Copyright Warning & Restrictions

The copyright law of the United States (Title 17, United States Code) governs the making of photocopies or other reproductions of copyrighted material.

Under certain conditions specified in the law, libraries and archives are authorized to furnish a photocopy or other reproduction. One of these specified conditions is that the photocopy or reproduction is not to be "used for any purpose other than private study, scholarship, or research." If a, user makes a request for, or later uses, a photocopy or reproduction for purposes in excess of "fair use" that user may be liable for copyright infringement,

This institution reserves the right to refuse to accept a copying order if, in its judgment, fulfillment of the order would involve violation of copyright law.

Please Note: The author retains the copyright while the New Jersey Institute of Technology reserves the right to distribute this thesis or dissertation

Printing note: If you do not wish to print this page, then select "Pages from: first page # to: last page #" on the print dialog screen

ABSTRACT

NOVEL SCRUBBING SYSTEMS FOR POST-COMBUSTION CO_2 CAPTURE AND RECOVERY

by
Tripura Mulukutla

Power plant emissions of flue gas releases considerable CO_2 to the atmosphere; CO_2 is considered to be the main contributor to global warming. Several gas absorption techniques are being investigated to reduce the capital and operating costs for CO_2 capture from post-combustion flue gas. Conventional method of CO_2 capture by an aqueous solution of monoethanolamine (MEA) and its subsequent stripping in a separate tower with steam at 120^oC, is a highly energy intensive process. The low partial pressure of CO_2 in the flue gas inhibits the application of CO_2-selective membranes unless methods are employed to increase the CO_2 partial pressure in the flue gas to be treated. A novel technique to potentially bypass the shortcomings of many existing approaches is described.

A bench-scale CO_2 capture and recovery from simulated flue gas is demonstrated using an advanced polypropylene hollow fiber membrane contactor. This is achieved by the use of a novel non-volatile absorbent, consisting of the ionic liquid [bmim][DCA] containing 20 wt % polyamidoamine PAMAM dendrimer Gen 0. A simulated humidified flue gas containing around 14% CO_2 is used and successful removal of bulk of the CO_2 and its recovery in a CO_2-concentrated stream up to 92% is demonstrated. An estimate of the overall volumetric mass transfer coefficient, $K_l a$ for the current CO_2-IL-PAMAM Gen 0 system was obtained.

Apart from the capture of CO_2 by an absorption-stripping process in a liquid flowing absorbent, a lot of research involves capture of the anthropogenic CO_2 by the use of solid adsorbents. Solid amine adsorption renders higher adsorption capacities via fast CO_2 reaction with amines. Impregnations of solids, direct condensation of the organic amines onto large surface area porous solids are few of the approaches being practiced to capture the CO_2 via adsorption. Regeneration of $Ca(OH)_2$, Na(OH) based adsorbents are highly energy intensive. Some of the other physical adsorbents in practice, zeolites, mesoporous silica, activated carbons are known to require high temperatures for effective desorption of CO_2. It is reported that these physical adsorbents have relatively low selectivity towards CO_2.

The novel absorbent of a mixture of 80 wt % polyamidoamine dendrimer Gen 0 (PAMAM) and 20 wt % ionic liquid [bmim][DCA] is chosen for the absorption study. Equilibrium CO_2 sorption uptake and temperature swing absorption (TSAB) of this nonvolatile organic CO_2-reactive liquid amine absorbent is reported in the present study. A mixture of 80% PAMAM in [bmim] [DCA] is highly viscous at room temperature and acts like a superefficient adsorbent by capturing CO_2 via fast reaction CO_2 reaction with amines. The equilibrium sorption uptake of this absorbent is studied in a pressure decay dual transducer apparatus for different weights and different temperatures of the absorbent. For the study of the TSAB process, a two- hollow fiber system is designed with porous PVDF and solid nonporous PEEK hollow fibers. A highly porous hydrophobic polymeric hollow fiber membrane absorbent-based device will have on the shell side the nonvolatile organic CO_2-reactive liquid amine, 80 wt. % PAMAM – IL, which will absorb CO_2 for a brief period from flue gas flowing through the bore of many

hydrophobic hollow fibers whose thin walls have a high porosity. Temperature-swing desorption of the absorbed CO_2 gas is done to regenerate the 80 wt. % PAMAM – IL absorbent. Hot water is passed through the bore of the solid PEEK hollow fibers of the two fiber system in order to desorb the sorbent of the absorbed CO_2 gas. Regeneration of the absorbent is studied at different temperatures and reported as a part of the present study.

NOVEL SCRUBBING SYSTEMS FOR POST-COMBUSTION CO_2 CAPTURE AND RECOVERY

by
Tripura Mulukutla

A Dissertation
Submitted to the Faculty of
New Jersey Institute of Technology
in Partial Fulfillment of the Requirements for the Degree of
Doctor of Philosophy in Chemical Engineering

Otto H. York Department of Chemical Engineering

August 2014

APPROVAL PAGE

NOVEL SCRUBBING SYSTEMS FOR POST-COMBUSTION CO_2 CAPTURE AND RECOVERY

Tripura Mulukutla

Dr. Kamalesh K. Sirkar, Dissertation Advisor — Date
Distinguished Professor of Chemical, Biological & Pharmaceutical Engineering, NJIT

Dr. Robert B. Barat, Committee Member — Date
Professor of Chemical, Biological & Pharmaceutical Engineering, NJIT

Dr. Somenath Mitra, Committee Member — Date
Distinguished Professor of Chemistry and Environmental Science, NJIT

Dr. Xianqin Wang, Committee Member — Date
Associate Professor of Chemical, Biological & Pharmaceutical Engineering, NJIT

Dr. Zafar Iqbal, Committee Member — Date
Research Professor of Chemistry and Environmental Science, NJIT

BIOGRAPHICAL SKETCH

Author: Tripura Mulukutla

Degree: Doctor of Philosophy

Date: August 2014

Undergraduate and Graduate Education:

- Doctor of Philosophy in Chemical Engineering,
  New Jersey Institute of Technology, Newark, NJ, 2014

- Bachelor of Technology in Chemical Engineering,
  University College of Technology, Osmania University, Hyderabad, India, 2008

Major: Chemical Engineering

Presentations and Publications:

T. Mulukutla, G. Obuskovic; K.K. Sirkar, A Novel Technology for Post-Combustion CO_2 Capture and Recovery: Experimental Studies. Manuscript being revised for publication in Journal of Membrane Science, 2014.

T. Mulukutla, D. Singh, J. Chau, G. Obuskovic, K.K. Sirkar, PAMAM Dendrimer Generation Zero Acting Like a Superefficient Adsorbent for CO_2 Removal from Flue Gas (Manuscript submitted for publication).

J. Chau, G. Obuskovic, J. Xingming, T. Mulukutla, K.K. Sirkar, Solubilities of CO_2 and He in an Ionic Liquid Containing Poly (amidoamine) Dendrimer Gen 0 Ind. Eng. Chem. Res. 52 (2013) 10484-10494.

T. Mulukutla, D. Singh, J. Chau, G. Obuskovic, K.K. Sirkar, A Membrane-Based Technique for Carbon Capture and Sequestration from Flue Gas, selected for poster presentation at NAMS Annual Meeting, Houston, TX, May. 2014.

T. Mulukutla, G. Obuskovic, K.K. Sirkar, A Novel Membrane-Based Technology for Post-Combustion CO_2 Capture and Recovery, oral presentation at AIChE Annual Meeting at San Francisco, CA. November. 2013.

T. Mulukutla, G. Obuskovic, K.K. Sirkar, A Novel Technology for Post-Combustion CO_2 Capture at AIChE Annual Meeting at Pittsburgh, PA, October. 2012.

T. Mulukutla, V. Kesiraju, Pre-Treatment of Sweet Sorghum Biomass: An Alternative Source of Energy at CHEMCON, Kolkata, India. December 2007.

T. Mulukutla, V. Kesiraju, A Study of Biomass as a Fuel and its Sustainability at IChESCON at NIT Warangal, India. January 2005.

Dedicated to
My loving parents, Venkata Sastry and Swarnalata Mulukutla

ACKNOWLEDGMENT

I would like to begin by conveying my deepest gratitude to my advisor, Dr. Kamalesh K. Sirkar. I am indebted to him and feel fortunate to work under the guidance of Distinguished Professor in Membrane Science and Technology. I have greatly benefited from his discussions, which motivated me to analyze and think critically. Without his encouragement, this dissertation would not have materialized.

I am really thankful to my committee members, Dr. Somenath Mitra, Dr. Xianqin Wang, and Dr. Zafar Iqbal for taking their time off the busy schedule and to be able to serve on my committee members and for their constructive comments and warm encouragement. I am particularly grateful to Dr. Robert B. Barat for his insightful comments and suggestions.

I owe a very important debt to the Chemical Engineering Department for their financial support during my course of study. I would like to particularly thank Dr. Sunil Saigal, Dr. Norman Loney and Dr. Basil Baltzis. I also want to thank Eaton Corporation in Midland, Michigan, as well as Martin J. Nadeau and David Y. Lee of Eaton Corporation for their support and encouragement.

I would like to thank Ms. Brenda Arthur for her generous support. I would like to offer my special thanks to Yogesh for his timeless assistance. I would like to thank all my lab mates and colleagues for their technical support. My special mention to Dr. Gordana Obuskovic, Dr. Dhananjay Singh, Dr. Sagar Roy, Dr. John Chau, Ying Ye, Shawn Yetman and George Barnes.

I am very grateful for the help and encouragement from my brother, Bhanu Chandra Mulukutla, who has been a strong pillar of support. Thank you very much. The

enormous support, patience and encouragement from Vishal Javvaji and Prasanna Dasari were invaluable. I would like to thank Lavanya Polepalli, Anusha Makineni, Sneha Kasireddy, Sharmila Yejella, Maneesh Merwade and all others who have shown their kind support and love directly or indirectly during this course of life.

All this would not have been possible without the unequivocal support, enduring patience and unconditional love of my parents for giving me this chance to pursue my dream. Thank you very much for everything.

TABLE OF CONTENTS

TABLE OF CONTENTS
(Continued)

TABLE OF CONTENTS
(Continued)

Chapter **Page**

TABLE OF CONTENTS
(Continued)

LIST OF TABLES

LIST OF TABLES
(Continued)

LIST OF FIGURES

LIST OF FIGURES
(Continued)

LIST OF FIGURES
(Continued)

LIST OF SYMBOLS

A_m	Membrane area, m^2
c	Concentration, mol/cm^3
c_i	Hypothetical liquid phase CO_2 concentration in equilibrium with the bulk gas
$C_{co_{2,g,in}}$	Concentration of CO_2 in the gas stream inlet, mol/cm^3
$C_{co_{2,g,out}}$	Concentration of CO_2 in the gas stream outlet, mol/cm^3
D_g	Diffusion coefficient of CO_2 in N_2, m^2/s
$D_{g,k}$	Knudsen diffusion coefficient of CO_2, m^2/s
$D_{g,b}$	Bulk diffusion coefficient of CO_2, m^2/s
H_i	Henry's law constant, bar
k_{im}	Membrane mass transfer coefficient of CO_2, m/s
k_{il}	Liquid mass transfer coefficient of CO_2, m/s
k_{ig}	Gas mass transfer coefficient of CO_2, m/s
K_l	Overall liquid film-based mass transfer coefficient, m/s
K_g	Overall gas film-based mass transfer coefficient, m/s

LIST OF SYMBOLS
(Continued)

N_{co_2}	Molar flux of CO_2, gmol/m^2s
N_i	Molar flux of species i, gmol/m^2s
P_t	Total pressure, atm
p	Partial pressure
p_i*	Equilibrium CO_2 partial pressure in gas in equilibrium with the bulk liquid
Q_g	Inlet feed gas flow rate, cm^3/min
R	Gas constant, cm^3atm/K gmol
r_p	Pore radius, μm
Re	Reynolds number
Sc	Schmidt Number
Sh	Sherwood Number
T	Temperature, K
$y_{co_{2,g,in}}$	CO_2 mole fraction at absorption module inlet
$y_{co_{2,g,out}}$	CO_2 mole fraction at absorption module outlet
y_{in}^*	Hypothetical inlet gas phase mole fraction in equilibrium with liquid phase
y_{out}^*	Hypothetical outlet gas phase mole fraction in equilibrium with liquid phase

Greek Symbols

Δy_{lm} = Logarithmic mean mole fraction

δ = Membrane thickness, μm

τ = Membrane tortuosity

ε = Membrane porosity

Superscripts and subscripts

b bulk

g gas phase

i species i ; phase interface location

k knudsen

m membrane

l liquid phase

lm log mean

t total

CHAPTER 1

INTRODUCTION

1.1 Background

1.1.1 Carbon Capture and Storage

According to the Intergovernmental Panel on Climate Change (IPCC) of the United Nations, the observed increase in globally averaged temperatures since the mid-twentieth century is very likely to have occurred due to the increase in anthropogenic greenhouse gas concentrations that leads to the warming of the earth's surface. In its turn, CO_2 is essentially blamed to be the main factor causing the greenhouse effect because it is the most important anthropogenic greenhouse gas [1, 2]. Table 1 shows the CO_2 emissions from various sources. According to International Energy Agency (IEA) (2003), it has been reported that the power sector is the single largest source of CO_2 emission, followed by the automotive sector. It is predicted that by 2050, the amount of CO_2 release into the atmosphere by the electric and the industrial sector will increase significantly. It is estimated that the global CO_2 emission range from 29-44 Gt CO_2 per year in 2020, and will be 23-84 Gt CO_2 per year in 2050 [3]. Hence, there is an immediate need to capture and store this CO_2.

Table 1.1 Sources of CO_2 emissions from fossil fuel combustion (2001)

	Emissions	
	($MtCO_2\ yr^{-1}$)	($MtC\ yr^{-1}$)
Public electricity and heat production	8,236	2,250
Autoproducers	963	263
Other energy industries	1,228	336
Manufacturing & construction	4,294	1,173
Transport	5,656	1,545
of which: Road	4,208	1,150
Other sectors	3,307	903
of which: Residential	1,902	520
TOTAL	23,684	6,470

Source: [3]

1.1.2 Options for Carbon Capture

There are three main options currently being used for carbon dioxide capture. The schematic diagram in Figure 1.1 shows three main methods of carbon capture.

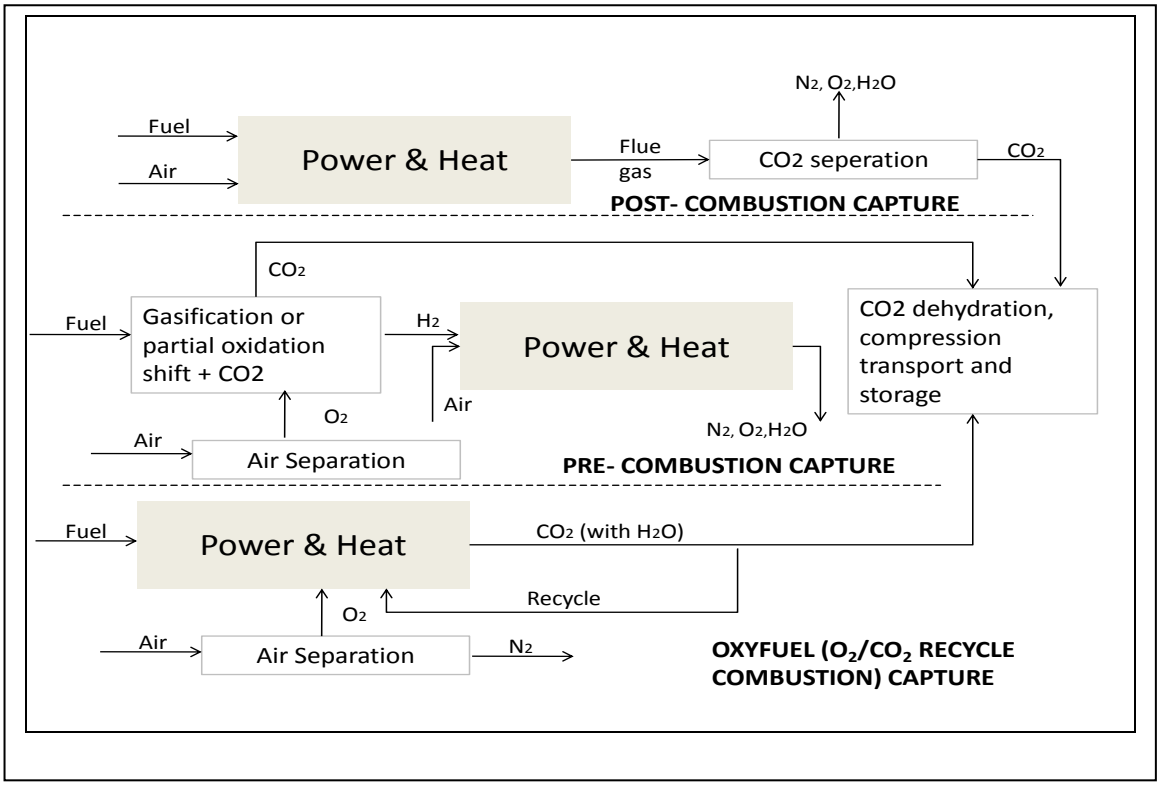

Figure 1.1 Principles of three main CO_2 capture options.
Source: [4]

a) **Pre-Combustion Capture:** Carbon capture prior to the combustion of fossil fuels is usually difficult. However, all types of fossil fuels can be gasified with sub-stoichiometric ratios of oxygen, which produces synthesis gas (CO and H_2) [3]. But addition of water to the mixture allows the water gas shift reaction to approach equilibrium and thereby leads to the conversion of residual CO to CO_2 and production of more hydrogen. The pre-combustion mixture has typically 15-60 vol% of CO_2.

Water –gas shift reaction: $CO + H_2O <=> CO_2 + H_2$ (1.1)

Separation of CO_2 from the hydrogen – rich gas typically uses a physical solvent and no heat is required to regenerate the solvent. Thus the CO_2 can be released above the atmospheric pressure, compressed and stored.

b) **Oxy-fuel Recycle Capture:** In this method, the fuel is burnt in a mixture of oxygen and recycled flue gases. During this combustion, the flue gas gets cooled down which is recirculated back into the combustion chamber. This recirculated mixture usually contains high amounts of carbon dioxide and water vapor. From this mixture of flue gas, carbon dioxide can be easily separated and compressed [4]. The oxy-fuel mixture has very high concentrations of CO_2 (about 80 vol% of CO_2).

c) **Post-Combustion Capture:** This strategy involves capturing the carbon dioxide from the combustion products, before they are vented to the atmosphere. Commercially advanced methods use wet scrubbing with aqueous amine solutions. CO_2 is removed from the waste gas by the amine solvent at a low temperature, after which the solvent is regenerated for re-use by heating at higher temperature, before being cooled and recycled continuously. The so removed carbon dioxide is dried, compressed and transported to safe geological storage [4]. The post-combustion mixture has typically 3-15 vol% of CO_2.

1.1.3 Existing Industrial Techniques for CO_2 Capture

Power plants release enormous volumes of CO_2 into the atmosphere. The combustion of fossil fuels not only releases CO_2 but also other acidic gas components, such as carbon monoxide, oxides of nitrogen, (NO_x), sulphur (SO_2) and other particulate matter including soot, fly ash, etc. The flue gas is typically much above 100 °C when it is released from the power plants. It is essential to remove these particulates and cool down the flue gas before it is subjected to CO_2 capture. The presence of such gases and particulates can pose operational challenges such as loss in absorption capacity; formation of heat stable salts, unwanted wastes in the CO_2 stream, leading to an overall high energy consumption of the process [3]. The major pretreatment of flue gas includes NO_x removal and flue gas desulfurization to remove SO_2. Non- Selective Catalytic Reduction (NSCR), Selective Catalytic reduction (SCR), adsorption and alkaline absorption of nitrogen oxides are some of the NO_x removal methods [5]. Furuta [6] has scrubbed NO_x from flue gas using calcium and magnesium hypochlorites with 95-100% efficiency.

Flue gas desulfurization refers to the removal of SO_2 from exhaust gases. The SO_2 concentration in the flue gas is about 300-5000 ppm. Common methods used for the removal of SO_2: Wet scrubbing by alkaline sorbents, limestone, lime, etc. Spray-dry scrubbing systems; Wet sulfuric acid process and SNOX flue gas desulfurization. Ortiz et al. [7] have used limestone for the desulfurization of the wet flue gas and have shown efficiencies of about 59-99% using three different types of limestone in a pilot plant setting. Zhao Yi et al. [8] have studied the SNOX removal of flue gas using an oxidizing manganese compound additive in a circulating fluidized bed (CFB). They reported the efficiencies of desulfurization and denitrification to be 92.3% and 60.8% respectively.

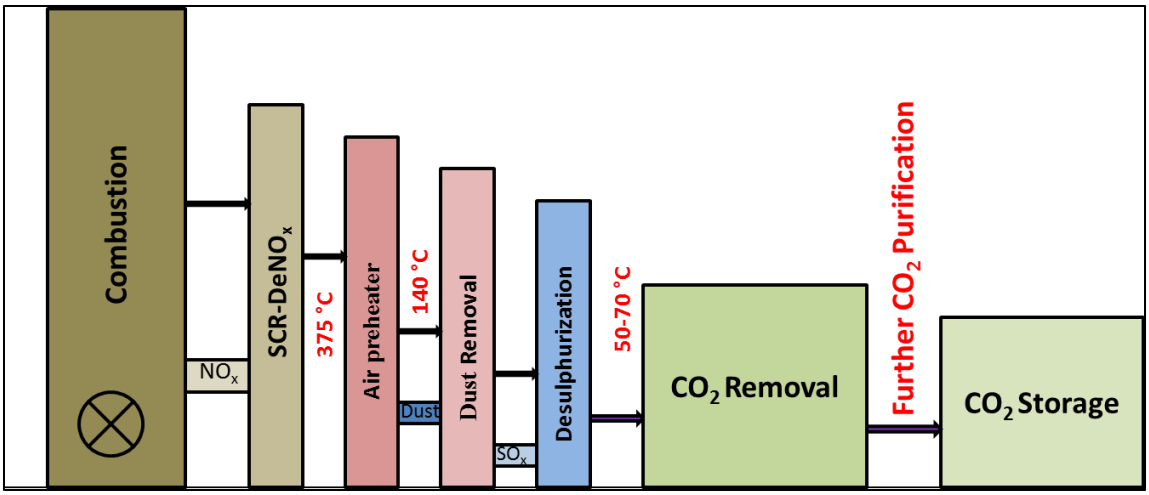

Figure 1.2 Schematic showing the steps involved in flue gas scrubbing.

After removal of the particulate materials, the post combustion mixture contains usually about 3-15 vol% CO_2, upto 2 vol% O_2 and rest N_2. This gas is first sent through the cooler section, where the temperature of the flue gas is cooled down to 40-50 °C from 100 °C. Figure 1.2 shows the steps involved in flue gas scrubbing.

In many existing industrial plants in chemical, petrochemical and other industries, CO_2 is removed by scrubbing the gas stream with a liquid solution flowing countercurrently in say, a packed tower; the CO_2 – loaded absorbent is then regenerated in another packed or tray tower generally at a higher temperature simultaneously producing a purified CO_2 stream. Scrubbing of CO_2- containing gas streams with a variety of CO_2 – reactive amine-containing solution is widely practiced in industry. However, such a process is expected to increase the cost of electricity production from PC power plants substantially. Absorption of the acid gas is done using alkaline amine solvent, typically MEA. The absorber is typically maintained at around 40-60 °C. The flue gas from the blower comes in contact with the amine solvent in the absorbent, when CO_2 is absorbed into the solvent via chemical reaction with the aqueous amine solvent.

This flue gas then undergoes water wash which helps in removing any fine particulates in the feed gas stream or solvent droplets. The CO_2 loaded solvent is then pumped into the stripper via a heat exchanger. This CO_2- loaded solvent is then stripped of CO_2 and the solvent is regenerated at about 100 °C – 140 °C in the stripper. Steam produced in the stripper which acts a stripping gas is condensed in the condenser and then fed back to the stripper. Reboiler provides the required heat in order to maintain the stripper at the elevated temperature. The lean CO_2 solvent from the stripper is then pumped back into the absorber via the heat exchanger where the temperature is reduced to the absorber temperature with a cooler [3]. Figure 1.3 shows a commercial amine scrubbing unit.

Kohl and Nielsen [9] have emphasized a number of acid gas removal processes; these include CO_2 absorption-stripping processes with a number of amines, some of them being monoethanolamine (MEA), diethanolamine (DEA), diisopropanolamine (DIPA), diglycolamine for high pressure natural gas treating, etc.

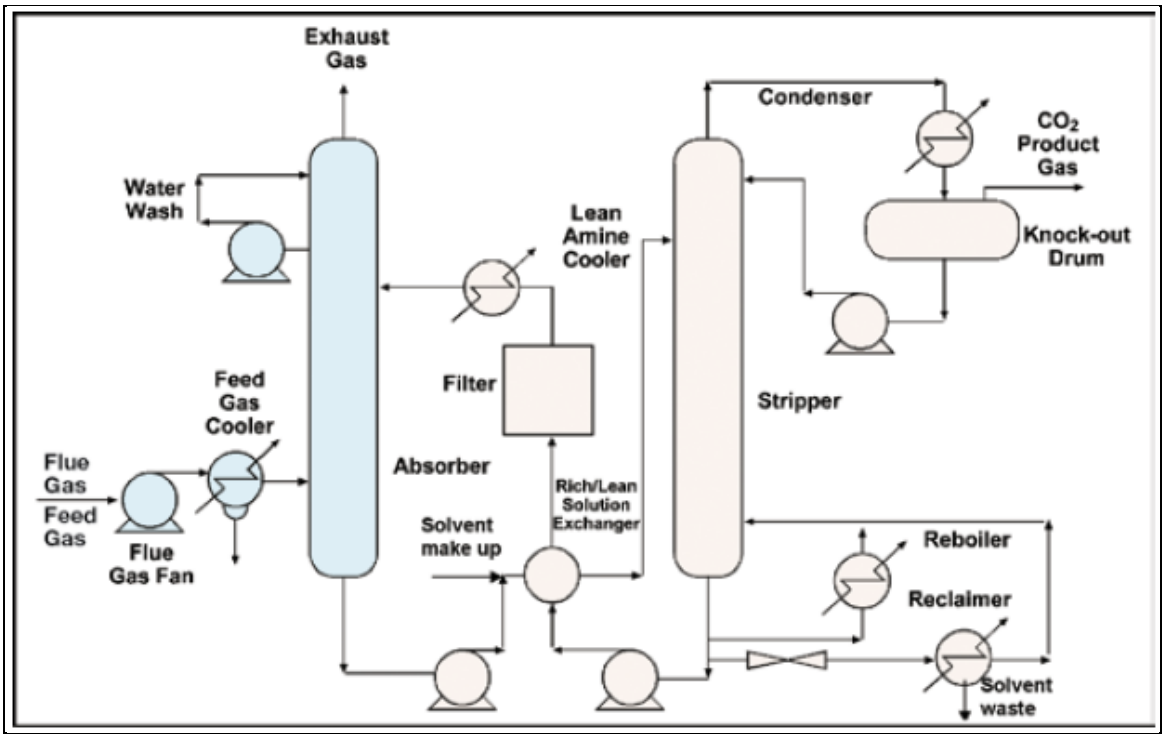

Figure 1.3 Commercial amine based gas scrubbing system.
Source: [3]

1.1.4 Disadvantages of Conventional Techniques

In spite of such cost estimates, Rochelle [10] has suggested that amine scrubbing will probably be the dominant technology for CO_2 capture from coal-fired plants in 2030. A number of changes are needed if a liquid scrubbing and regeneration strategy is to succeed in substantially reducing the cost of post-combustion CCS. Amine scrubbing technologies share a few common features:

(1) The reactive amine is in an aqueous solution. (2) The amines are most likely to be volatile and therefore slowly lost by evaporation. (3) During solution regeneration and release of the absorbed CO_2, considerable heat is supplied to raise the solution temperature to 110-120° C and around 2 atm from ~ 50 °C used during scrubbing using say, an aqueous monoethanolamine (MEA) solution. This leads to considerable evaporation of water and creates the need for providing substantial

sensible heat and latent heat due to water evaporation. (4) Generally the heat of absorption is high; the value of ΔH_f decreases as one goes from primary amines to tertiary amines. (5) Hindered amines have a larger capacity of CO_2 absorption and undergo easier desorption. (6) There is significant degradation of amines via oxygen or otherwise. (7) The scrubbing and stripping columns provide low gas-liquid interfacial area. As a result, they are tall and costly structures. (8) There is a significant possibility of foaming in such scrubbing towers which are either packed or tray towers. (9) The flue gas may be assumed to be essentially saturated with water.

Conventional absorption towers in the amine sweetening system are usually very large in size and heavy in weight. They pose operational challenges such as liquid channeling, flooding, emulsions, entrainment and foaming [11].

Foaming: Expansion of liquid due to the passage of gas refers to foaming. Though it provides high interfacial gas-liquid contact, excessive foaming leads to liquid hold up, thereby reducing separation efficiency.

Entrainment: At high gas velocities, the gas leaving the columns may carry droplets of the solvent as mist. Entrainment losses are caused by inefficient mist extraction or carry-over of the solution. To overcome this loss, installation of additional equipment (such as mesh etc.) is required.

Flooding: At high gas flow rates, the chances of flooding are very high in packed columns. This is because as the gas flow rate is increased, the pressure drop per unit length of the packing increases. The increase in the pressure from the high gas flow rates

may retard the liquid flow, resulting in liquid hold up. Flooding causes a significant decrease in the separation efficiency.

Apart from the conventional techniques, a variety of approaches are being investigated for removing CO_2 from post-combustion flue gas and recovering it in a substantially purer form suitable for sequestration. These approaches include: Adsorption, cryogenic (condensation) processes, liquid solvent absorption, membrane processes, and dry absorbent-based processes [12].

Gas separation membranes involve separation of the individual gas component of a gas mixture on the basis of the gas permeation rate through the membrane. The gas permeation rate depends on the characteristics of the gas component, the type of the membrane and the partial pressure differential of the gaseous component across the membrane [9].

1.2 Membrane-based Gas Absorption and Stripping

Membrane based gas absorption is primarily implemented in hollow-fiber membrane devices. These hollow fibers can be packed into the membrane contactors in a number of ways. Either hydrophilic or hydrophobic membrane fibers can be used depending on the type of use. In membrane based gas absorption, the gas is either passed on the shell side or the tube side of the membrane module and the solvent is passed on the other side, i.e. either lumen side or shell side of the membrane device. Figure 1.4 shows a schematic of membrane based gas absorption.

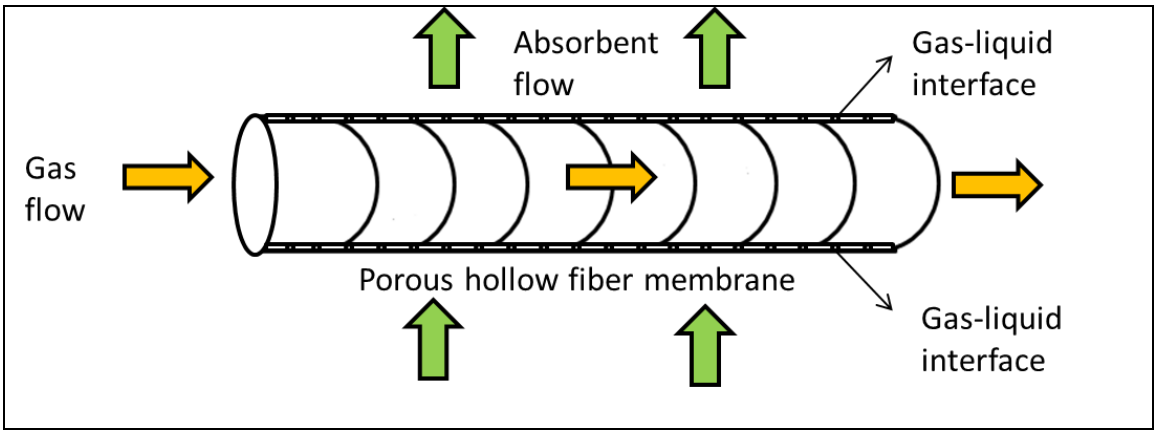

Figure 1.4 Schematic of membrane based gas absorption with the absorbent in cross flow over the hollow fiber.

Gas absorption into the solvent or the stripped liquid occurs at the gas-liquid interface. The gas usually diffuses into the solvent through the pores/pore mouth of the hollow fiber membrane module/contactor. These pores can be either gas filled or absorbent filled depending on the mode of the operation. If the pores are filled with gas, it is called a non-wetted mode of operation. If the pores are liquid filled, it is a wetted mode of operation.

To ensure a non-dispersive mode of operation, the gas pressure has to be lower than that of the liquid pressure in order to prevent dispersion of the gas as bubbles into the liquid. Unless a certain critical pressure (Δp_{cr}) is exceeded by the liquid pressure over the gas pressure, the liquid does not enter the pores [13, 14]. This maximum allowable value of the differential pressure is defined as the breakthrough pressure. Figure 1.5 shows the non-wetted mode of operation. Equilibrium separation processes of gas absorption and gas stripping take place with one phase interface, the gas/liquid interface, immobilized at the membrane pore mouth in a membrane-based gas/liquid contactor.

If the microporous membrane could be modeled as a collection of parallel cylindrical pores of radius r_p, then the breakthrough pressure is related to the other relevant variables by the Young-Laplace equation:

$$\Delta p_{cr} = \frac{2\,\gamma_l\,cos\theta_c}{r_p} \tag{1.2}$$

where γ_l is the surface tension of the absorbent liquid, θ_c is the contact angle and r_p is the pore radius.

The first nondispersive gas absorption was introduced in blood oxygenation. Esato and Eiseman [15] used the Gore-Tex hydrophobic flat membranes of polytetrafluroethylene for oxygenation of blood. Tsuji et al. [16] used hydrophobic microporous hollow fibers of polyprolyene for absorption oxygen into blood. Sirkar (1992) [14] reviewed microporous membrane-based gas absorption process.

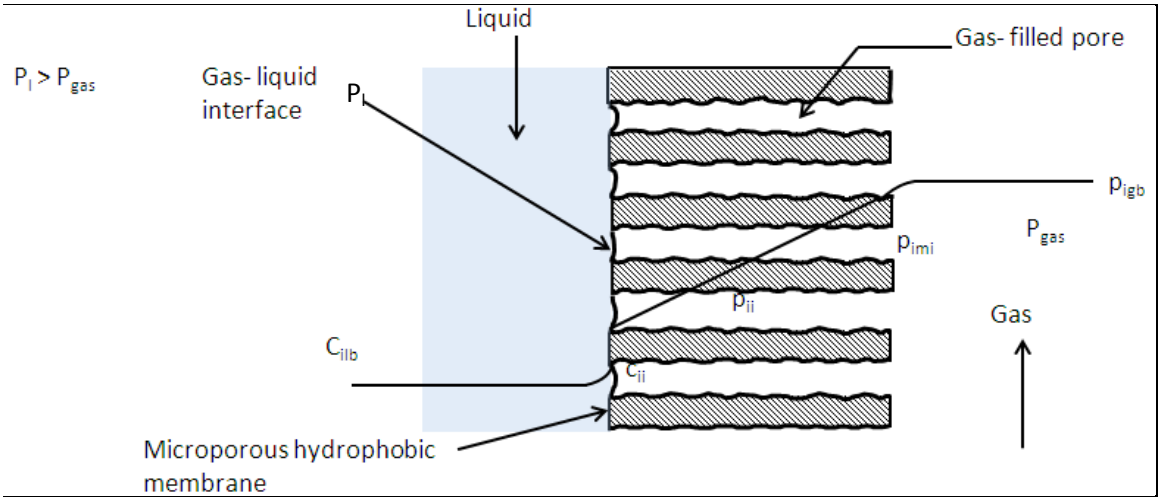

Figure 1.5 Concentration profile for a gas-filled pore system (non-wetted mode).
Source: [13]

In the wetted mode of operation, a porous hydrophilic membrane is spontaneously wetted by an aqueous absorbing liquid. In this mode, the gas pressure has to be higher

than the liquid pressure in order to prevent the liquid from dispersing as drops in the gas. Karoor and Sirkar [13] have studied non-dispersive gas absorption with the gas at higher pressure by incorporating an aqueous solution in hydrophobic membrane pores via an exchange process. Figure 1.6 shows the concentration profile in an absorbent filled pore.

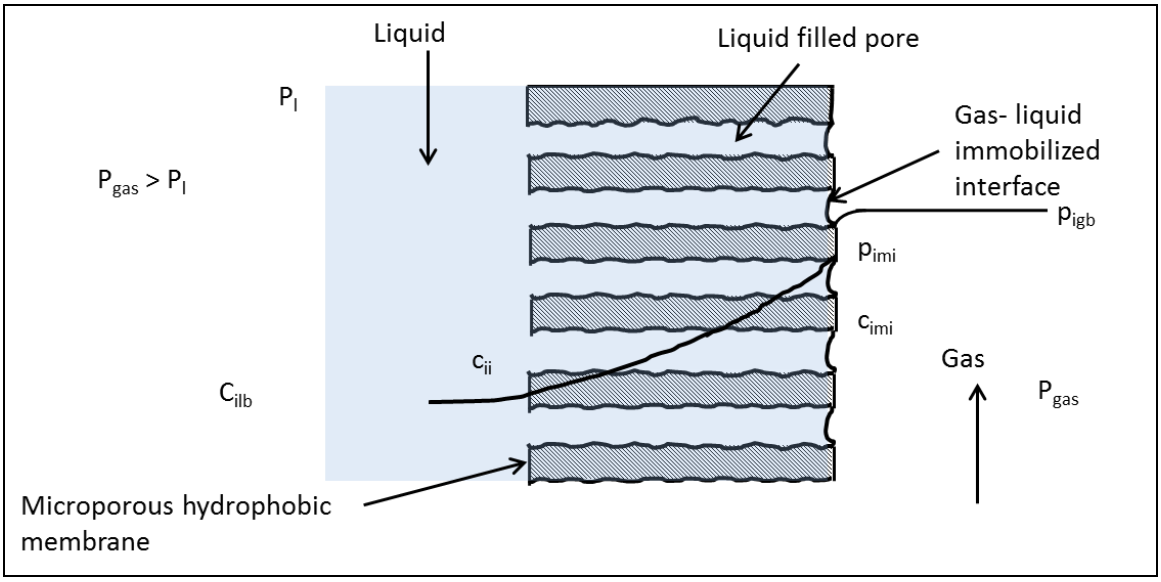

Figure 1.6 Concentration profile in an absorbent filled pore system (wetted pore).
Source: [13]

1.2.1 Advantages of Gas-Liquid Membrane Contactors

Membrane based gas separation offers a number of advantages compared to tray columns, packed columns, spray towers, etc. Membrane gas contactors/ modules have much less weight and are smaller in size, thereby offering low capital investment and labor costs, when compared to the conventional separation techniques. Owing to its compact size and nondispersive mode, it is easy and flexible to operate. Also, the compact porous membrane like device provides high gas liquid contacting surface area per unit volume. Due to its modularity and low maintenance, it is easy to scale up and can be operated over a wide range of capacities [17]. Membrane modules can be successfully

operated under high gas/liquid flow ratios. Since the gas and liquid flow independently, solvent dispersion, entrainment, flooding, solvent hold-up etc. are avoided, thereby offering excellent mass and hear transfer capability. Such an operation provides high solubility selectivity of the liquid solvents and potential reduction in energy requirements.

1.2.2 State of the Art CO_2 Removal Solvents – Membrane Processes

Due to the increasing popularity of the use of physical solvents in gas treating, a plethora of room temperature ionic liquids (RTIL) have been investigated for capturing carbon dioxide from earth's atmosphere. These green solvents are stable molten ionic salts at room temperature with high thermal decomposition temperatures, high ionic conductivities, low melting points, and negligible vapor pressure [18]. These molten salts come in a number of bulky organic cation and anion combinations. Berthod et al. [19] reviewed the physicochemical properties of a large number of ionic liquids. Therefore these ionic liquids (ILs) can serve as better physical solvents compared to conventional candidates e.g.,sulfolane, N- Methyl-2-Pyrrolidinone (NMP) and propylene carbonate [20].

Andrzej et al. has reviewed the solubility parameters and enthalpies of evaporation of a number of ionic liquids [21]. Jalili et al. [22] have studied the solubility and diffusion of CO_2 and H_2S in ionic liquid [emim][$EtSO_4$] and have shown that H_2S is more soluble in [emim][$EtSO_4$] and the corresponding diffusion coefficient being two orders magnitudes higher than that of CO_2. Anthony et al. [23] have shown the feasibility of using [bmim][PF_6] to capture CO_2 by static absorbers where experiments were done with variations in temperature and pressure. Chau et.al [24] have reported solubility of CO_2 in [bmim][DCA], mixture of [bmim][DCA] and 20 wt% Poly(amidoamine)

dendrimer Gen 0 (PAMAM) with and without moisture; they had studied a mixture containing 30 wt% PAMAM as well.

A number of CO_2 capture studies were also done with various blends of amines. The enhancement in CO_2 capture was achieved by the reactive absorption of CO_2 with the amines. Vaidya et al. [25] have studied the capture of CO_2 via reaction of CO_2 with aqueous solutions of various members of alkanolamines. Matsuyama et al. [26] have studied the facilitated transport of CO_2 through polyethylenimine/poly (vinyl alcohol) blend membranes.

1.2.3 Significance of PAMAM Dendrimer

Room temperature ionic liquids (RTILs) are a category of polar organic solvents with significant solubility for CO_2 over N_2. If we now dissolve a high concentration of a hyperbranched amine such as polyamidoamine (PAMAM) dendrimer of generation 0 (MW 517) in the RTIL, we may achieve a high $CO_2 - N_2$ selectivity. The studies by Kovvali et al. of immobilized liquid membranes (ILMs) [27, 28, 29] of this amine indicated a CO_2/ N_2 selectivity of upto 15,000-18,000 for low CO_2 concentrations and 700 for higher CO_2 concentrations upto 25 cm Hg CO_2 partial pressure. As long as there was considerable moisture present in the gas phase, the highest values were obtained with the pure dendrimer. Further ILM selectivity can only suggest what may be achieved in absorption. Kazama et al. have demonstrated the in-situ modification method which was used to develop large-sized dendrimer ILM - based membrane modules for CO_2 separation with high CO_2 permeance from an ambient temperature flue gas [30, 31, 32].

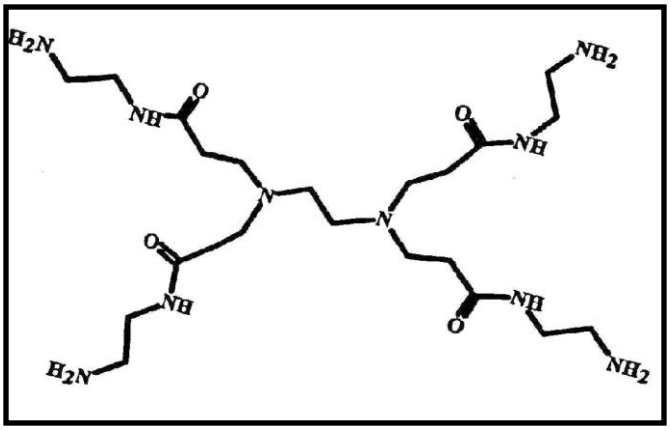

Figure 1.7 Structure of PAMAM dendrimer generation 0.

The PAMAM dendrimer has four primary amines and two tertiary amines. Tertiary amines require the presence of moisture before being activated. Kovvali et al. observed that the reactivity of the hyperbranched amine PAMAM Gen 0 is strongly dependent on the presence of moisture in the gas phase [27, 28, 29]; reduced environmental humidity drastically reduced CO_2-N_2 selectivity since the tertiary amines could not be activated in the absence of moisture. The studies by Chau et al. [24] of equilibrium absorption of CO_2 - He into a 20-30 wt % PAMAM Gen 0 solution in the ionic liquid [bmim][DCA] (1-butyl-3-methylimidazolium dicyanamide) at various temperatures indicated a CO_2 – He selectivity of ~50 at 50 °C in the presence of moisture; without moisture it was reduced to ~ 30. Therefore when the spent CO_2-saturated amine – containing organic solvent is brought to a heater, heated to, say, 85-90 °C and released into a porous hollow fiber membrane contactor-based stripper, the immediate loss of moisture from the liquid phase will substantially enhance the stripping of CO_2 from the RTIL as long the gas phase is removed via vacuum. One may not need to go to a high temperature of 110-120 °C currently used in MEA-based systems. Further, the evaporation of bulk water encountered in conventional processes would be absent

here except for the dissolved water evaporation leading to a substantial reduction of the stripper heat requirement. There will be no loss of ionic liquid via evaporation; nor will there be a loss of the amine by volatilization and consequent corrosion of the downstream equipment.

Replacement of water and conventional volatile amines (MEA et al.) respectively by RTIL and a hyperbranched oligomer, PAMAM Gen 0, will raise the solution viscosity substantially. The scrubber pressure drop will be determined by Reynolds number (Re), flow path length, viscosity and form friction vs. skin friction.

1.3 Objectives of this Thesis

Two membrane based absorption-stripping technique to potentially bypass the shortcomings of many existing approaches are described here.

- Develop a novel CO_2-reactive nonvolatile mixed organic solvent-based system for capturing CO_2 from simulated cooled post combustion flue gas mixture in lab-scale advanced hollow fiber membrane contactors and then recover purified CO_2 from a membrane stripper.
- Demonstrate successful removal of bulk of the CO_2 and its recovery in a CO_2-concentrated stream.
- Estimate of the overall volumetric mass transfer coefficient ($K_l a$) for the proposed CO_2-IL-PAMAM Gen 0 system, and its comparison with CO_2- aq.MEA and CO_2-aq.DEA systems.
- Develop a novel CO_2-reactive nonvolatile mixed organic solvent-based system to study the equilibrium CO_2 sorption uptake of the solvent.

- Design and demonstrate a dynamic temperature swing absorption (TSAB) based on this novel solvent in a two-fiber system to simulate rapid temperature swing absorption process for CO_2 absorption and recovery.

1.4 Approach

In the first part of this thesis, the ionic liquid [bmim][DCA] containing 20 wt % PAMAM dendrimer generation 0 is used to absorb CO_2 at around 40-50 °C from simulated flue gas in advanced hollow fiber membrane contactors; the spent absorbent solution is then regenerated continuously in similar hollow fiber membrane contactors at around 85-90 °C. Short hollow fiber - based membrane contactors were employed; here the absorbent liquid will flow slowly through the bore or around the hollow fiber outside surface in cross flow. Sirkar group observed in direct contact membrane distillation (DCMD) studies [33,34,35] that hot saline waters in cross flow yielded high heat and mass transfer coefficients with very little pressure drop and very low Re values. Kovvali et al. have also obtained high values of CO_2 permeances (permeability/membrane thickness) in the studies of ILMs based on organic solvents and amines at higher temperatures [28, 29]. Therefore, one can expect to obtain not too low a mass transfer coefficient with viscous liquids flowing at a very low Re [36].

Further the contactor lengths are going to be quite limited from the liquid path length point of view; therefore the absorbent flow pressure drop or the gas pressure drop are unlikely to be high. Such a process of CO_2 absorption-stripping is illustrated here. The separations achieved as well as the values of the mass transfer coefficient of CO2 for a variety of conditions have been reported. Alternative methods of stripping including a sweep gas and/or a vacuum were investigated.

The sorption performance of CO_2 in a porous hollow fiber based absorption-stripping system via a temperature swing absorption (TSAB) process and the equilibrium sorption of CO_2 uptake by 80 wt % dendrimer in ionic liquid is studied in the second part of the thesis. Temperature swing based regeneration of CO_2 using a variety of adsorbents is being widely studied. The key to a successful process will be an adsorbent that has an extremely high CO_2 sorption capacity with very high selectivity over N_2 and yet can be regenerated at reasonably low temperature preferably hot water. The sorption capacity must be very high since the heating and cooling load (correspondingly cost) is inversely proportional to the sorption capacity. Ma et al. [37] employed a molecular basked sorbent to achieve 140 mg CO_2/g of sorbent at 15 kPa CO_2 partial pressure; this amounts to 3.18 mmol CO_2/g of sorbent. Ma et al. compared their material with a variety of adsorbent materials from literature and claimed a higher sorption performance including those from zeolitic imidazolate frameworks (zifs) (Banerjee et al.,) [38]. Hicks et al. [39] achieved 3.1 mmol CO_2/g of the hyperbranced aminosilica material at room temperature.

More recently, Geoppert et al. [40] report 1.74 mmol/g adsorbent FS-PEI-33 (branced polyethylenimine (PEI) coated on fumed silica) under humid conditions for ambient air and claimed it to be the highest value (higher than that for hyperbranced aminosilica) with a 36% amine content. Stuckert and Yang [41] found zeolite type Li-LSX the best among a few sorbent materials including amine-grafted microporous silica with a measured capacity of 0.82mmol/g for low CO_2 concentration in air; however this value is based on dry air since this particular zeolite loses its sorption capacity under moisture, Pacheco et al. (2012) [42] obtained 1.46 mmol/g adsorbent at 5 atm/308 K in an aminosilane-functionalized cellulosic polymer sorbent. In the present study, a novel absorbent is presented; its CO_2 sorption capacity is higher than most of the adsorbents

reported in the literature. The development of the absorbent with high capacity, rapid uptake, easy recycling with suitable thermal and mechanical properties is a challenging task. The results of the equilibrium sorption capacity of CO_2 and hollow fiber system sorption with 80 wt% dendrimer in ionic liquid [bmim] [DCA] are obtained using a pressure decay apparatus for the equilibrium sorption process and TSAB process for hollow fiber sorption.

Recently, Lively et al. [43] have reported a similar kinetic sorption performance of Zeolite 13X adsorbent. In the current study, the simulated flue gas is passed through the porous hollow fibers for CO_2 absorption. Regeneration of the sorbent bed is done by passing hot water through the solid fibers. The dispersed sorbent bed around the packed fiber bed allows fast heat and mass transfer rates. In the breakthrough absorption-desorption experiments of the sorbent bed, 44 mol % of CO_2 was obtained.

CHAPTER 2

CARBON DIOXIDE CAPTURE FROM POST COMBUSTION FLUE GAS USING 20 WT % PAMAM IN [BMIM] [DCA]

2.1. Materials, Membranes and Chemicals

2.1.1 Materials and Chemicals

The absorbent liquids used were pure ionic liquid (IL) [bmim] [DCA], [bmim] [DCA] containing the PAMAM dendrimer Gen 0, pure water and an aqueous solution of the dendrimer. Ionic liquid [bmim] [DCA] was obtained from EMD Chemicals, Philadelphia, PA; PAMAM dendrimer Gen 0 was procured from Dendritech Inc., Midland, MI as a 64.05 wt% solution in methanol. LiCl and K_2SO_4 were from Sigma Aldrich for calibration of the humidity probes. Nylon was used as material of construction for the body of the hollow fiber membrane contactor modules with mobile absorbent solution. In the case of the gas leaks or solvent leakages, West System # 105 Epoxy Resin and # 209 Extra Slow Hardener were used to fix the hollow fiber membrane modules. Physical solvents, N- Methyl-2-Pyrrolidinone (NMP), tetramethylene sulfolane (Acros Organics) and propylene carbonate (Sigma Aldrich) were used to test the degradation properties of nylon and the epoxy at 95 °C. This study also showed the basis for the selection of ionic liquid [bmim][DCA] against the physical solvents for CO_2 capture at temperature at 95 °C.

2.1.2 Material and Solvent Selection

Polar organic solvents e.g propylene carbonate, NMP, sulfolane, etc having high boiling points have considerable CO_2 solubility and selectivity for CO_2 over N_2, O_2; their CO_2 solubilities are in the same order of magnitude as that of water. In the field of industrial

gas treating by solvents, the process in which NMP is used as a solvent is referred to as the Purisol process. The Fluor solvent process uses propylene carbonate for gas treating. Table 2.1 shows that the physical solvent ionic liquid is the best suited for the present study. The epoxy and nylon were placed in a 10 ml solvent of each and tested over a period of 10 days for the dissolution properties against the ionic liquid [bmim][DCA] at 95 °C.

Table 2.1 Material and Solvent Selection
Resin 105+ Hardner 209 (R105 +H209): Amber Color.

Solvent / Material	Propylene Carbonate **(Fluor Solvent)**	Tetra Methylene Sulfolane **(Sulfolane)**	N- Methyl-2-Pyrrolidinone – NMP **(Purisol)**	Ionic Liquid [bmim][DCA]
Nylon	No dissolution	No dissolution	Color changes from white to pale yellow.	No dissolution
R105 + H209 (Epoxy)	Color Change from amber yellow to dark yellow.	Color Change from amber yellow to dark red.	Color Change from amber yellow to dark yellow along with dissolution of epoxy.	No color change
Solvent Evaporation	Considerable Evaporation	Little Evaporation	Significant Evaporation	No Evaporation

2.1.3 Membranes and Modules

Fourteen cross-flow hollow fiber membrane contactors in the form of picture frames containing the hollow fibers were received from Applied Membrane Technology, Inc. (AMT, Minnetonka, MN) per NJIT specifications. These specifications included: Nylon as the material of construction for the frame; denser coating on the fibers in the stripping module. Figure 2.1 shows the photographs of the bare membrane contactor on

the right, membrane contactor assembly with the facebox and the flow distribution plates (facebox and plates fabricated at NJIT). Table 2.2 provides the details of the modules. Membrane contactors were prepared using porous hydrophobic polypropylene (PP) hollow fibers of inside diameter (ID)/outside diameter (OD) of 240μm/290μm; these hollow fibers have a thin plasma polymerized hydrophobic porous fluorosilicone coating on the outer surface of the fiber. Two types of coatings were prepared, one set having a thinner coating for the absorption modules and one set of thicker coating for the stripping modules. These membrane contactor modules are typically suitable for feed gas flow rates between 50 -500 cm^3/min; each had a surface area of 500 cm^2 based on the hollow fiber ID.

Table 2.2 Characteristics of cross flow hollow fiber membrane module

Fiber ID (cm)	0.024
Fiber OD (cm)	0.029
Active fiber length (cm)	6.35
Fiber bed dimensions	2.5”x 1”x 3/4”
Porosity of hollow fiber (%)	40
Effective membrane surface area (cm^2)*	500
Number of fibers, n	1064
Bed volume (cm^3)	61.75
Membrane module volume (cm^3)	81.75
Interfacial area, (m^2/m^3)	2102.5
Membrane tortuosity (τ)	2.6
Average pore size (μm)	0.03

*based on fiber ID

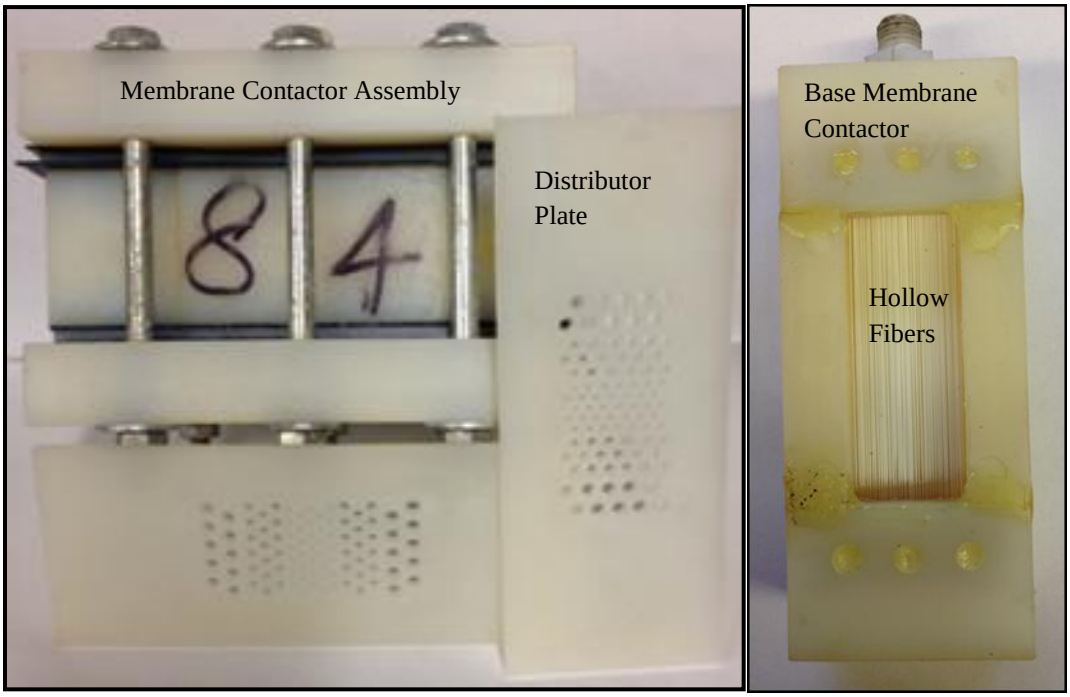

Figure 2.1 Rectangular assembly of cross flow hollow fiber membrane module contactor with face box and distribution plates.

2.2 Analytical Instruments

- Gas Chromatograph (GC) (Agilent, Santa Clara, CA; Model HP 5890 Series II) equipped with GC column. (Alltech, HAYESEP D 100/120).
- Solid-State IR-based CO_2 Analyzers (Model 906, Quantek Instruments, Grafton, MA)
- Humidity Probe Model HMP76 and a digital readout display unit Model MI70, (Vaisala Inc., Woburn, MA)
- Perkin Elmer Spectrum One – FTIR Spectrometer.

2.3 Viscosity Measurements

Canon-Fenske routine viscometer from Induchem Lab Glass Co. Viscometer of size 200 was used having a viscometer constant (c) 0.1. 20% dendrimer in ionic liquid was tested at four different temperatures. Times for the drop in liquid level from mark A to mark B was noted. The efflux time (second) was multiplied with the viscometer constant to get the kinematic viscosity for the particular temperature. [kinematic viscosity = t * c]. Density measurements were done with a 10 ml density bottle.

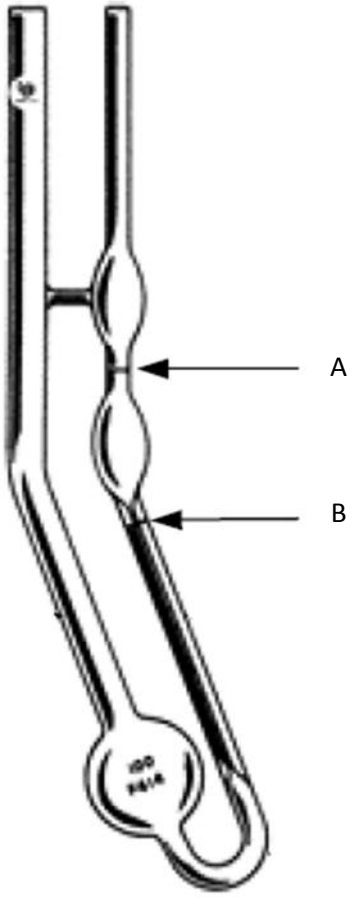

Figure 2.2 Canon-Fenske Viscometer.

Table 2.3 Viscosity Measurements

Temperature (°C)	Size	Viscometer Constant	Time (s)	Kinematic Viscosity (cst)	Density (gm/cc)	Dynamic Viscosity (cP)
Room temp	200	0.1	1153	115.3	1.08	106.75
50	200	0.1	382	38.2	1.07	40.87
55	200	0.1	342	34.2	1.065	36.42
60	200	0.1	270	27.0	1.065	28.75
65	200	0.1	240	24.0	1.060	25.44

2.4 Surface Tension Measurements

Interfacial Tensiometer (Model K8, KRUSS, Hamburg, Germany) was used for surface tension measurements. All surface tensions are reported in dynes/cm, were taken at 25 °C, 55 °C, 85 °C. Three readings were taken for each measurement. For the measurement procedure, the operational manual of the device was consulted.

Table 2.4 Surface tension values in dyne/cm for ionic liquid [BMIM] [DCA]

At 22-25°C	At 50-55°C	At 80-85°C
42.5	41.0	39.5
43.0	40.5	39.5
42.5	40.5	39.5
Avg : 42.6	40.6	39.5

Table 2.5 Surface tension values in dyne/cm for 20 wt % PAMAM in ionic liquid [BMIM] [DCA]

At 22-25°C	At 50-55°C	At 80-85°C
46.5	44.5	43.5
46.5	44.5	43.0
46.0	45.0	42.5
46.0	45.0	43.5
Avg : 46.25	44.75	43.0

2.5 CO_2-Amine Theory- Mechanism

a) *With primary amines:* CO_2 can readily react with primary amines via Zwitterion mechanism to give carbamic acid. This zwitterion is usually very unstable and reacts with base leading to the formation of carbamate [44].

$$CO_2 + 2RNH_2 \Leftrightarrow RNHCOO^- + RNH_3^+ \tag{2.1}$$

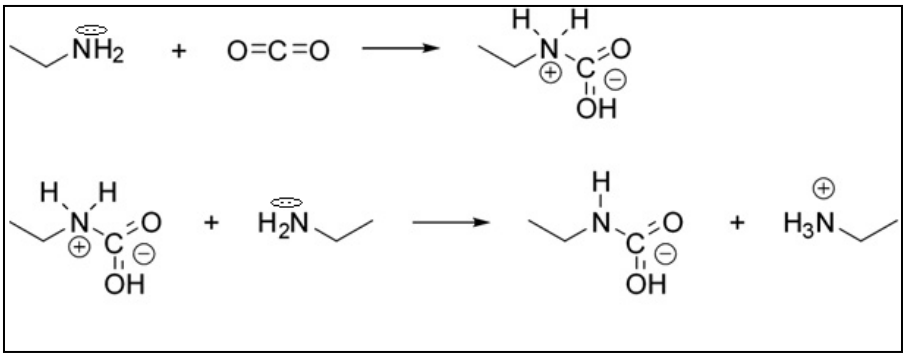

Figure 2.3 Carbamate formation by reaction of CO_2 with primary amines.

Mechanism: The two-step mechanism was first introduced by Caplow [45] and later re-introduced by Danckwerts [46, 47]. In the first step the lone pair of electrons of amine attacks the carbon of CO_2 making a zwitterion intermediate of carbamate. The free base then deprotonates the zwitterion leading to the formation of carbamate. One mole of CO_2 required 2 moles of primary amines. The maximum amine efficiency under dry condition in any primary amine solvent is 0.5 mol CO_2 per mole of primary amine [48]. In the present work, PAMAM dendrimer Gen 0 used has four primary amines, which means the 4 primary amines acting as base, increase the amine efficiency to 2 mol CO_2 per mol of primary amine.

b) With tertiary amines: CO_2 cannot directly react with tertiary amine. The opening of one double bond of carbon dioxide molecule to yield a zwitterionic species is strongly favored in the case of only primary and secondary amines. This is because the loss of one

proton from the nitrogen atom allows the formation of a partial N=C double bond, which cannot occur with tertiary amines. Hence the chance of formation of this zwitterion is very less in tertiary amines [49].

$$H_2O \Leftrightarrow H^+ + OH^- \tag{2.2}$$

$$CO_2 + R_1R_2R_3N + H_2O \rightarrow R_1R_2R_3NH^+ + HCO_3^- \tag{2.3}$$

$$HCO_3^- \Leftrightarrow CO_2 + OH$$

Mechanism: The reaction between CO_2 and tertiary amine takes place only in presence of water. Tertiary amines undergo base-catalyzed hydrolysis of CO_2 [44]. In the first step; tertiary amine dissociates water to form a quaternary cationic species and OH^- which in turn attacks CO_2 to form the bicarbonate anion. The last step is the ionic association of the protonated amine and bicarbonate [48, 50**].**

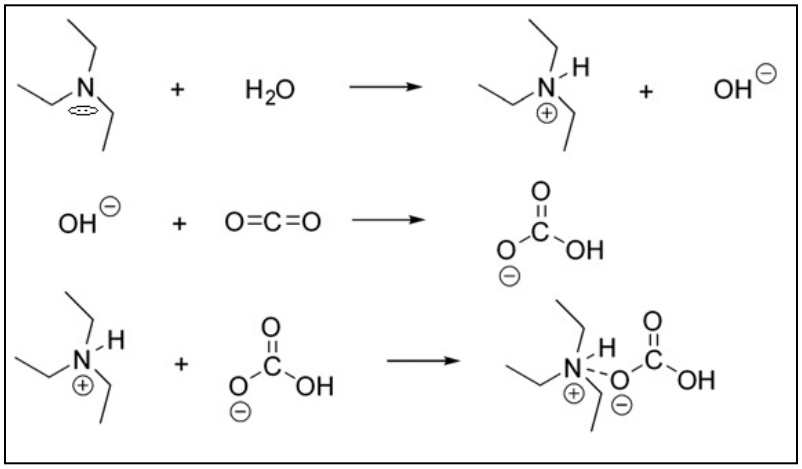

Figure 2.4 Mechanism for the reaction of CO_2 with tertiary amines. [48, 50]

2.5.1 Spectroscopic Evidence: Formation of Carbamate and Bicarbonate

Figure 2.5 shows the superimposed spectra of fresh samples of both [bmim][DCA] and 20% dendrimer in ionic liquid. These observed spectra were over same range of absorbance and wavelength (cm^{-1}). The peaks between 3200-2900 cm^{-1} denotes the –C-H- bond stretching, indicating the presence of imidazolium ion $[bmim]^{+}$. The peaks around 2200-2100 cm^{-1} indicate the presence of symmetric and asymmetric C≡N bond [51]. Figure 2.5 also shows that pure [bmim] [DCA] did not have any band at around 1655 cm^{-1} on the IR spectra, whereas 20wt% dendrimer Gen 0 in [bmim] [DCA] without any exposure to CO_2 had the band at 1655 cm^{-1}, indicating the presence of amines in the solution.

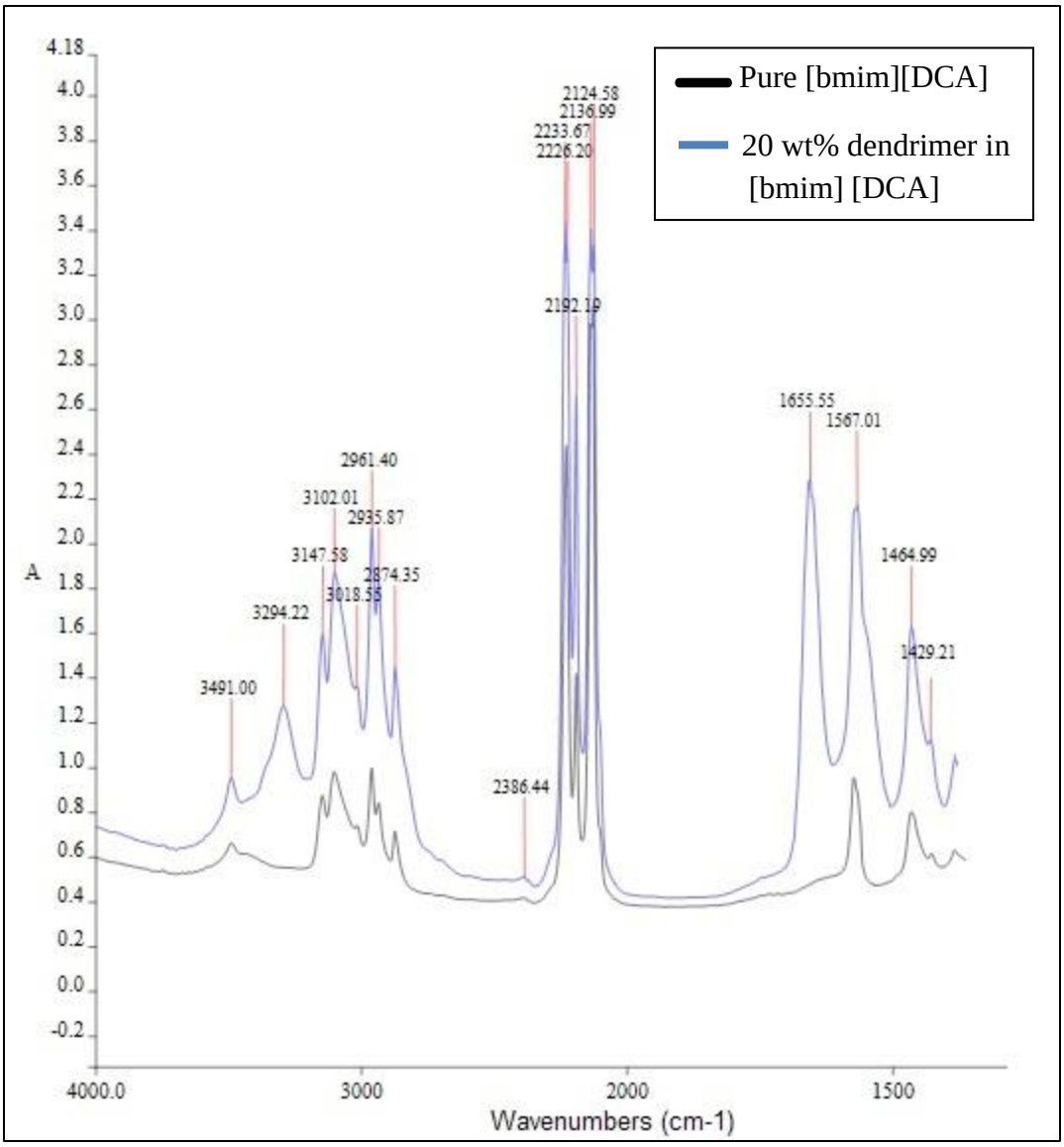

Figure 2.5 IR spectra of pure [bmim][DCA] and 20 wt% of dendrimer Gen 0 in [bmim][DCA] not exposed to CO_2.

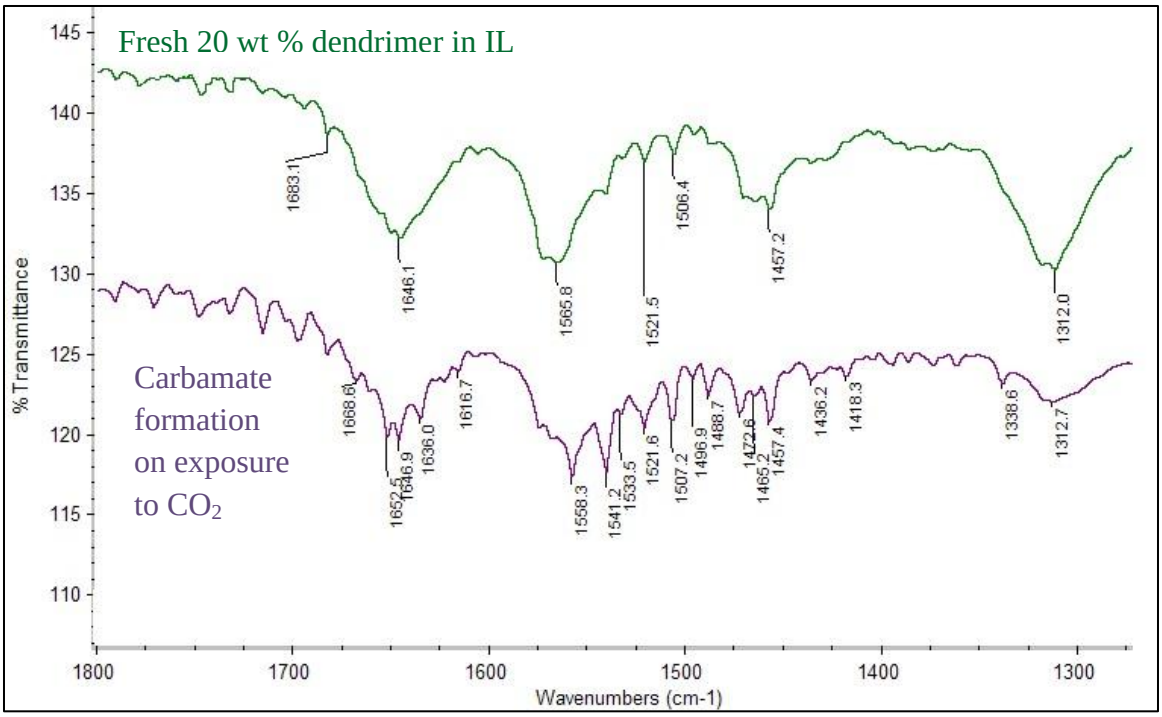

Figure 2.6 IR spectra of 20 wt% of dendrimer Gen 0 in [bmim][DCA] and formation of carbamate when exposed to CO_2.

Figure 2.6 shows the IR spectra of fresh 20 wt% dendrimer in [bmim] [DCA] and the spectra of 20 wt % dendrimer in [bmim][DCA] on exposure to CO_2. The bands 1646.1 cm^{-1} and 1565.8 cm^{-1} indicate the presence of amines in the solvent. One can clearly see the shifts in the wavelengths, on exposure to CO_2 indicating the formation of the reaction products. The bands 1616.7 cm^{-1} and 1558.3 cm^{-1} indicate the zwitterionic formation. The bands around 1500 cm^{-1} indicate the C=O asymmetric bend of the $NH_2CO_2^-$ group, indicating the formation of carbamate. The bands around 1400-1300 represent the asymmetric and symmetric bends of NH_3^+. Khanna et al. [52] have shown that bands 1628 cm^{-1}, 1543 cm^{-1}, 1448 cm^{-1}, 1400 cm^{-1}, 1300 cm^{-1}, etc. indicate the formation of ammonium carbamate, which are almost in coherence with the current obtained bands for carbamate formation.

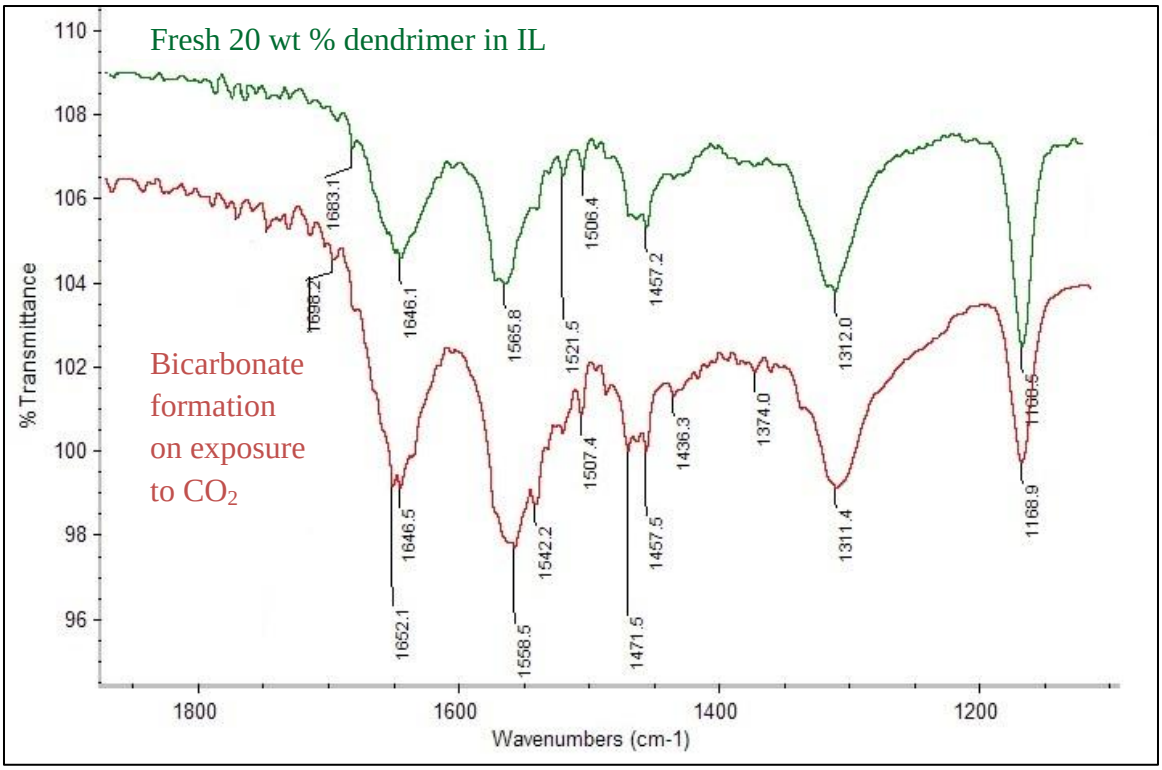

Figure 2.7 IR spectra of 20 wt% of dendrimer Gen 0 in [bmim] [DCA] and formation of bicarbonate upon addition of water (excess) and exposure to CO_2.

Figure 2.7 shows the IR spectra of fresh 20 wt% dendrimer in [bmim][DCA] and the spectra of 20 wt % dendrimer in [bmim][DCA] on addition of water (excess) and exposure to CO_2. The bands 1471.5 cm^{-1}, 1436.3 cm^{-1}, 1374.0 cm^{-1} indicate the formation of bicarbonate due to the reaction of CO_2 and dendrimer with addition of water. The bands reported by Khanna et al. [52] for the formation of ammonium bicarbonate: 1597 cm^{-1}, 1498 cm^{-1}, 1480 cm^{-1}, 1441 cm^{-1}, 1370 cm^{-1}, 1290 cm^{-1}, etc. are similar to the current obtained bands.

2.6 Experimental set up and procedure

A simulated flue gas mixture of composition 14.1% CO_2, 1.98% O_2 and balance N_2 (Welco-CGI Gas Technologies, Newark, NJ) was introduced from the gas cylinder into

the membrane absorption module. Feed gas flow rate was controlled by a Multi-channel Mass flow Controller Model 8248A and Mass flow Controller Transducer Model (MTRN-1002-SA, Matheson TRI-GAS, Montgomeryville, PA). Experiments were conducted generally with the following gas flow rates unless otherwise mentioned: 50 cm^3/min, 100 cm^3/min, 150 cm^3/min and 200 cm^3/min.

In experiments where humidity was needed in the feed gas, a porous hydrophobic PP hollow fiber membrane-based humidification module-based arrangement was made as shown in Figure 2.8a. A humidity probe placed between the outlet of the humidification module and the inlet of the absorption module allowed monitoring of the humidity. A stainless-steel liquid reservoir (Alloy Products Corp., Waukesha, WI. Model No. B501-0228-00-E Vessel 1 gal 304 s. steel) was used to push deionized water into the shell side of the humidification module, whose other end was closed with a plug. The humidity of the feed gas was checked with a Humidity Probe Model HMP76 and a digital readout display unit Model MI70, (Vaisala Inc., Woburn, MA). Initial calibration of the humidity probe was done in an instrument using salts LiCl and K_2SO_4 for the probe calibration. A water trap was placed between the humidification module and the humidity probe. Any leakage of water from the module was collected in the water trap. This was essential to prevent clogging of the humidity probe with water, which in turn would affect the relative humidity reading.

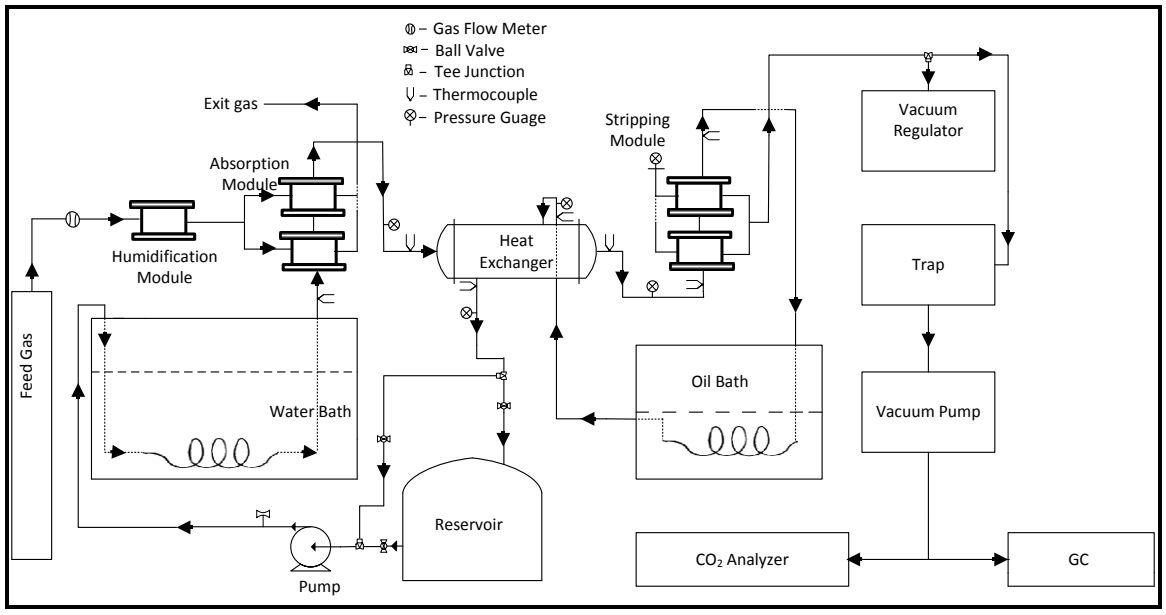

Figure 2.8a Schematic of the experimental setup for CO_2 absorption- stripping process.

For experiments involving no humidity, a bypass arrangement of the gas stream allowed direct flow of the simulated flue gas into the absorption modules. Carbon dioxide concentrations in the purified gas stream and the stripped gas stream were monitored using two solid-state IR-based CO_2 analyzers (Model 906, Quantek Instruments, Grafton, MA). In some cases, CO_2 concentrations in the treated feed outlet stream and the stripped gas stream were double checked for accuracy with a gas chromatograph (GC) (Agilent, Santa Clara, CA; Model HP 5890 Series II). The GC column (Alltech, HAYESEP D 100/120) was accordingly calibrated for CO_2 and N_2.

At the beginning of the experiment the absorbent liquid was initially circulated from a stainless steel liquid reservoir (Alloy Products Corp., Waukesha, WI. Model No. B501-0228-00-E Vessel 1 gallon 304 stainless steel) to fill up the system with the absorbent liquid. This liquid was pumped by a micropump (Pump Head Model GJ-N21-JF1S.J., Pump Motor Model DG-F61.G1T2P5.J.B., Micropump, Vancouver, WA) through a flow meter (1-GPI Model GM001S2C41-2 1/8" NPT S. steel oval gear meter,

Great Plains Industries, Wichita, KS) and passed either through the bore or the shell side of the hollow fibers in the membrane absorption module(s) via a coiled nylon tubular loop immersed in a water bath (Model HCTB-3020, 12 liter BATH-12, LID-12, Omega Engineering, Stamford, CT). Heat tracing was done, to ensure that the liquid flowing on the absorption side was at 50-55°C (unless otherwise mentioned) and the liquid on the stripping side was at 85-90°C in experiments conducted at elevated temperatures.

The CO_2-loaded absorbent liquid was next introduced to a heat exchanger (Model 00256-03, Exergy LLC, Garden City, NY; supplied by Burt Process Equipment, Hamden, CT) to raise its temperature to around 85-95°C. At the exit of the heat exchanger, the heated and CO_2-loaded absorbent was introduced to the shell side of the membrane stripper module(s). The absorbent liquid stripped of CO_2 and cooled a bit in the stripper was passed through a coiled nylon tubular loop immersed in an oil bath (Model HCTB-3030, 26 liter, BATH-26, LID-26, Omega Engineering, Stamford, CT) heated up to 95 - 110°C. During the experimental studies only one liquid pump was used (unlike that shown Figure 2.8b) since the pressure drop through the system was not high enough for the second pump (pump 2) to pump the stripped liquid into the heat exchanger. The heated and stripped liquid was ready again for absorption of CO_2 after it was cooled down in the heat exchanger. During regular and continuous operation, the stainless steel vessel based liquid reservoir was bypassed.

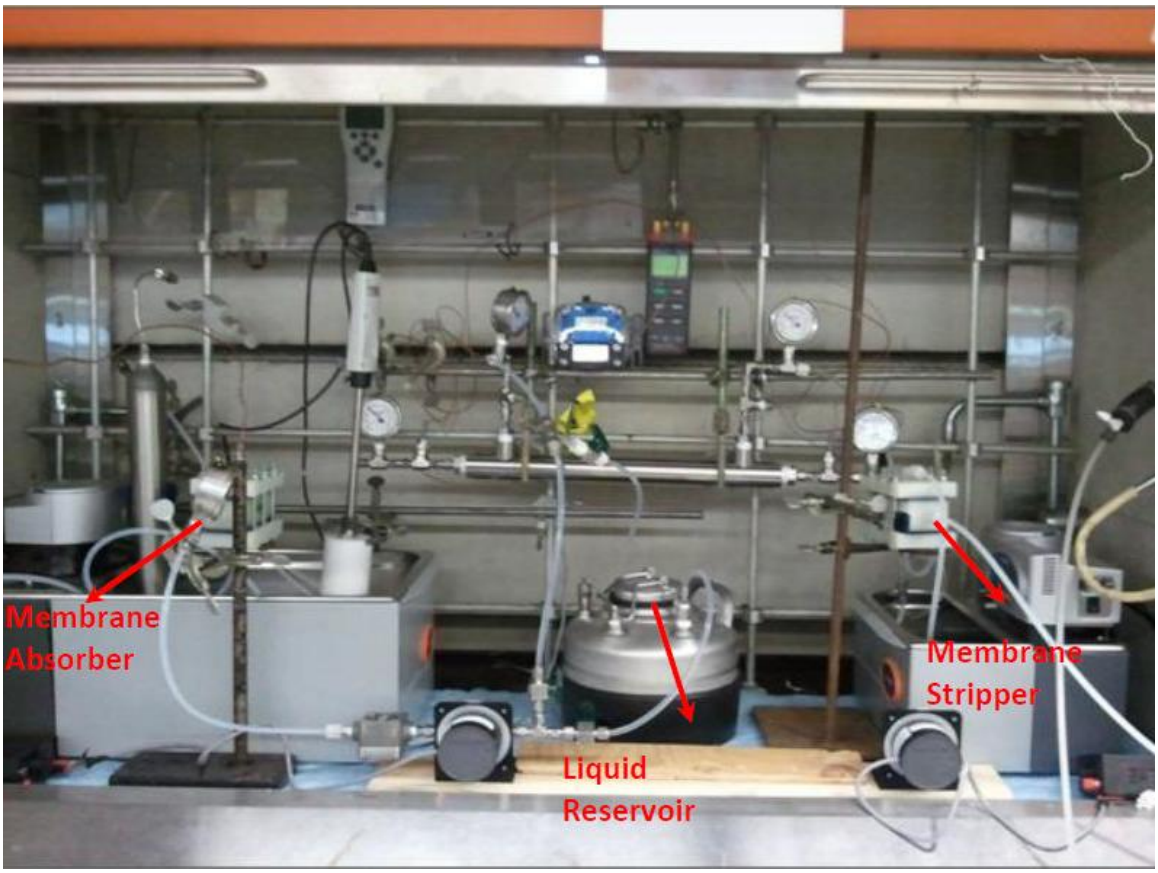

Figure 2.8b Photo of the experimental setup of the CO_2 absorption-stripping process with one absorption and one stripping membrane contactor.

On the stripping side, the tube side of the membrane modules was subjected to vacuum or helium or air as sweep gas, to remove and collect the stripped CO_2 from the CO_2-loaded absorbent. When both were used simultaneously, it is identified as the combo-mode of operation. In experiments where vacuum was used as the mode for stripping, one end of the bore of the fibers in the stripper module was closed using a plug. The stripped gas leaving the other end of the tube side of the membrane stripper was first introduced into a vacuum regulator (Model DVR-1000, PSV-2 Proportioning Valve, J-Kem Electronics, and St. Louis. MO) controlling the level of vacuum desired. The gas stream then was passed through a dry ice trap (Model Z154253-1EA Double Channel Vacuum Trap, Sigma-Aldrich, and St. Louis, MO) to prevent any condensable and/or

possible absorbent liquid leakage to enter the vacuum pump (Model N810.3 FTP, KNF Neuberger, and Trenton, NJ). The vacuum pump exhaust gas stream at atmospheric pressure was passed through a CO_2 analyzer to determine the CO_2 concentration in the stripped stream; alternately it was sent to a GC (HP 5890, Series II). The GC calibration plots for both high and low CO_2 concentrations can be seen in Figures 2.9a and 2.9b.

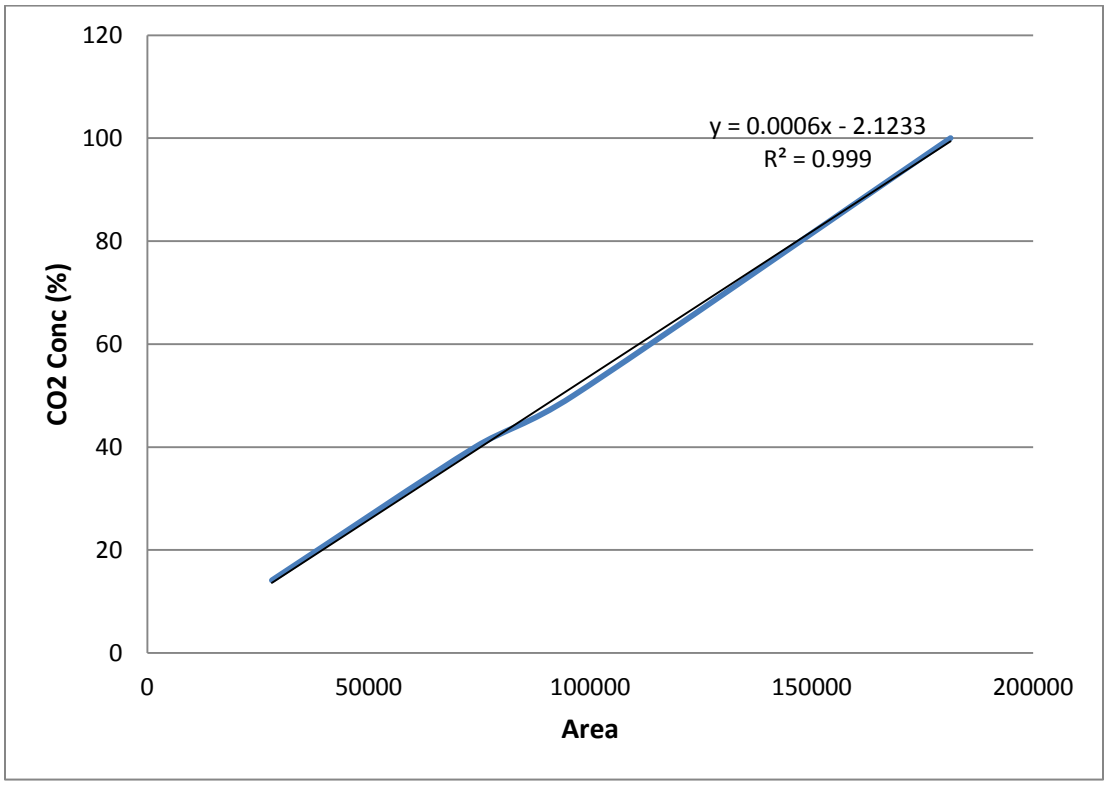

Figure 2.9a GC calibration plot for high CO_2 concentrations.

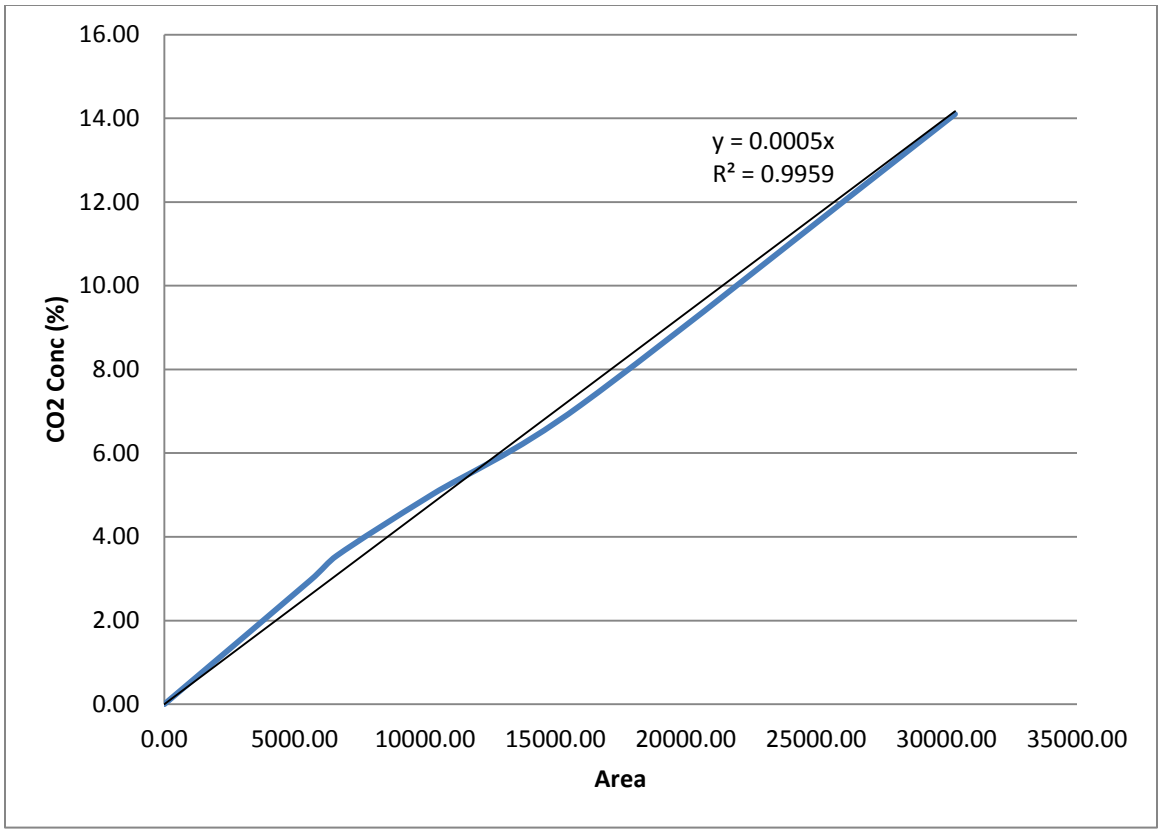

Figure 2.9b GC calibration plot for low CO_2 concentrations.

The temperatures of the absorbent liquid at the inlet and exit of the heat exchanger and the absorption and stripping module(s) were measured via thermocouples (Model EW-08516-74 Type K Pipe Plug Thermocouple Probes, ¼" NPT, 0.5"L; Cole Parmer, Vernon Hills, Il). The pressures of the absorbent liquid at all four locations were also measured by pressure guages (Swagelok, Wyoming & MI) to ensure that the pressure at the inlet of the absorber module was not too high. The excess liquid phase pressure over the gas phase pressure should preferably not exceed 10 – 20 psig (~103.5 kPa). A pressure gauge connected at one end of the stripping module was used as a check for the vacuum level.

All other miscellaneous parts needed for the experimental setup, e.g., valves, nuts, tubing, fitting, gaskets, etc., were obtained from either McMaster-Carr, Robbinsville, NJ or R.S. Crum & Co., Mountainside, NJ. A conceptual schematic of the absorbent flow around the fiber outside is shown in the Figure 2.10. The same configuration is also valid for the stripper. Figure 2.11 illustrates a rectangular box arrangement for large scale operation.

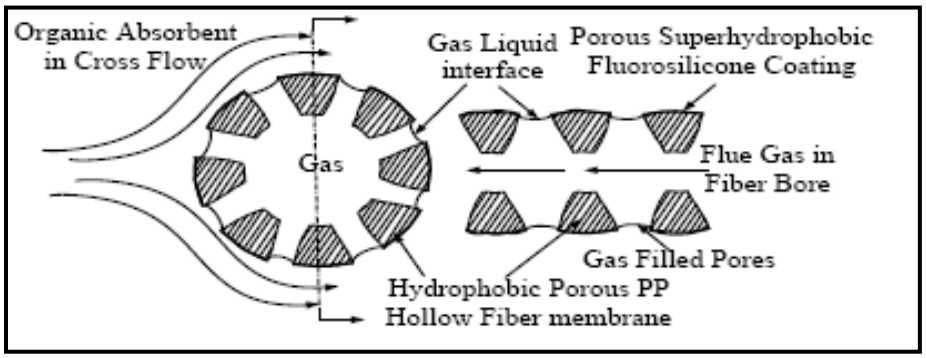

Figure 2.10 Novel super hydrophobic hollow fiber membrane in CO_2 scrubbing membrane contactor: Absorbent on shell side.

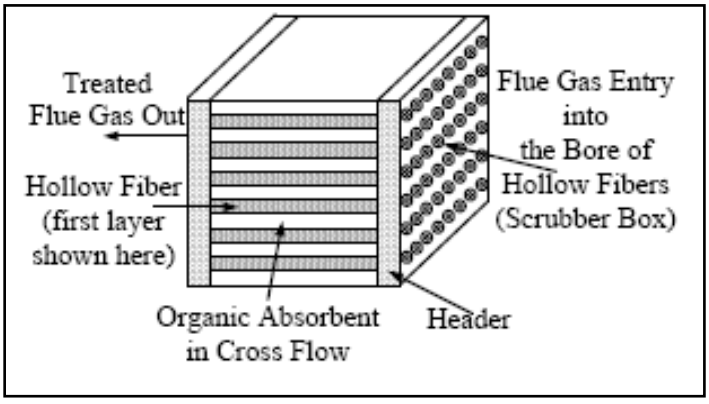

Figure 2.11 Hollow fiber membrane contactor for CO_2 scrubbing from post combustion cooled flue gas.

2.7 Results and Discussion

The experimental results reported here employ the following quantities: CO_2 concentration in the treated gas; percentage recovery of the absorbed CO_2 in the stripped gas; CO_2 concentration in the stripped gas; volumetric rate of CO_2 absorption; mass transfer coefficients for CO_2 absorption.

2.7.1 Water or Aqueous Dendrimer Solution as Absorbent

The first set of experiments was done with water as absorbent with one absorption module and one stripping module at room temperature (24 °C). The simulated flue gas was flowing on the shell side of the cross-flow module and water was passed through the fiber bores at a constant flow rate of 12.9 gal/h. For stripping, either vacuum or pure He or air sweep gas through the vacuum line was used. Only low feed gas-flow rates of 7.50 - 14.90 cm^3/min were used.

Depending on the stripping mode, the CO_2 concentration at the absorber outlet decreased from 14.1 vol% to around 3.5% - 4.0% at 7.3 cm^3/min feed gas flow rate (Figure 2.12). With sweep air as the stripping mode, the treated feed gas outlet concentration of CO_2 doubled to 6 ~ 6.5 vol % when the feed gas flow rate was doubled from 7.5 to 14.7 cm^3/min. For a feed gas flow rate of 14.9 cm^3/min, when a combo stripping mode was used using 60 mm Hg vacuum and 15 cm^3/min sweep He sweep gas, a value of 5.2 % was achieved as the CO_2 absorber outlet concentration. For other combo-mode runs the CO_2 level in the stripping stream was below the detection limit of the CO_2 analyzer of 0.01% due to rather high sweep gas flow rate (12-16 lit/min) that caused dilution. The results of Figure 2.12 show that the reduction in the feed CO_2

concentration generally depended on the stripping conditions; the quality of the stripped water affected gas absorption behavior.

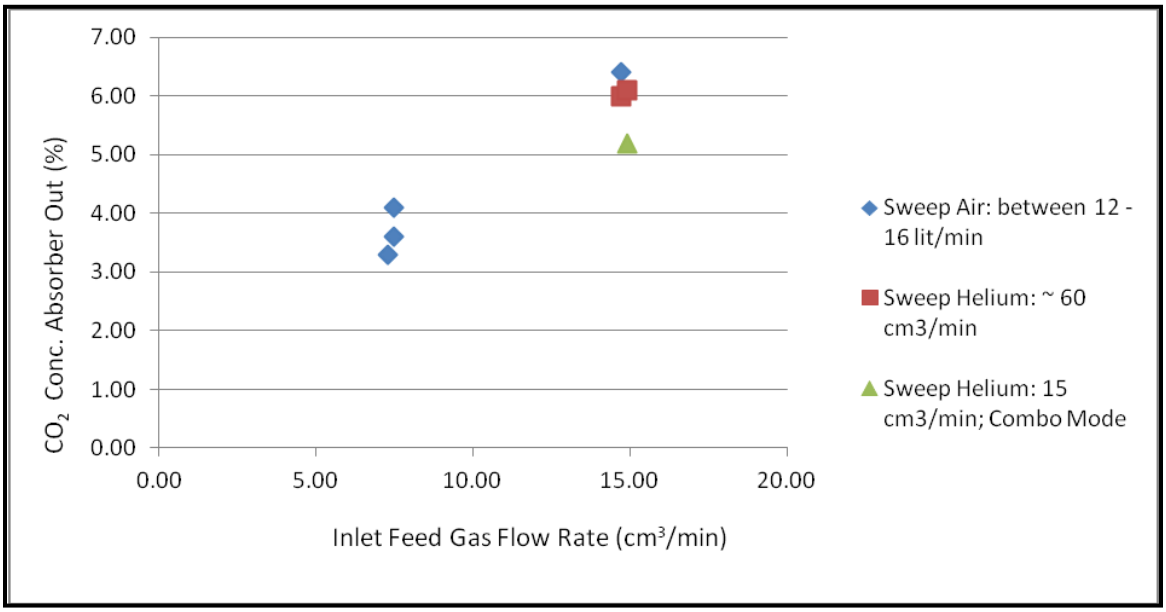

Figure 2.12 Dry feed gas and water as absorbent for various stripping conditions at 24°C.

Experimental results for a 16 wt% aqueous dendrimer solution as the absorbent at room temperature are presented in Figure 2.13 for a dry feed gas. For a liquid flow rate of 12 gal/h and a low vacuum of 30 mmHg, CO_2 concentration in the absorber outlet was 3.0% and in the stripped stream was 9.0%. For a similar feed gas flow rate and a sweep He gas flow rate of around 14 cm^3/min, a reduced liquid flow rate of 0.9 gal/hr yielded a purified CO_2 composition of 2.0%. Another experiment with a much higher feed gas flow rate of 102 cm^3/min and He sweep gas flow rate of 125 cm^3/min resulted in a CO_2 concentration in the feed gas outlet stream of 11.8% and a stripper outlet stream of 3.6%. CO_2 is chemically absorbed into the 16 wt% dendrimer solution when compared to its absorption into water. The tertiary amines get activated in humid conditions and react

with CO_2, leading to more absorption of CO_2. Therefore, in spite of high stripping gas flow rates, dilution of the purified CO_2 on the stripping side was not as high as compared to that with water as absorbent.

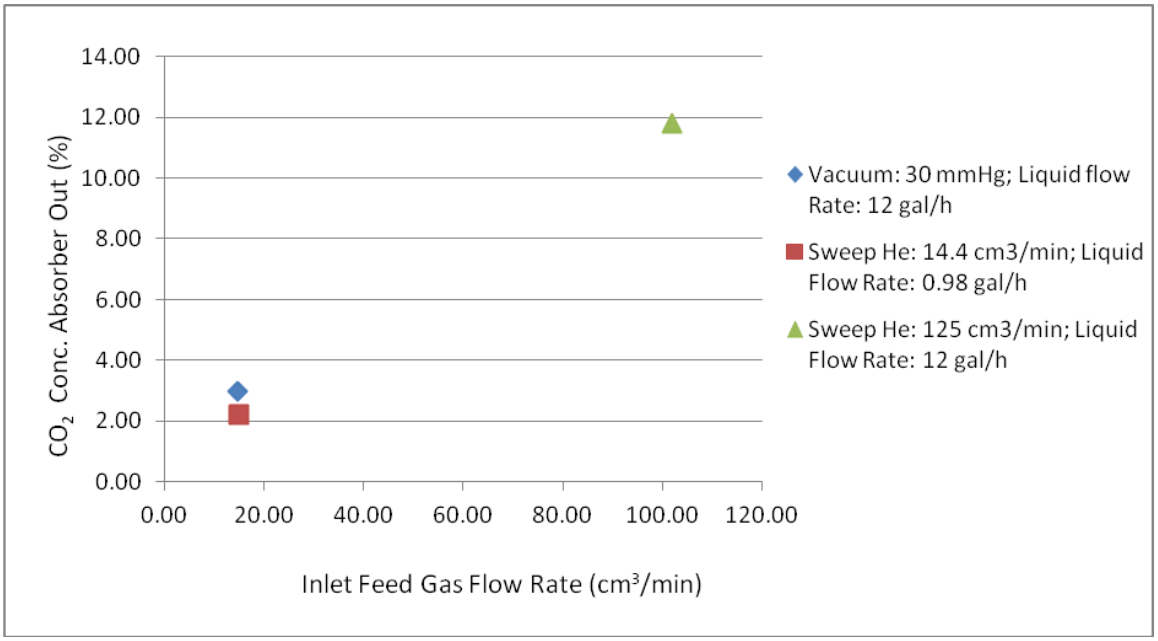

Figure 2.13 Dry feed gas and 16 wt% aqueous dendrimer solution as absorbent for various stripping conditions at 24 °C.

2.7.2 Absorbent [bmim] [DCA] and Different Stripping Methods

Results for the pure IL, [bmim] [DCA], as the absorbent at room temperature using either He as a sweep gas or the combo mode stripping method are provided in Figure 2.14. One absorption and one stripping module were used in the absorption and stripping sections. The IL was passed through the tube side of the module with flue gas on the shell side. The first two experiments were performed at low liquid flow rates 0.36 and 0.24 gal/h using He sweep gas flow rates of 31.1 and 62.9 cm^3/min respectively, yielding 9.32 % and 12.5% CO_2 concentration in the purified gas stream. Although the sweep gas flow rate was doubled, the feed gas outlet concentration increased since the feed gas flow rate

was increased from 3.54 to 9.6 cm^3/min. The CO_2 recovery in the stripped gas from the amount of CO_2 absorbed was 75.3 % and 62.2% respectively indicating insufficient regeneration of the absorbent. Here, CO_2 recovery is defined as the ratio of the volumetric rate of the stripped CO_2 to the volumetric rate of absorption of CO_2. Carbon dioxide concentration in the stripped stream was only 0.5 and 0.24% due to high dilution.

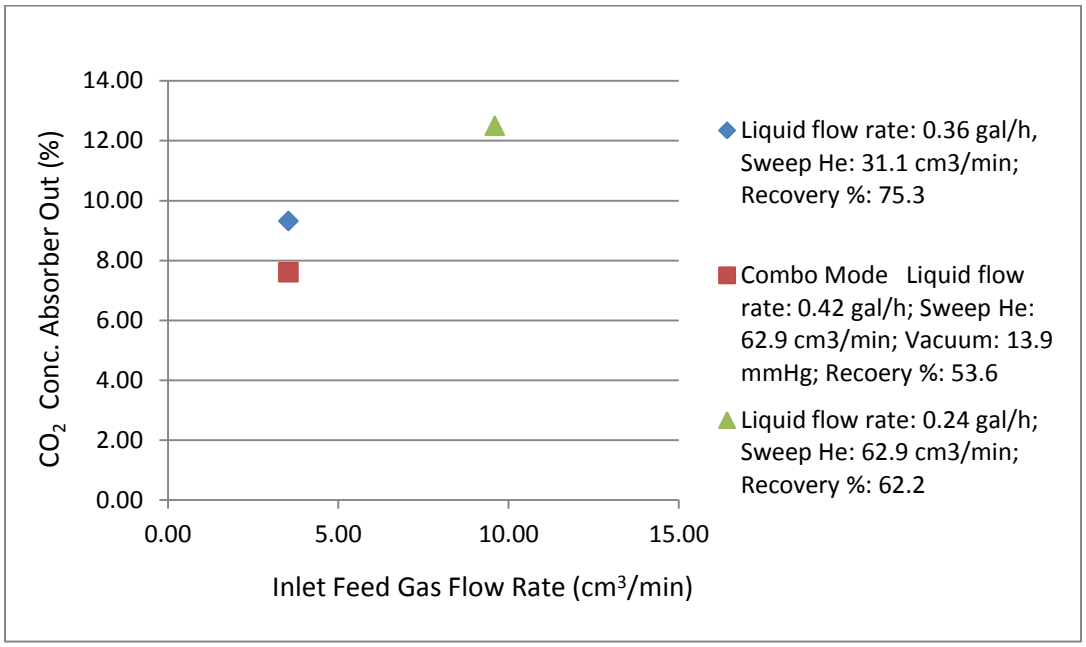

Figure 2.14 Dry feed gas and [bmim][DCA] as absorbent for various stripping conditions at 24 °C.

For the combo mode (sweep helium and vacuum) at the same feed gas flow rate of 3.54 cm^3/min, a sweep helium gas flow rate of 62.9 cm^3/min and a vacuum of 13.9 mmHg, the CO_2 product outlet concentration was 7.61% while percent recovery from the absorbed amount was 53.6%. Comparing the first three results using pure ionic liquid at room temperature, the highest rate of absorption and stripping CO_2 was achieved when the combo mode was used. IL based runs at room temperature were done to develop a perspective and provide a better foundation for the following experiments.

As the percent CO_2 recovery was not very high, additional absorption and stripping modules were added. A plot of the treated gas outlet concentration and the feed gas flow rate is shown in Figure 2.15. Two absorption and two stripping modules were used in the parallel mode of operation (see Figure 2.8) with the ionic liquid in cross-flow through the shell side of the modules. The operating temperatures were also increased to improve regeneration of the solvent. In these experiments the absorbent flow rate was 4.16 gal/h; the sweep He flow rate was 23.24 cm^3/min. The pressure drop along the length of the module was 3-5 psig (27.5 kPa) for the absorption modules operating at 50-52 °C and the stripping modules at 79-82 °C.

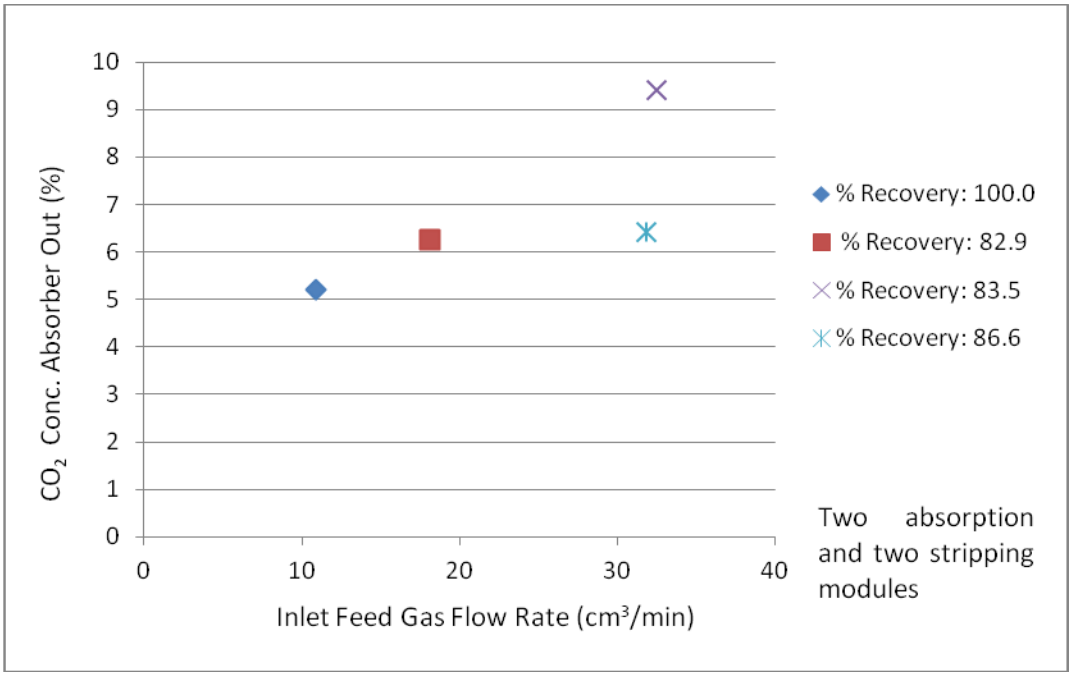

Figure 2.15 Dry feed gas and [bmim] [DCA] absorbent at 4.16 gal/h**;** absorption temp: 50- 52 °C; stripping temp: 79 - 82 °C; Stripping mode: Sweep He at 23.24 cm^3/min.

As the feed gas flow rate was varied between 10.9, 18.1, 29.6 and 32.5 cm^3/min (Figure 2.15), the feed gas outlet composition increased to 5.2, 6.2, 7.0, and 9.4%

respectively; the corresponding CO_2 removal rates increased from 1.02 cm^3/min to 1.74 cm^3/min. The highest feed gas flow rate data point was repeated to check the reproducibility, e.g, gas flow rate around 32 cm^3/min, liquid flow rate 4.16 gal/h, sweep He flow rate 23.24 cm^3/min yielded product concentration of around 9%, CO_2 concentration in the sweep stream was around 6% and CO_2 recovery in the stripped gas between 83 and 86%. The results presented above provide an idea of the effects of changing the liquid flow rate, the feed gas flow rate and the CO_2 partial pressure in the feed. High absorbent flow rates were achieved when the absorbent was passed through the shell side of the modules. Therefore, due to the higher amount of fresh solvent and higher liquid mass transfer coefficient, CO_2 absorption rate and the absorption capacity increased. By reducing the feed gas flow rate, the extent of CO_2 removal was increased which is directly related to the amount of available CO_2 in the feed gas stream.

2.7.3. Ionic Liquid - 20 wt% PAMAM system

To increase the CO_2 absorption capacity, 20 wt% dendrimer solutions in IL [bmim] [DCA] was used. All experiments with dendrimer solution were performed at an elevated temperature to account for increased solution viscosity. The absorbent was passed through the shell side of the absorption modules (flow across the hollow fiber membrane) to avoid high pressure drop, possible fiber damage and pore/fiber wetting. Two absorption and stripping modules were used in both absorption and stripping sections. PAMAM Gen 0 dendrimer in ionic liquid solvent was used as the absorbent. An absorbent flow rate range of 2.57 gal/h - 4.16 gal/h and a feed gas flow rate range of 50 cm^3/ min – 200 cm^3/ min were employed.

2.7.3a Mode of stripping: Sweep He

The first set of experiments was done at a feed gas flow rate of around 50 cm^3/min and absorbent flow rate at 2.57 gal/h. Table 2.6 shows the results of these experiments. For the gas flow rate of 54.08 cm^3/min and the sweep gas flow rate of 47.84 cm^3/min, CO_2 recovery was about 54.3%. Increased feed gas flow rate of 54.08 cm^3/min and a sweep He gas flow rate of 78.87 cm^3/min resulted in a marginal increase in per cent CO_2 recovery of the amount of CO_2 absorbed to 55.17% (Table 2.6). The volumetric rate of absorption of CO_2 into the absorbent got reduced from 5.6 cm^3/min to 4.97 cm^3/min.

Reduction in the sweep helium gas flow rate reduces the driving force for stripping CO_2 from the loaded absorbent; this is the basis for the observed reduction in the recovery of CO_2 in the stripped stream. Another reason that can be attributed to the lower recovery is the temperature; during these runs the temperature difference along the length of two modules on the stripping side was about 12 – 15 °C. In all runs with pure [bmim] [DCA], the difference in temperature across the modules was ≤ 5° C with 4.16 gal/h as the absorbent flow rate.

Table 2.6 CO_2 absorption/stripping results of 20 wt% Dendrimer in IL with Sweep He stripping mode for liquid flow rate 2.57 gal/h with an inlet CO_2 Conc being 14.1 %*

Feed gas flow rate cm^3/min	Conc. CO_2 absorber out (%)	Sweep He flow cm^3/min	Conc.CO_2 stripper out (%)	Rate of CO_2 absorption cm^3/min	Rate of CO_2 removal cm^3/min	CO_2 Recovery (%)
54.08	5.4	47.8	5.6	4.9	2.70	54.3
54.08	4.5	78.8	3.4	5.6	3.09	55.1

*Temperature of dry feed gas at 25 °C.

2.7.3b Mode of stripping: Vacuum

When a similar experiment was repeated for the same feed gas flow rate of 54.08 cm^3/min and a constant absorbent flow rate at 4.16 gal/h, much higher recovery values were obtained using vacuum compared to the sweep He stripping mode (Figure 2.11). The vacuum level was maintained at 29 inch Hg. The absorbent temperatures at the inlet of two absorber modules was 50-55°C and at the inlet/outlet of two stripping modules were 85-90°C. For the selected feed gas flow rate, the treated feed gas outlet CO_2 concentration was 5.29% with a volumetric rate of CO_2 absorption of 5 cm^3/min. Vacuum pump outlet flow rate was 6.08 cm^3/min yielding 82% CO_2 concentration in the stripped stream when analyzed by the GC and 85.4% when analyzed by the Quantek CO_2 analyzer. This clearly shows that, although the rate of CO_2 absorption into the solvent is similar, the rate of desorption/ recovery was less in the case of sweep He stripping mode.

Similar experiments were carried out for feed gas flow rates of 52 cm^3/min, 106 cm^3/min, 145 cm^3/min and 210 cm^3/min (Figure 2.16). The CO_2 concentrations in the treated outlet gas stream were 6.5%, 7.75%, 9.9% and 11.5 vol % of CO_2 respectively, with CO_2 concentrations in the stripped gas ranging between 82-92 vol % (Figure 2.16). For these experiments, Figure 2.17 shows an increase in volumetric CO_2 absorption rate with an increase in the feed gas flow rate. The volumetric rate of absorption of CO_2 absorbed into the solvent increased from 4.3 cm^3/min to 7.5 cm^3/min with an increase in the feed gas flow rate from 52 to 210 cm^3/min. Figure 2.17 also shows that the percent recovery increased as the feed gas flow rate was increased. High percent recovery ≈ 99% of the absorbed CO_2 was achieved while using 20 wt% dendrimer solution in IL, [bmim] [DCA]. Since the volumetric rate of CO_2 absorption increased with an increase in the feed gas

flow rate, under the same stripping conditions the percent of CO_2 recovered also increased.

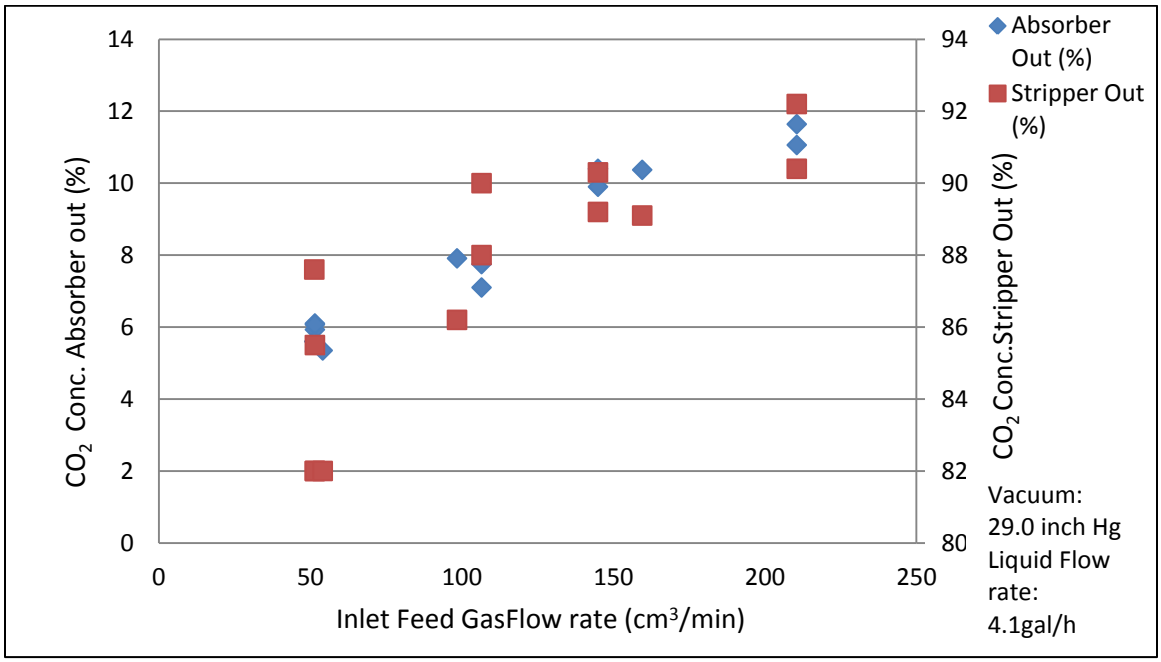

Figure 2.16 Variation in CO_2 concentration under different dry feed gas flow rates and 20 wt% dendrimer in [bmim][DCA] solution as absorbent; absorption temp : 50-55 °C ; Stripping temp : 85-90 °C; absorbent flow : 4.16 gal/h; vacuum on the sweep side, 29 inch Hg.

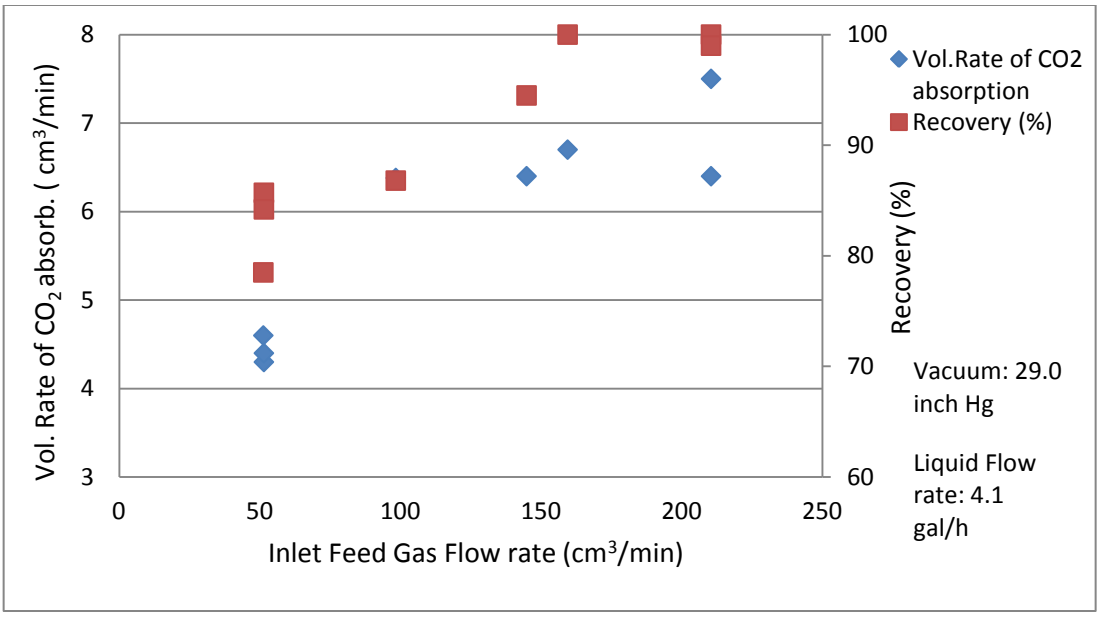

Figure 2.17 Rate of CO_2 absorption (cm^3/min) and % Recovery under dry feed condition with vacuum stripping using 20wt% dendrimer in [bmim][DCA] as absorbent; 50-55 °C ; Strip temp : 85-90 °C.

There are two explanations for this increase in the amount of CO_2 absorbed. First, increased gas flow rate decreases the residence time which will increase the CO_2 concentration in the gas phase leading to a higher rate of reactive absorption. Secondly, the gas phase mass transfer coefficient of CO_2 is increased and for a fast reaction higher CO_2 flux is expected. Figure 2.18 shows that the gas phase - based overall mass-transfer coefficient (defined in the next chapter) increased with an increase in the feed gas flow rate.

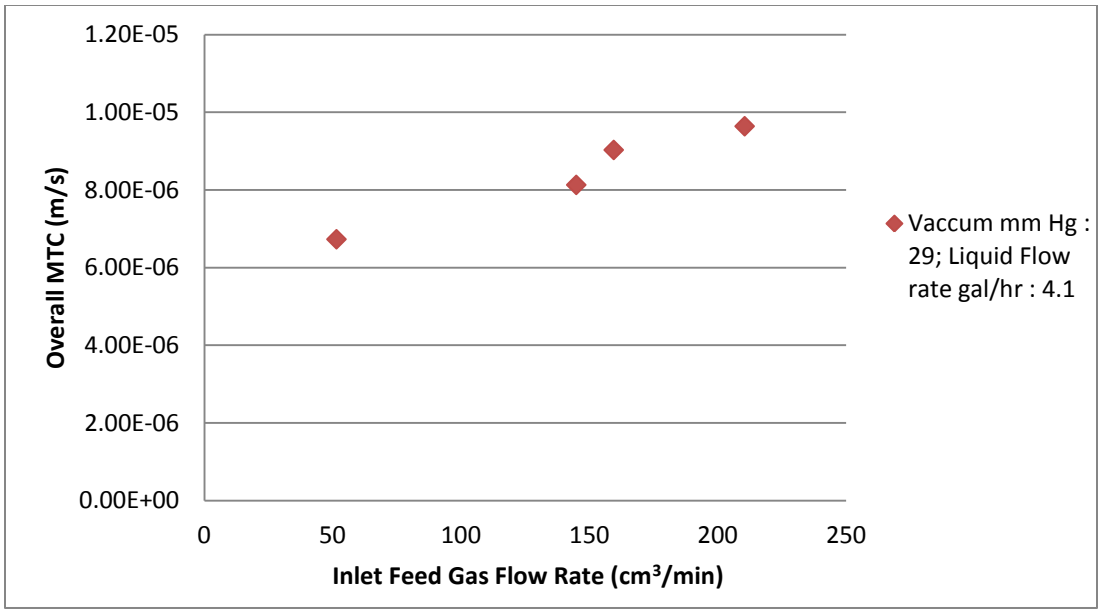

Figure 2.18 Overall MTC for a dry feed gas with 20 wt% dendrimer in [bmim][DCA] solution as absorbent; absorption temp : 50-55 °C ; Strip temp : 85-90 °C.

2.7.4 Performance with Humidified Feed Gas

A high value of ~ 155 cm^3/min humidified feed gas flow rate was used for a 20 % PAMAM Gen 0 in [bmim] [DCA] flow rate of 4.16 gal/h. Three consecutive experiments were performed for stability testing and reproducibility of the results (Figure 2.19). All three experiments yielded CO_2 feed gas outlet composition between 7.2 and 7.7%, and CO_2 stripper out concentration in the range 89-92 vol % shown in Table 2.7. A comparison of the overall mass transfer coefficient (defined in the next section) for the dry and humidified feed gas mixture at a feed flow rate of ~150 cm^3/min, is shown in Chapter 3. Amongst all moist gas experiments, the highest rate of absorption of CO_2 was about 11.44 cm^3/min.

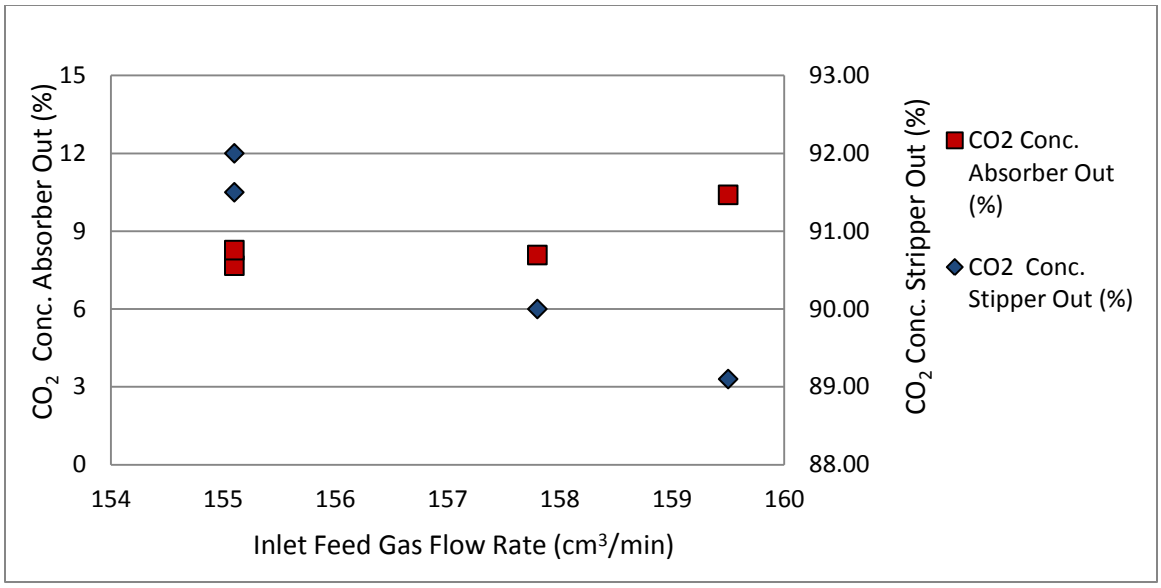

Figure 2.19 Humidified feed gas using 20 wt% dendrimer in IL; Absorption temp: 50-55 °C; Strip temp: 85-90 °C; absorbent flow: 4.16 gal/h.

Table 2.7 CO_2 absorption/stripping results of 20 wt% dendrimer in IL for humidified feed gas with an absorbent flow of 4.16 gal/h

Feed gas flow rate, Q_g (cm^3/min)	Conc. CO_2 in (%)	Conc.CO_2 absorber out (%)	Conc.CO_2 stripper out (%)	Rate of CO_2 absorption (cm^3/min)
144.9 (dry)	14.1	9.9	89.2	7.0
159.5 (dry)	14.1	10.37	89.1	6.7
157.8 (moisture)	14.1	7.2	92.0	11.44

CHAPTER 3

MASS TRANSFER IN MEMBRANE CONTACTORS

3.1 Overall mass transfer coefficient for the absorbent modules

The flux of CO_2 through the membrane depends on a number of factors including the liquid film mass transfer coefficient, gas film mass transfer coefficient, porosity of the hollow fiber membrane, absorption temperature and chemical kinetics in the case of a reactive solvent. Based on the inlet and outlet gas concentrations of CO_2, inlet gas flow rate (Q_g) and the membrane area (A), the molar CO_2 flux (N_{co_2}) can be calculated from

$$N_{co_2} = \frac{Q_g (C_{co_{2,g,in}} - C_{co_{2,g,out}})}{A} \tag{3.1}$$

The overall gas phase based mass-transfer coefficient (MTC), K_g , for the experimentally obtained molar CO_2 concentrations at a total pressure P_t can be obtained from

$$N_{co_2} = K_g \frac{\Delta y_{lm} P_t}{RT} \tag{3.2}$$

where, the logarithmic mean gas phase CO_2 mole fraction Δy_{lm} is defined by

$$\Delta y_{lm} = \frac{(y_{co_{2,g,in}} - y^*_{in}) - (y_{co_{2,g,out}} - y^*_{out})}{ln(\frac{(y_{co_{2,g,in}} - y^*_{in})}{(y_{co_{2,g,out}} - y^*_{out})})} \tag{3.3}$$

where y^*_{out} and y^*_{in} indicate the hypothetical gas phase mole fractions in equilibrium with the liquid phase at the two ends of the module and $y_{co_{2,g,in}}$ and $y_{co_{2,g,out}}$ indicate the CO_2 mole-fractions of the inlet and outlet gas respectively.

Along with physical absorption in the ionic liquid, acid gas CO_2 is chemically absorbed into the dendrimer solution via a reversible chemical reaction between CO_2 and amines. Since CO_2 reaction with amines is a fast pseudo first order reaction, it is known that mass transfer in the case of a fast reaction does not depend on the liquid film thickness; furthur the effect of y_{in}^{*} and y_{out}^{*} at the gas- liquid interface is almost negligible. However, the gas film thickness is likely to affect the CO_2 flux. An estimate of the overall gas-phase-based mass transfer coefficient has been made based on the inlet and outlet mole fractions of CO_2 obtained experimentally. Table 3.1 includes these values and shows the effect of moisture on the mass-transfer of CO_2 at the gas-liquid interface. Sample calculations are shown in Appendix B.

Table 3.1 Gas phase based overall mass transfer coefficient for absorbent flow rate of 4.16 gal/h*

Feed gas flow rate, Q_g (cm^3/min)	Conc. CO_2 in (%)	Conc.CO_2 absorber out (%)	Conc.CO_2 stripper out (%)	Vacuum stripping (inch Hg)	Rate of CO_2 absorption (cm^3/min)	Overall MTC** (m/s)
144.9 (dry)	14.1	9.9	89.2	28.8	7.0	9.2×10^{-6}
159.5 (dry)	14.1	10.37	89.1	29.0	6.7	9.0×10^{-6}
157.8 (moisture)	14.1	7.2	92.0	28.9	11.44	1.67×10^{-5}

* Absorption temp: 50-55 °C; Stripping temp: 85-90 °C
** Mass Transfer Coefficient

It can be seen from Table 3.1 that for humidified feed gas, the outlet gas concentration of the purified CO_2 was reduced from 10.37 vol % to 7.2 % compared to that for the dry feed gas. The volume rate of CO_2 absorption in these runs increased from 7 cm^3/min to 11.44 cm^3/min. The value of K_g for the wet gas and 20 wt% dendrimer solution in the ionic liquid is 1.67 $x10^{-5}$ m/s; the corresponding value for the dry gas is

9.0 x 10^{-6} m/s. For a comparison Albo et al. [53] obtained a value of 7.5x10^{-7} m/s using a pure ionic liquid [emim] [$EtSO_4$] at room temperature in a membrane contactor. It is clear that the mass transfer coefficient obtained here is more than an order of magnitude higher than this value. The only valid explanation for it is that we have primary and tertiary amines, furthur the tertiary amines are active with the wet gas leading to doubling of the CO_2 absorption rate since the tertiary amine groups in dendrimer Gen 0 have as much CO_2 absorption capacity as the primary amines.

3.2 Considerations of Individual Mass Transfer Coefficients

When the absorbent is passed on the shell side of the membrane contactor with the gas on the tube side, gas diffuses through the pores of the hollow fiber membranes into the liquid. The gas absorption occurs at the gas-liquid interface. The highly porous superhydrophobic flourosilicone coating on the porous polypropylene fibers enables a non-wetted mode of operation. Also, the absorbent pressure should be higher than that of the gas pressure to prevent dispersion of gas as bubbles into the absorbent [13]. The concentration profile in a gas filled pore has already been shown in Figure 1.5.

At the gas-liquid interface, for a species i, the p_{ii} of the gas side and c_{ii} of the liquid side are at equilibrium and are related by Henry's law constant, *H*,

$$c_{ii} = H \times p_{ii} \tag{3.4}$$

Species i, diffuses through the gas film, gas-filled membrane pore and liquid film in series. The steady state flux expressions for species i the three regions are given by

Gas - Side

$$N_i = k_{ig} (p_{igb} - p_{imi}) \quad (3.5)$$

Membrane - Side

$$N_i = k_{im} (p_{imi} - p_{ii}) \quad (3.6)$$

Liquid - Side

$$N_i = k_{il} (c_{ii} - c_{ilb}) \quad (3.7)$$

Therefore,

$$N_i = k_{ig} (p_{igb} - p_{imi}) = k_{im} (p_{imi} - p_{ii}) = k_{il} (c_{ii} - c_{ilb}) \quad (3.8)$$

where,

k_{ig} = local gas film mass transfer coefficient

k_{im} = local membrane mass transfer coefficient

k_{il} = local liquid film mass transfer coefficient.

Based on the definition of an overall mass transfer coefficient

$$N_i = K_g (p_{igb} - p_i^*) = K_l (c_i^* - c_{ilb}) \quad (3.9)$$

where, $$c_{ilb} = H_i p_i^* \quad (3.10)$$

$$c_i^* = H_i p_{igb} \quad (3.11)$$

From Figure 1.5, we know that

$$p_{igb} - p_i^* = (p_{igb} - p_{imi}) + (p_{imi} - p_{ii}) + (p_{ii} - p_i^*) \quad (3.12)$$

$$N_i/K_g = N_i/k_{ig} + N_i/k_{im} + N_i/H_i k_{il} \quad (3.13)$$

Therefore,

Overall gas film-based resistance: $$\frac{1}{K_g} = \frac{1}{k_{ig}} + \frac{1}{k_{im}} + \frac{1}{H_i k_{il}} \quad (3.14)$$

Also, by substituting equations (3.11), (3.10) in equation (3.12) we get,

$$c_i^*/H_i - c_{ilb}/H_i = (p_{igb} - p_{imi}) + (p_{imi} - p_{ii}) + (p_{ii} - p_i^*) \quad (3.15)$$

$$(c_i^* - c_{ilb})/H_i = (p_{igb} - p_{imi}) + (p_{imi} - p_{ii}) + (p_{ii} - p_i^*) \quad (3.16)$$

$$N_i/H_i K_l = N_i/k_{ig} + N_i/k_{im} + N_i/H_i k_{il} \quad (3.17)$$

Overall liquid film-based resistance: $$\frac{1}{K_l} = \frac{H_i}{k_{ig}} + \frac{H_i}{k_{im}} + \frac{1}{k_{il}} \quad (3.18)$$

Relation between K_g and K_l

Multiplying equation (3.14) by H_i

$$H_i/K_g = H_i/k_{ig} + H_i/k_{im} + 1/k_{il} \quad (3.19)$$

$$K_l = K_g / H_i \quad (3.20)$$

3.2.1 Determination of Individual Mass Transfer Coefficients

3.2.1a Membrane Mass Transfer Coefficient

Membrane resistance depends on porosity, pore size, tortuosity, membrane thickness and effective membrane diffusion coefficient. The effective membrane diffusion coefficient is governed by the type of flow regime of the gas in the membrane pore. It depends on both molecular diffusion and Knudsen diffusion transport regime [54]. Table 2.2 shows the characteristics of the hollow fiber membrane used in the current study.

The membrane mass transfer coefficient is given by

$$k_m = \frac{D_{g,e}.\ \varepsilon}{\delta\ \tau} \tag{3.21}$$

where, $D_{g,e}$ = effective membrane diffusion coefficient

ε = membrane porosity

δ = membrane thickness

τ = membrane tortuosity (τ =2.6)

The effective membrane diffusion coefficient is given by

$$D_{g,e}^{-1} = D_{g,b}^{-1} + D_k^{-1} \tag{3.22}$$

where $D_{g,b}$ = bulk diffusion coefficient; D_k = Knudsen diffusion coefficient.

The ratio of the membrane pore radius (r_p) to the mean free path (λ) determines the nature of the gas flow regime in the membrane fiber; if $r_p/\lambda < 1$, Knudsen diffusion dominates.

To determine the nature of the gas flow regime (Calculation shown in Appendix B)

$$\text{Mean free path } (\lambda) = \frac{RT}{(1.414.d^2.N_A.P.\pi)} \tag{3.23}$$

$$= 8.39 \times 10^{-8} \text{ m}$$

We know, if $r_p/\lambda < 1$, Knudsen flow dominates

$r_p / \lambda = 1.5 \times 10^{-8}$ m / 8.39×10^{-8} m = 0.178 < 1 → therefore Knudsen diffusion dominates.

Therefore the effective membrane diffusion coefficient becomes

$$D_{g,e} = D_k \tag{3.24}$$

The Knudsen diffusion coefficient is calculated by using equation

$$D_k = K_o (8RT/\pi M)^{0.5} \quad (3.25)$$

where, $$K_o = 2r_p\varepsilon_m/3\tau_m \quad (3.26)$$

Substituting the values in (3.25), $D_k = 1.18 \times 10^{-6}$ m^2/s.

Therefore, membrane mass transfer coefficient (k_{im}) is calculated substituting the above values in equation (3.21):

$k_{im} = 1.18 \times 10^{-6} \times 0.40 / (2.5 \times 25 \times 10^{-6})$

$= 1.16 \times 10^{-2}$ m/s.

3.2.1b Liquid Side Mass Transfer Coefficient

A number of correlations are available to evaluate the liquid and gas side mass transfer coefficients. Yang and Cussler [55] have measured the liquid side coefficients for water flow in cross-flow for different membrane fiber arrangements. Wickramasinghe et al. [56] arrived at correlations for flow outside and across the membranes for a Re ≈ 2.5. The range of Re values obtained for the present experimental conditions is shown in Table 3.2. Bhaumik et al. [57] have proposed the following correlation to estimate the liquid side mass transfer coefficient for crossflow hollow fiber membranes; (the range of Re in this study is in the range of Bhaumik et al. [57].

$$Sh = 0.57\, Re^{0.31} Sc^{0.33} \quad ; \quad 0.01<Re<1 \quad (3.27)$$

Table 3.2 Parameters for CO_2 absorption for pure ionic liquid and PAMAM in ionic liquid

Parameters	Membrane Module
Feed gas composition	14.1 % CO_2
Gas flow rate**, cm^3/min	51.2-210.5
Gas flow rate per fiber x10^{10}, m^3/s	4.2-16.5
Characteristic length, d, m	0.00005
Gas Reynolds number, Re	0.006-0.13
Gas Phase Sherwood number, Sh	0.00075-0.0022
Mean free path , λ, m	8.39 x 10^{-8}
Knudsen diffusion coefficient, $D_{g,k}$ x10^6, m^2/s	1.18
Diffusion coefficient, D_g x10^5, m^2/s	1.58
Diffusion coefficient of CO_2 in liquid[58], x10^9, m^2/s	2.20
Membrane mass transfer coefficient, k_{im} x10^2 , m/s	1.16
Shell –side liquid velocity x 10^3, m/s	4.8
Liquid Reynolds number, Re	0.044-0.036
Liquid Phase Sherwood number, Sh	2.54-4.06
Liquid mass transfer coefficient, k_{il} x 10^5, m/s	1.93-0.91
Molecular Mass of [bmim][DCA],gm/gmol	205.26
Heat Capacity, J/mol.K	1.80

** Two absorption modules

Liquid side mass transfer coefficients for the liquid flow rates of 4.16 gal/h and 2.57 gal/h are calculated using equation 3.27. Table 3.3 shows the K_l for pure ionic liquid DCA and Table 3.4 shows K_l for 20 wt % dendrimer in ionic liquid. In the calculation (detailed calculation in Appendix B) of the Reynolds number Re, fiber o.d. and interstitial velocity are used for shell-side crossflow; where,

$$\text{Interstitial velocity (m/s)} = \frac{\text{Solvent flow rate}}{\text{Open area for flow through the shell side}} \quad (3.28)$$

Table 3.3 Liquid mass transfer coefficient, k_l for pure ionic liquid [bmim] [DCA] (ρ = 1050 kg/m^3; CO_2 diffusivity = 6.5E-10 m^2/s [24])

Solvent flow rate (gal/h)	Solvent flow rate (cc/min)	Viscosity of solvent (pa.s)	Interstitial velocity (cm/min)	Velocity m/s	Reynolds Number (Re)	Schmidt Number Sc	Sherwood Number Sh	Liquid Mass Transf. k_l(m/s)
4.16	262.45	0.0331	29.16	0.00486	0.04469	7121.27	4.06	9.1E-06
2.57	162.14	0.0331	18.01	0.00300	0.02761	4399.44	2.98	6.6E-06

Table 3.4 Liquid mass transfer coefficient, k_l for 20 wt% dendrimer in ionic liquid [bmim] [DCA] (ρ = 1070 kg/m^3; CO_2 diffusivity = 2.20 E-09 m^2/s [58])

Solvent flow rate (gal/h)	Solvent flow rate (cc/min)	Viscosity of solvent (pa.s)	Interstitial velocity (cc/min)	Velocity (m/s)	Reynolds (Re)	Schmidt Number (Sc)	Sherwood Number Sh	Liquid Mass Transf. k_l(m/s)
4.16	262.45	0.0408	29.16	0.004860	0.03699	2.06E+03	2.54	1.93E-05
2.57	162.14	0.0408	18.01	0.003002	0.02279	1.28E+03	1.86	1.41E-05

3.2.1c Gas Side Mass Transfer Coefficient

For tube side mass transfer correlations of a fully developed laminar flow in a tube, Yang and Cussler [55] have used Sieder and Tate equation. Wickramasinghe et al. [56] have evaluated tube side coefficient for Gz > 4. To estimate the gas side mass transfer coefficient, the equation by Pachecho (1998) was used [59]

$$Sh = 1.096 \{Re\ Sc\ (d/h)\}^{0.80} \quad (3.29)$$

where, d is (outer diameter- inner diameter) ; h is the length of the fiber.

Individual gas-mass transfer coefficients of the feed gas flow rates are reported in Table 3.5. A sample calculation of Reynolds number, Schmidt number, Sherwood number and the gas film mass transfer coefficient is shown in Appendix B.

Table 3.5 Gas Film Mass Transfer coefficient, k_g, for all feed gas flow rates

Feed gas flow rate (cc/min)	Reynolds Number (Re)	Schmidt Number (Sc)	Sherwood Number (Sh)	Gas Film Mass Transf. k_g (m/s)	Gas Film Mass Transf. k_g (mol/m^2.s.Pa)
10.91	6.78E-03	0.88	6.002E-05	1.90E-05	7.66E-09
18.16	1.13E-02	0.88	0.0003164	1.00E-04	4.03E-08
32.46	2.02E-02	0.88	0.0005036	1.59E-04	6.41E-08
54.08	3.36E-02	0.88	0.0007576	2.39E-04	9.64E-08
51.2	3.18E-02	0.88	0.0007251	2.29E-04	9.24E-08
98.4	6.11E-02	0.88	0.0012229	3.86E-04	1.55E-07
106.5	6.61E-02	0.88	0.0013028	4.12E-04	1.66E-07
144.9	9.00E-02	0.88	0.0016667	5.27E-04	2.12E-07
159.5	9.91E-02	0.88	0.0017997	5.69E-04	2.29E-07
210.5	1.31E-01	0.88	0.002247	7.10E-04	2.86E-07

3.2.4d Henry's law constant (H_i)

Chau et al. [24] have reported solubility of CO_2 in [bmim][DCA], mixture of [bmim][DCA] and 20 wt% Poly(amidoamine) dendrimer Gen 0 (PAMAM) with and without moisture. Table 3.6 shows the Henry's law constant for CO_2 in three different units.

Table 3.6 Henry's law constant for pure [bmim][DCA] and 20 wt% dendrimer in [bmim][DCA]
Source : [24]

Solvent	Henry's law constant (bar)	Henry's law constant ($gmol/atm.cm^3$)	Henry's law constant (dimensionless)
Pure [bmim][DCA]	74.4±0.5	$6.96x10^{-5}$	$184.34x10^{-5}$
20 wt% Dendrimer in [bmim][DCA]	28.5±1.0	$1.39x10^{-4}$	$36.81x10^{-4}$

Overall gas phase based mass transfer coefficient based on individual mass transfer coefficients are calculated using equations (3.14). Table 3.7 shows the valves K_g for pure DCA and Table 3.8 shows K_g for 20 wt % dendrimer in ionic liquid.

Table 3.7 Overall K_g from individual mass transfer coefficients for pure [bmim][DCA]

Gas flow	k_{ig} $x10^4$ (m/s)	k_{im} $x10^2$ (m/s)	k_{il} $x10^6$ (m/s)	H $x10^3$	$1/k_{ig}$ $x10^{-3}$	$1/k_{im}$	Hk_{il} $x10^8$	$1/Hk_{il}$ $x10^{-7}$	$1/K_g$ $x10^{-7}$	K_g $x10^8$ (m/s)
10.91	0.19	1.16	9.10	1.84	52.7	86.2	1.68	5.96	5.97	1.68
18.16	1.00	1.16	9.10	1.84	10	86.2	1.68	5.96	5.96	1.68
32.46	1.59	1.16	9.10	1.84	6.28	86.2	1.68	5.96	5.96	1.68

Table 3.8 Overall K_g from individual mass transfer coefficients for 20 wt% dendrimer in [bmim][DCA]

Feed flow	k_{ig} $x10^4$ (m/s)	k_{im} $x10^2$ (m/s)	k_{il} $x10^5$ (m/s)	H $x10^3$	$1/k_{ig}$ $x10^{-3}$	$1/k_{im}$	Hk_{il} $x10^8$	$1/HK_{il}$ $x10^{-7}$	$1/K_g$ $x10^{-7}$	K_g $x10^8$ (m/s)
54.08	2.39	1.16	1.93	3.68	4.18	86.2	7.10	1.41	1.41	7.10
51.2	2.29	1.16	1.93	3.68	4.36	86.2	7.10	1.41	1.41	7.10
98.4	3.86	1.16	1.93	3.68	2.59	86.2	7.10	1.41	1.41	7.10
106.5	4.12	1.16	1.93	3.68	2.43	86.2	7.10	1.41	1.41	7.10
144.9	5.27	1.16	1.93	3.68	1.90	86.2	7.10	1.41	1.41	7.10
159.5	5.69	1.16	1.93	3.68	1.76	86.2	7.10	1.41	1.41	7.10
210.5	7.10	1.16	1.93	3.68	1.41	86.2	7.10	1.41	1.41	7.10

Revisiting equations (3.14) and (3.20) to calculate the $K_g\,a$ and $K_l a$ where a is the interfacial area Table 3.9 shows the values of K_g, K_l

Table 3.9 Overall volumetric mass transfer coefficient K_la (mol/m^3.Pa.s) for 20 wt. % PAMAM in [bmim] [DCA] for a liquid flow rate: 4.16 gal/h

K_g (mol/m^2.s.Pa)	K_g.a (mol/m^3.Pa.s)	K_l (mol/m^2.Pa.s)	K_la (mol/m^3.Pa.s)
2.86E-11	6.02E-08	7.78E-09	1.62E-05

Table 3.10 Overall volumetric mass transfer coefficient K_la (m/s) for 20 wt. % PAMAM in [bmim] [DCA] for a liquid flow rate: 4.16 gal/h

K_g (m/s)	K_g.a (1/s)	$K_l = K_g/H_i$ (m/s)	K_l.a (1/s)
7.10E-08	1.49E-04	1.93E-05	4.06E-02

The K_la for the current CO_2 – IL- dendrimer study is about 1.63 x 10^{-5} mol/m$^{2.}$Pa.s.The K_la reported by Nishikawa et.al [60] for CO_2 – MEA system for a similar interfacial area is about 1.19 x 10^{-3} mol/m$^{2.}$Pa.s. These results are reported in Table 3.9. This result is expected owing to the highly viscous nature of 20 wt% dendrimer in [bmim] [DCA] solvent compared to the aqueous MEA solvent. Rangawala [61] has reported K_la (m/s)

for CO_2- DEA system. These results are reported in Table 3.10. These $K_l a$ values reported in Table 3.11 are almost comparable to the $K_l a$ obtained for the current CO_2 – IL-dendrimer system.

Table 3.11 Comparison of $K_l a$

System	Interfacial area a (m^2/m^3)	$K_l a$ ($mol/m^{2\cdot}Pa.s$)	$K_l a$ (1/s)
CO_2 - aq.MEA[60]	2078	1.19×10^{-3}	-
CO_2-IL-dendrimer (This work)	2102	1.63×10^{-5}	4.6×10^{-2}
CO_2 – aq. DEA[61]	2324	-	4.3×10^{-1}

3.3 Considerations on Energy Needed

An estimate of the energy used for CO_2 absorption at an elevated temperature by the ionic liquid [bmim] [DCA] is calculated by [62]

$$Q\ (KJ/Kg\ CO_2) = \Delta H_{abs} + m*C_p*\Delta T \qquad (3.30)$$

Where, ΔH_{abs} the heat of absorption for [bmim] [DCA] is -295 KJ/Kg CO_2 [63], m is the mass of the solvent, the Henry's law constant of CO_2 in [bmim] [DCA] at 50° C is 74.4 bar [24], $C_{p,}$ is the heat capacity [64] of [bmim][DCA] (its value provided in Table 3.2) and ΔT being the temperature difference between the absorption and stripping temperatures. As mentioned in Section 2.7, the absorption and the stripping temperatures were about 50-52 °C and 79-82 °C with the corresponding $\Delta T \sim 30$ °C.

Therefore, the energy required for [bmim] [DCA] at 0.1 bar partial pressure of CO_2 is about 1.36×10^5 KJ/kg. Table 3.12 provides a comparison between the two IL's [bmim][PF_6] and [bmim][DCA] with regard to energy consumption.

Table 3.12 Energy usage comparison between [bmim][PF_6] and [bmim][DCA]

	[bmim][PF_6]	[bmim][DCA] (This Work)
Mass of solvent/kg CO_2	5914	2586.7
ΔH_{abs} (KJ/kg CO_2)	-366	-295
C_p (KJ/kg K)	1.0	1.8
Q(KJ/kg CO_2)	4.4×10^5	1.36×10^5
Q(million BTU/ton CO_2)	382	120.09

CHAPTER 4

CO_2 CAPTURE FROM POST COMBUSTION FLUE GAS USING 80 WT % PAMAM IN [BMIM] [DCA] IN A THERMAL SWING ABSORBENT BED

4.1 Introduction

Flue gas from power plants based on coal combustion is one of the primary sources of CO_2 emissions. The capital and operating costs of the utilities for CO_2 capture and sequestration (CCS) can be substantially reduced via the following: (1) Employ a highly compact device to reduce capital cost; (2) a compact device will also reduce the amount of heat needed to regenerate the sorbent for adsorption or absorption-based processes; (3) avoid using high-cost energy such as electricity instead use hot water if heating is needed; (4) avoid using high vacuum requiring huge vacuum pumps. Solid amine-based adsorption carried out in porous ceramic supports allows higher adsorption capacities via fast CO_2 reaction with amines. Efforts have been focused on grafting, impregnating or immobilizing preformed polymeric amines of various types on porous solid supports/adsorbents for CO_2 adsorption. The absolute CO_2 adsorption capacity of such supported basic groups/g of the adsorbent material is however, considerably reduced by the support mass.

Temperature swing regeneration of the adsorbent will involve heating of this support mass which does not generally contribute much to CO_2 adsorption. One can bypass these problems altogether if we let a nonvolatile amine itself function as if it were an adsorbent. Here I illustrate a Temperature Swing Absorption (TSAB) technique that allows an almost pure highly viscous liquid amine to function as if it were an adsorbent even though it functions as an absorbent; one can thereby increase the CO_2 sorption capacity per unit weight drastically.

A novel hollow fiber membrane based device whose shell side is filled with the amine base is employed in the present study; it demonstrates how such an amine absorbent will be functioning as if it were an adsorbent in a temperature swing process over a temperature range of 25-95 ^{0}C. An illustration of the transient CO_2 absorption in the liquid absorbent followed soon after by feed CO_2 concentration breakthrough after which an arrangement of rapid heating of the bed by hot water, to strip the absorbed CO_2 from the liquid amine is provided. The first focus is on the sorption characterization of the amine base that can be used efficiently as if it were a superefficient adsorbent for CO_2; the next focus is on a device where such an amine base can function in a temperature swing absorption process.

As discussed in Chapters 1, 2 & 3, polyamidoamine (PAMAM) dendrimer generation 0 (MW, 517 dalton) can act as a molecular gate for selective CO_2 removal since it was providing extremely high selectivities for CO_2 over N_2/O_2 in the range of 700-18,000 depending on the partial pressure of CO_2. This performance was achieved only in the presence of considerable moisture which is needed for activation of the tertiary amine groups in the dendrimer of interest which has four primary amines and two tertiary amines. Since then the RITE group in Japan has developed successful CO_2 separation membranes using this amine in particular ways and scaled it up [30, 31, 32].

Membrane separation of CO_2 from flue gas requires however considerable vacuum on the permeate side which may be reduced only if the partial pressure of CO_2 can be raised. An alternative strategy using such a nonvolatile dendrimer amine is suggested. The author initially reported its extremely high CO_2 sorption capacity due to reversible reactions of the four primary amines (which do not require moisture for the reaction) and two tertiary amines in the presence of moisture. A porous polymeric

hydrophobic hollow fiber membrane-based device wherein the PAMAM dendrimer Gen 0 is immobilized on the shell side of the thin-walled porous hollow fiber membranes through the bore of which the flue gas is passed for part of the temperature swing cycle. In the device there is another set of solid polymeric nonporous and impervious hollow fiber through the bore of which hot water is passed in the rest of the cycle to desorb CO_2 at a high partial pressure from the PAMAM Gen 0 absorbent; this CO_2 exits through the bore of the first set of porous hollow fibers.

4.2. Materials and Methodology

4.2.1 Chemicals

Pure ionic liquid [bmim] [DCA] was bought from EMD chemicals, Philadelphia, PA. PAMAM Gen 0 (M.W= 517) was obtained from Dendritech Inc., Midland, MI as a 64.05 wt% solution in methanol. To get pure dendrimer, the solution was vacuumed for several days under a relatively high temperature around 60^0C to remove methanol. After evaporation of methanol from dendrimer, 80 wt% dendrimer in ionic liquid [bmim] [DCA] was prepared as an absorbent in the current study.

4.2.2 Materials and Membrane Module Characterization

The properties of the porous and solid hollow fibers employed in the two-fiber set up are listed in Table 4.1. The two-hollow-fiber-set based compact membrane device was fabricated using a PTFE plastic shell, having an ID 0.45 cm of and two Y-fittings at each end; the Y-fittings were potted at the each end of the PTFE tubing. Once the epoxy was dry, porous PVDF and solid PEEK fibers were then inserted into the membrane device through the arms of Y-fittings. Eleven 35.5 cm long hydrophobic porous hollow fibers of

polyvinylidene fluoride (PVDF) commingled with another eleven solid nonporous hollow fibers of PEEK of the same length were potted with epoxy in Y-fittings of the PTFE plastic shell.

Table 4.1 Properties of the hollow fibers used in the two-fiber-set membrane module

Membrane	ID of the fiber (µm)	OD of the fiber (µm)	Pore size (µm)	Porosity
PVDF E[a]	691	925	0.2	0.54
Solid PEEK	420	575	0	0

ID = Internal Diameter; OD = Outside Diameter.
[a] Arkema Inc., King of Prussia, PA.

Once the whole membrane device was ready after curing of the epoxy, 80 wt% dendrimer in ionic liquid absorbent was introduced to the shell side of the novel hollow fiber membrane-based device to carry out the temperature swing absorption (TSAB) process as follows. About 21.25 cm^3 volume (ρ= 1.18 gm/ cm^3; weight of absorbent = 25 gm) of 80 wt% dendrimer in ionic liquid was needed to fill the membrane module device. For introduction of this absorbent in the module shell side, 80% dendrimer in ionic liquid was mixed with a small amount of water and then poured onto the shell side of the module. Then water was removed by vacuum applied through the porous hollow fibers. This process was repeated a few times to completely fill out the shell side with this liquid. Although PAMAM dendrimer is a somewhat novel and expensive absorbent (per Aldrich catalog for an analytical grade), the manufacturer proposes to supply an industrial grade of this compound in large scale at a reasonable price of ~ $10-20/lb since its potential application involves very large scale (Dendritech Inc., Midland, MI).

4.2.3 Sorption Characterization Method

Before conducting the TSAB process, the absorbent was first subjected to equilibrium CO_2 uptake measurements to determine the sorption isotherms of the absorbent. Equilibrium sorption experiments were done in a pressure-decay dual-transducer apparatus shown in Figure 4.1, originally designed by Chau et al. [24].

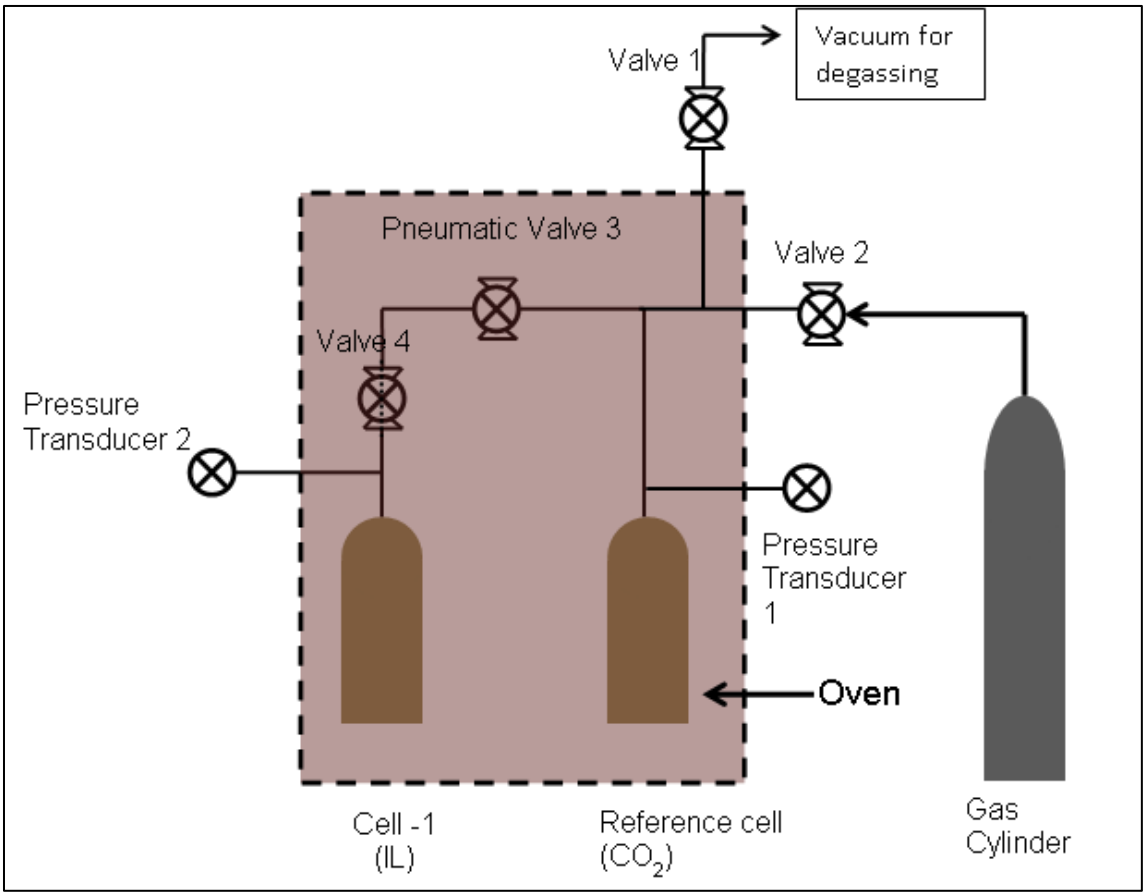

Figure 4.1 Pressure-decay dual transducer apparatus for equilibrium sorption experiments.

Ultrahigh grade pure CO_2 was obtained from Air gas. The desired amount of sorbent was placed in a stainless steel cell – 1 (Product No. 304L-05 SF4-150, R.S. Crum & Company, Mountainside, NJ) and connected to the system. In dry gas experiments, the system with all the valves (Product No. SS-2P4T-BK, R.S. Crum & Company,

Mountainside, and NJ) open was subjected to vacuum (Model UN 726.3 FTP, KNF, Trenton, NJ) for about 4 hours to remove any trace amounts of moisture or CO_2. In the measurements under humid conditions, the desired amount of water was added to the cell and connected back to the system. The three valves, valve 1, 2 and 3 were opened for vacuuming the system with valve 4 opened only for 5 minutes. Once the degassing was done, all valves were closed with valve 2 and valve 4 opened in humid gas experiments. Then, the gas (pure CO_2) at the desired pressure is loaded into the stainless steel reference cell (Product No. 304L-05 SF4-150, R.S. Crum & Company, Mountainside, NJ) through valve 2 and the initial pressure (P1) was noted from the pressure transducer (Model PX32B1-250GV, Omegadyne Inc., Sunbury, OH). Then the valve 2 was closed, and the oven temperature was turned on to allow the system to reach the desired temperature. Once the desired temperature was reached, the pneumatic controller (PneuMagnetic, Quakertown, PA) was turned on for the measurements. Upon reaching equilibrium, the final pressure (P2) was noted. The number of moles absorbed were calculated from, the difference in the final pressure and initial pressure, volume of the sorbent and temperature of the system. This pressure decay recorded over the time, determines the gas sorption kinetics. These results are reported in Section 4.4.

4.3 Experimental Procedure of the Rapid Temperature Swing Absorption

The simulated flue gas mixture of composition 14.1% CO_2, 1.98% O_2 and rest N_2 (Welco-CGI Gas Technologies, Newark, NJ) was introduced from the gas cylinder into the two – fiber absorption-thermal stripping module. Figure 4.2 shows the schematic of the TSAB system. Feed gas flow rate was controlled by a Multi-channel Mass flow Controller Model 8248A and Mass flow Controller Transducer Model (MTRN-1002-SA,

Matheson TRI-GAS, Montgomeryville, PA). Various feed gas flow rates were studied in this process. Carbon dioxide concentrations in the treated flue gas stream and the stripped gas stream was monitored continuously by a solid-state IR- based CO_2 analyzer (Model 906, Quantek Instruments, Grafton, MA) connected at the gas outlet of the two fiber module. Complete capture of CO_2 from the flue gas took place until the onset of the CO_2 breakthrough, followed by a slow increase in CO_2 concentration in the outlet gas as observed in the CO_2 analyzer. The feed gas was further allowed to pass through the fibers until the liquid absorbent was completely saturated as indicated by the feed CO_2 concentration of 14.1% showing up at the module outlet at which time the feed gas flow was stopped completely. Then the system was very rapidly purged with a burst of helium replacing the feed gas in the porous hollow fibers. The two gas valves at the inlet and the outlet of the two-fiber system were then closed.

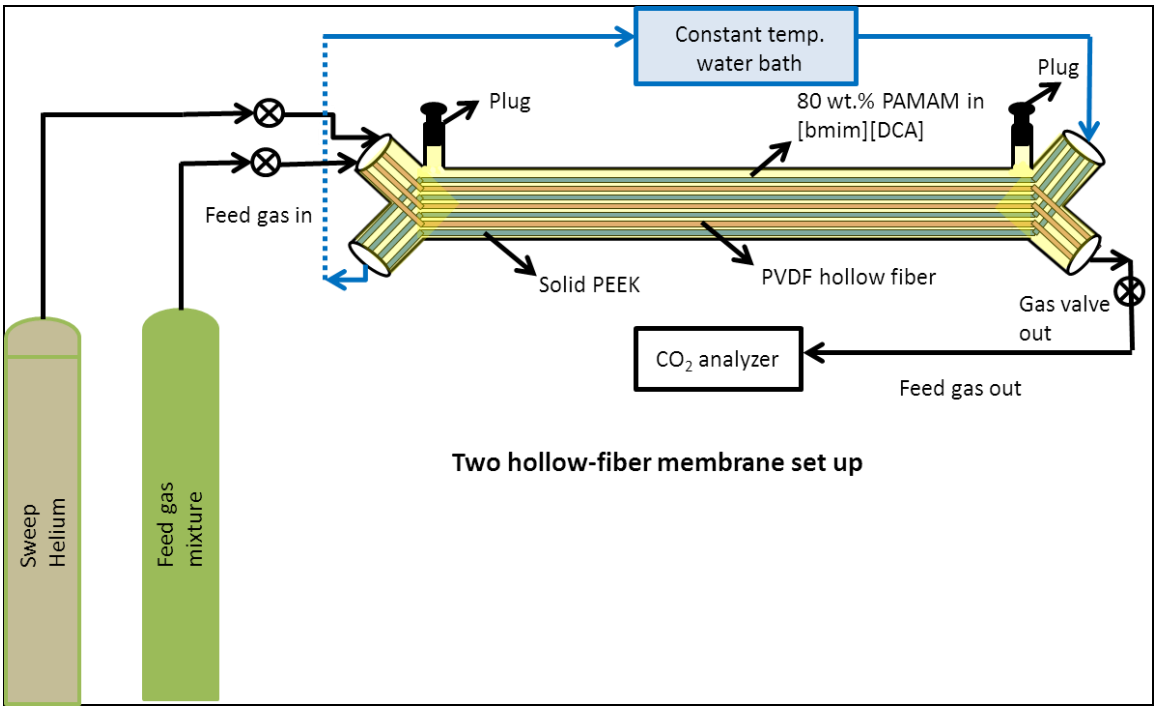

Figure 4.2 Schematic of temperature swing absorption - desorption setup (membrane module enlarged in the picture).

In order to desorb the absorbed CO_2, hot water from a constant temperature bath was pumped through the bore of the solid PEEK hollow fibers. The thin polymeric solid hollow fibers function as an extremely efficient heat transfer device and are ideal for very rapid heating up of the absorbent liquid residing in the inter-fiber space between the two sets of hollow fibers if we introduce hot water or low temperature steam through their lumen. These solid hollow fibers are also useful for absorbing the exothermic heat of absorption during CO_2 absorption in the shell-side absorbent liquid if we pass cold water through their lumen to achieve isothermal absorption. The thermocouples at the inlet and the outlet of the solid PEEK fibers were connected to the temperature read-out in order to record the inlet and the outlet water temperature. Hot water was passed for about 10 min, in order to desorb from sorbent the absorbed CO_2 gas. After passing the hot water for 10 min, the two inlet and the outlet gas valves were quickly opened and sweep He (carrier

gas) was passed though the PVDF porous hollow fibers. The CO_2 concentration in the treated gas stream was recorded by the CO_2 analyzer. This temperature swing absorption-regeneration of the absorbent was studied at different temperatures in the presence of various sweep helium flow rates. The highest concentration recorded on the analyzer was noted. After the sorption run, the bed was completely regenerated by passing the sweep He maintaining the same bed temperature as in the experiment for about 45 min to 1 hour, to make it ready for the next sorption run.

4.4 Results and Discussions of Sorption Characterization of Solvent

4.4.1 Equilibrium CO_2 sorption capacity measurements of 80 wt. % PAMAM in ionic liquid [bmim][DCA] with pure CO_2 at 100 psig

4.4.1a Effect *of weight loading at 50 °C (323K)*

In the first experiment, 11.6 cm^3 of 80 wt. % PAMAM in IL (ρ = 1.18 gm/cm^3) was introduced into the stainless steel cylinder cell-1. The corresponding weight of the 80 wt. % PAMAM in IL measured about 13.69 g (containing 10.95 g PAMAM and 2.74 g IL). Once the desired temperature was reached and the pneumatic controller valve was opened, a sharp decrease in the pressure was seen, indicating the onset of the equilibrium process. Once the equilibrium (10 days needed to reach equilibrium) was reached, a total of 18.01mmol of CO_2 was absorbed by 13.69 g of absorbent, indicating of about 1.32 mmole CO_2 per gm of absorbent. In another measurement, about 3 g of absorbent was subjected to the same working conditions (50 °C (323K) with pure CO_2 at 100 psi) and tested for sorption capacity. On reaching equilibrium (3 days needed to reach

equilibrium), a total of 10.36 mmole of CO_2 was absorbed by 3 g, representing 3.45 mmole CO_2 per gm of absorbent.

Figure 4.3 shows the mole fraction of CO_2 absorbed at the end of the equilibrium process. The mole fraction of CO_2 increased with time in the case of 3g absorbent when compared to that of 13.69 g. This difference in the behavior can be attributed to the highly viscous nature of the dendrimer 80 wt % solution of dendrimer in IL. The thickness of 3g of sorbent, is much less compared to that of 13.69 g absorbent. Due to this, CO_2 diffusion through the layers of the 3 g absorbent took much less time leading to much quicker equilibrium where the mole fraction of CO_2 was stable at 0.64 after 4 days, compared to the 13.69 g absorbent where the mole fraction achieved was only 0.35 even after 4 days. CO_2 gas diffusion is directly proportional to the thickness of the sorbent, because of which, some of the amines present in the 80 wt% dendrimer in ionic liquid may become unavailable for CO_2 absorption when using the high weight of the absorbent mixture for sorption measurements.

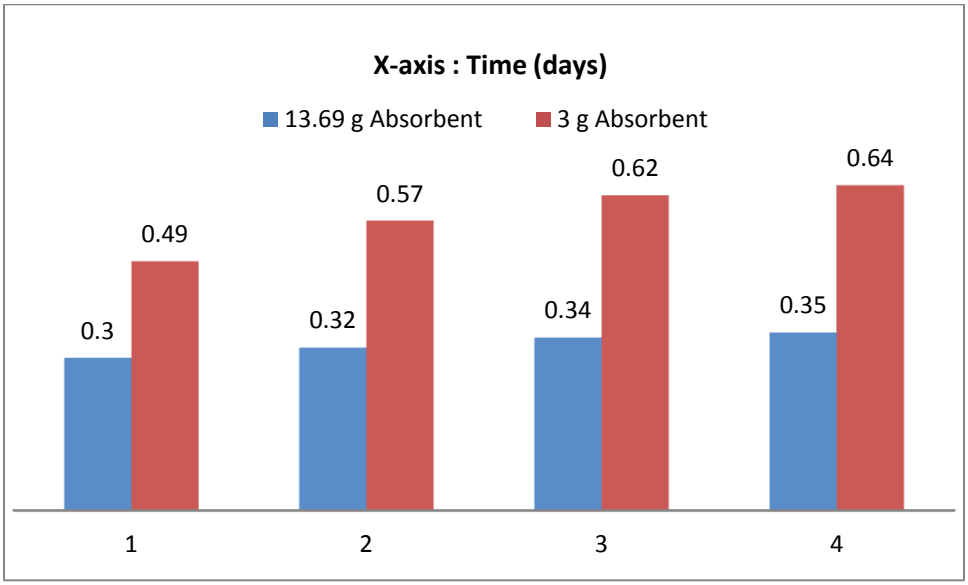

Figure 4.3 Mole fraction of CO_2 absorbed per gm of absorbent (y-axis) against time in days at 50 °C.

4.4.1b Effect *of temperature on CO_2 sorption capacity*

Equilibrium reactive sorption capacity (in mmol) of 80 wt. % dendrimer in ionic liquid at different temperatures is shown in Figure 4.4. The mmol of CO_2 absorbed by 3 g sorbent, reported at different temperatures were recorded over a period of 3 days. At 50 °C, a total of 10.36 mmol of CO_2 was absorbed by 3 g, representing 3.45 mmole CO_2 per gm of absorbent. At 40 °C, a total of 9 mmol were absorbed representing 3 mmol of CO_2 absorbed per gram of absorbent, where the capacity marginally decreased from 3.45 mmol at 50 °C. With the increase in the temperature the CO_2 sorption capacity should decrease. But this difference in behavior is seen here because, as the temperature increases, the viscosity of the 80 wt% dendrimer in ionic liquid decreases. This means that the apparent effect of thickness for diffusion through 3 g of sorbent at 50 °C is less compared to that at 40 °C. Since CO_2 gas diffusion is proportional to the thickness of the sorbent, it is expected that the number of mmol absorbed at 50 °C are higher than at 40 °C unless much more time is allowed.

At 90 °C, only a total of about 1.36 mmol of CO_2 and therfore 0.45 mmol of CO_2 per gm of absorbent was achieved. This is likely to be due to the lower reactive sorption capacity of CO_2 at such temperatures. Chau et al. [24] have reported the solubility of CO_2 in 20 wt. % and 30 wt%. dendrimer in ionic liquid. They have also studied its effect with and without moisture. Figure 4.4 shows that, at 50 °C, 0.54 mmol CO_2/ gm absorbent and 0.59 mmol CO_2/ gm absorbent were absorbed by 20 wt % dendrimer in ionic liquid and 30 wt% dendrimer in ionic liquid respectively.

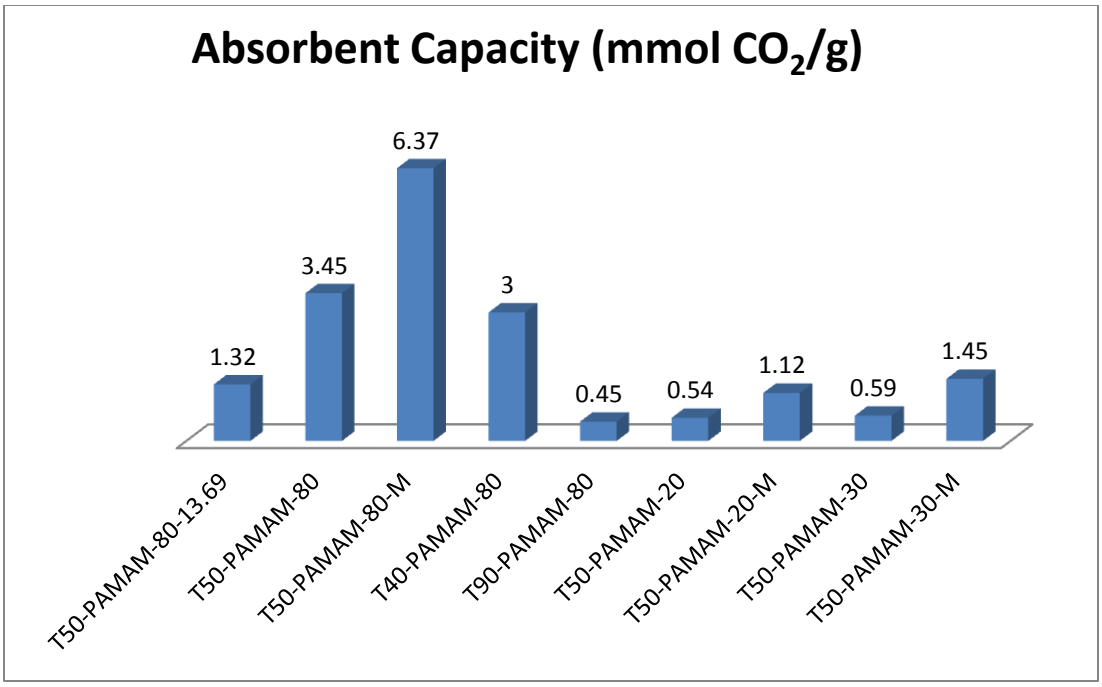

Figure 4.4 Absorbent capacity (mmoles CO_2/ gm absorbent) of 80 wt. % PAMAM in Ionic Liquid at various temperatures. The symbol T50-PAMAM-80-M means the temperature was 50 ^{0}C, PAMAM was present at 80 wt% level in [bmim][DCA] and M means moisture was present.

Generation 0 PAMAM dendrimer has four primary amine functional groups and two tertiary amines. Under no humidity conditions, only 4 primary amines react with CO_2. Primary amines react readily with CO_2 via zwitterionic mechanism to form carbamate (Equation 4.1), while tertiary amines cannot directly react with CO_2 to form carbamate; they facilitate base-catalyzed hydrolysis of CO_2 reaction forming bicarbonate in the presence of water (Equation 4.2). Hence, one PAMAM Generation 0 can react with 4 moles of CO_2 in the presence of water. Therefore, sorption measurements with humidity are needed in order to activate the tertiary amine groups.

$$CO_2 + 2RNH_2 \Leftrightarrow RNHCOO^- + RNH_3^+ \quad (4.1)$$

$$CO_2 + R_1R_2R_3N + H_2O \rightarrow R_1R_2R_3NH^+ + HCO_3^- \quad (4.2)$$

$$HCO_3^- \Leftrightarrow CO_2 + OH^-$$

4.1.1c Effect *of moisture on CO_2 sorption capacity*

In order to know how many grams of water are needed to facilitate the reaction, a theoretical estimation of the grams of water needed was made and absorption experiments with moisture were done.

Stoichiometrically, 1 mole of PAMAM can consume 4 moles of CO_2 and consume 2 moles of water

$$\frac{-n_{pamam}}{1} = \frac{-n_{water}}{2} = \frac{n_{carbon\ dioxide}}{4} \quad (4.3)$$

For 3 g absorbent (2.4 g of PAMAM; 0.6 g IL),

Moles of PAMAM = 2.4/ 517 = 4.6 mmol

$$\text{Moles of water for complete reaction} = \frac{-n_{pamam}}{1} = \frac{-n_{water}}{2} \quad (4.4)$$

$$n_{water} = 2 * n_{pamam} \quad (4.5)$$

= 9.2 mmoles

Weight of water required: 9.2 mmoles * 18 = 0.165 gm.

When 0.25 g of water was added to the 3 g absorbent, a total of 19.01 mmol of CO_2 were absorbed at 50 °C; i.e about 6.37 mmol per gm of absorbent which is about 280.2 mg CO_2/ gm of absorbent. Figure 4.5 shows a comparison in mg of CO_2 absorbed per gm of sorbent. Geoppert et al. [40] studied CO_2 sorption characteristics of PEI on fumed silica at two weight loadings: 33 wt%, 50 wt% of PEI. Under dry conditions the amount of CO_2 adsorbed per gm of FS- PEI- 33 was 156 mg/g and 150 mg/ g for FS-PEI-

50. In the presence of water, these values were 230 and 124 mg CO_2/g PEI, respectively. As the two tertiary amines begin to react with CO_2 in presence of water, the absorption capacity increased two-fold. At the same temperature 50 °C, Figure 4.4 shows that the mmoles of CO_2 per gm of absorbent increased from 3.45 to 6.37 on addition of just sufficient amount of water. This behavior is very similar to the solubility of CO_2 in 20 wt % and 30 wt % dendrimer in ionic liquid reported by Chau et al. [24]. The number of mmoles per gm of absorbent increased from 0.54 to 1.12 in the case of 20 wt% dendrimer in ionic liquid and from 0.59 to 1.45 in the case of 30 wt % dendrimer in ionic liquid. Kuwahara et al. [65] studied CO_2 adsorption characteristics of prototypical poly (ethyleneimine)/silica composite adsorbents whose sorption capacity was drastically enhanced by altering the acid/base properties of the oxide support via incorporation of Zr into the silica support. Samantha A et al. [66] have reviewed the CO_2 adsorption capacity of a number of amine-impregnated solid sorbents in mmol CO_2 per gram adsorbent. Table 4.2 shows a number of amines impregnated with different wt % on various solid supports. The CO_2 absorbent capacity of 80 wt % dendrimer in ionic liquid reported in the current study, 6.37 mmol CO_2/g is much more than those reported in the literature.

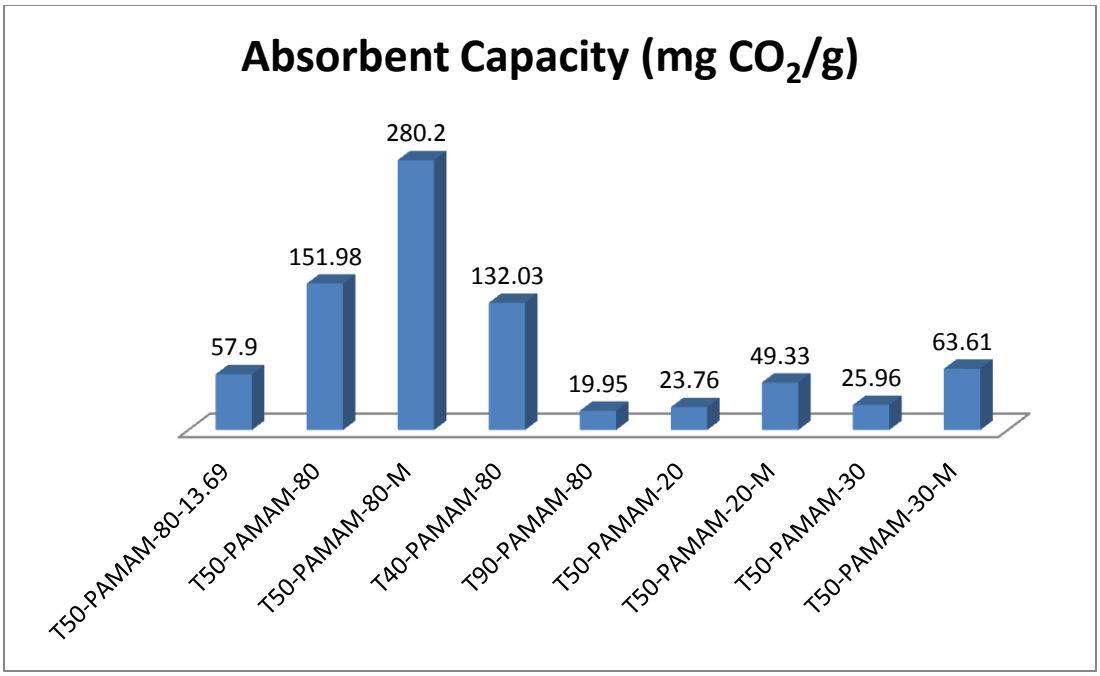

Figure 4.5 Absorbent capacities (mmol CO_2/ g absorbent) of 80 wt. % PAMAM in ionic liquid at various temperatures.

Table 4.2 CO_2 Adsorption Capacity of Amine-Impregnated Solid Sorbents (mmol CO_2/g)

support	amine	amine content (wt %)	adsorption capacity (humid) (mmol g^{-1})
MCM-41	PEI	75	3.02
MCM-41	PEI	50	2.05
PE-MCM-41	DEA	77	2.93
PE-MCM-41	DEA	73	2.81 (2.89)
MCM-41	PEI	50	(3.08)
MCM-41	TEPA	50	4.54
SBA-15	TEPA	50	3.23
SBA-15	DEA + TEPA	50 (30% TEPA, 20% DEA)	3.61
SBA-15	PEI	50	3.18
SBA-15	PEI	50	1.36
SBA-15	APTES		(2.01)
KIT-6	PEI	50	1.95
monolith	PEI	65	3.75
mesoporous silica	PEI	40	2.4
PMMA	DBU	29	(3.0)
PMMA	DBU	29	(2.34)
PMMA (Diaion)	PEI	40	2.40 (3.53)
SiO_2 (CARiACT)	PEI	40	2.55 (3.65)
Zeolite 13X	MEA	10	1.0
Zeolite Y60	TEPA	50	(4.27)

Source: [66]

4.4.2 CO_2 sorption performance in the two hollow-fiber membrane based liquid absorbent bed

The sorption performance of the absorbent in the module containing eleven 35.5 cm long hydrophobic porous hollow fibers of polyvinylidene fluoride (PVDF) having a bed void volume fraction of 0.767 will now be illustrated. The CO_2 absorption behavior of this bed of hollow fibers is studied as a simulated flue gas containing 14.1% CO_2 was passed through the lumen of these porous hollow fibers.

4.4.2a CO_2 absorption in the two-hollow fiber membrane device

Figure 4.6 displays the CO_2 breakthrough performance by the two fiber bed at different temperatures (both bed and feed gas temperatures) with variations in feed gas flow rates. The breakthrough performance was studied for three different dry feed gas flow rates: 9.1, 12.7 and 24.1 cm^3/min. During the absorption process, water at 50 ^{0}C was passed through the lumen of the solid hollow fibers for absorption at 50 ^{0}C to ensure that the bed remained at 50 ^{0}C.

For the same inlet feed gas temperature at 25 ^{0}C and bed temperature of 25 ^{0}C, a significant spreading in the CO_2 breakthrough curve is seen for the flow rate 12.7 cm^3/min when compared to that at 24.1 cm^3/min. A similar trend in the breakthrough performance is seen when the bed temperature was raised from 25 ^{0}C to 50 ^{0}C, for the same flow rates 12.7 cm^3/min and 24.1 cm^3/min. The CO_2 breakthrough curve is not very sharp indicating the role of diffusional processes in the shell-side absorbent liquid. The thickness of the absorbent liquid on the shell side in between two contiguous hollow fibers is considerable; this thickness is contributing to the not-so-sharp-a-rise in CO_2 concentration at the outlet. In the case of higher packing density of the porous hollow fibers for gas absorption, the thickness of the absorbent liquid in between the contiguous porous PVDF hollow fibers would be reduced leading to a quicker saturation and a sharper CO_2 breakthrough.

In another absorption experiment with feed gas flow rate of 24.1 cm^3/min, the feed gas was heated to 40 ^{0}C with bed temperature at 25 ^{0}C. A quicker breakthrough at 1.24 min with a sharper rise in the CO_2 curve, was seen in comparison to the breakthrough curve of the feed gas at 24.1 cm^3/min at 25 ^{0}C. The CO_2 bed breakthrough times for the feed gas flow rates 9.1, 12.7 and 24.1 cm^3/min were 7.24 min, 6.2 min and

2.4 minutes respectively for the room temperature bed and feed gas temperature. For the bed temperature at 50 ^{0}C, the breakthrough time for the gas flow rate of 12.7 cm^3/min, was about 3.5 min. A change in the bed temperature did not have any significant effect on the breakthrough time for the feed gas flow rate 24.1 cm^3/min.

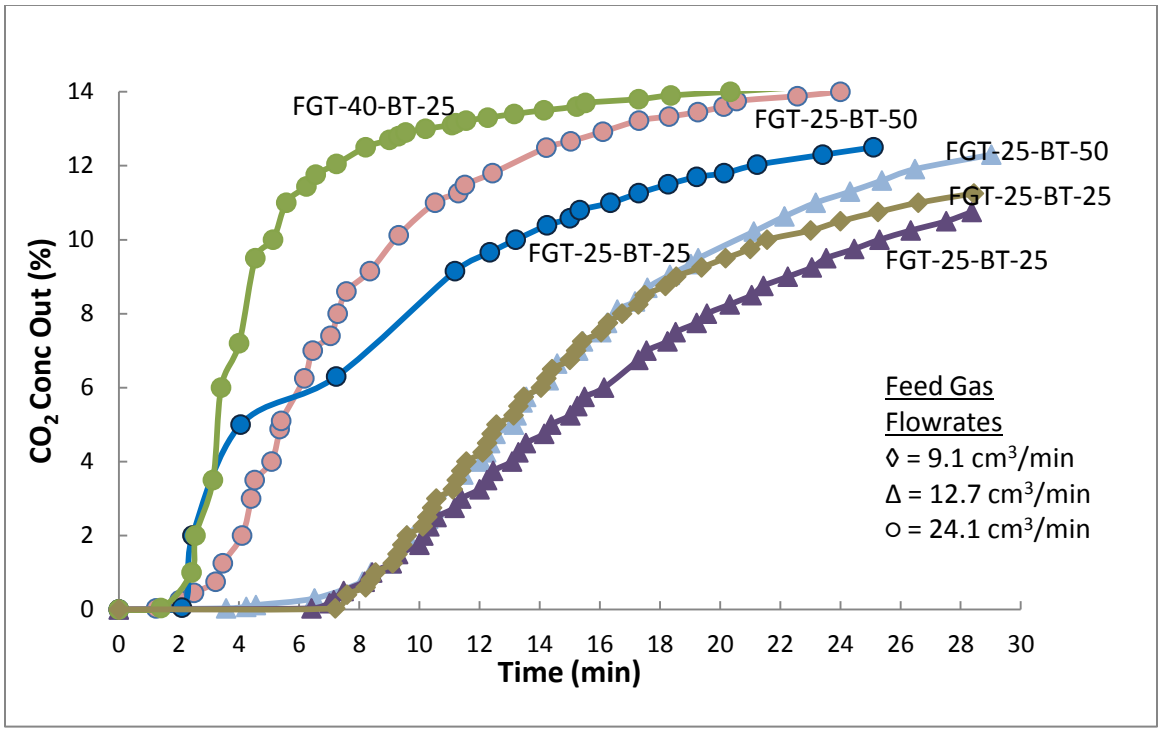

Figure 4.6 CO_2 breakthrough experiments with dry feed gas flow rates. The symbol FGT-25-BT-25: Feed gas flow rate temperature (FGT) at 25 ^{0}C with bed temperature (BT) at 25 ^{0}C.

Figure 4.7 illustrates the corresponding breakthrough behavior for 50 ^{0}C with moisture. The first experiment was done with the bed and feed gas temperature both at 25 ^{0}C. For the feed gas flow rate of 12.7 cm^3/min (RH= 91%), the breakthrough time was about 4.7 min. This breakthrough time is much less than the breakthrough time for the feed gas flow rate 12.7 cm^3/min with bed and feed gas temperature at 25 ^{0}C. This can mean that, though there was moisture, it did not help in effectively facilitating the

reaction between CO_2 and tertiary amines at room temperature. Also, gas diffusion resistance may have existed due to the presence of the moisture and already viscous nature of the 80 wt % dendrimer in ionic liquid at room temperature.

The hollow fiber bed showed better performance when the bed temperature was raised during absorption. At a bed temperature of 50 ^{0}C the breakthrough times for the humidified feed gas flow rates 9.1, 12.7 and 24.1 cm^3/min, were about 12.13, 10.01 and 4 min respectively. It is clear that presence of moisture in the feed gas almost doubles the amount of CO_2 absorbed in so far as the breakthrough time is concerned. This is expected since the tertiary amine groups start absorbing CO_2 only in the presence of moisture. At a bed temperature of 60 ^{0}C, the breakthrough time of the bed was about 5.3 minute.

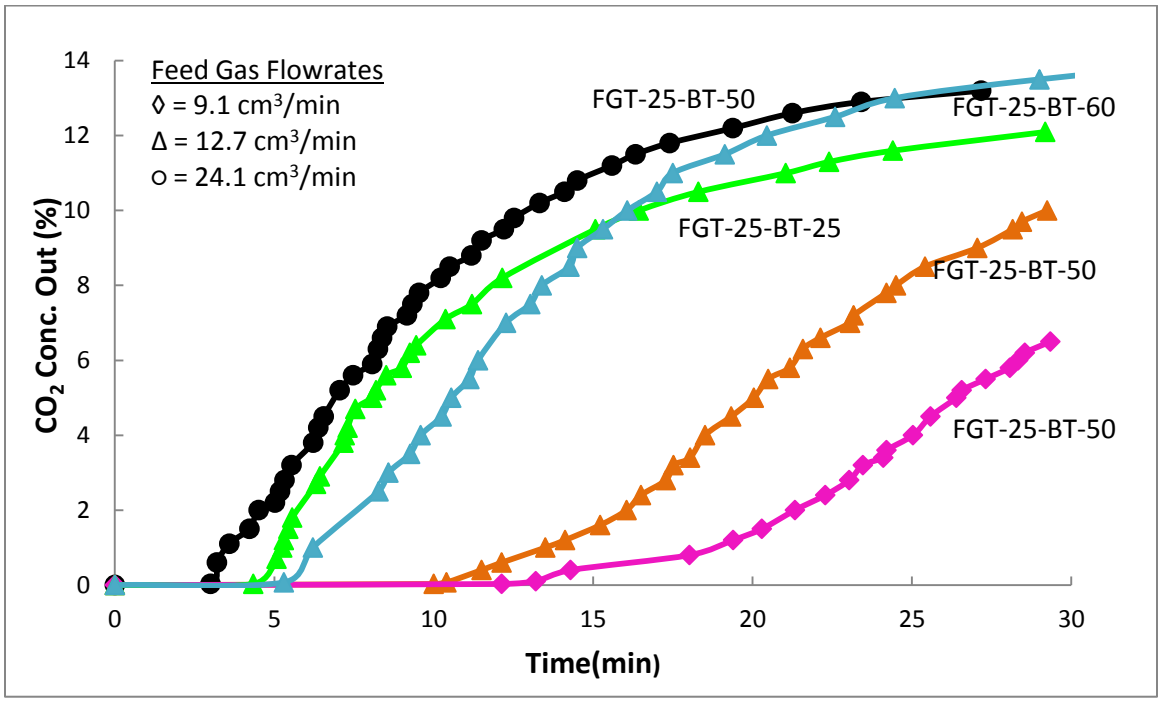

Figure 4.7 CO_2 breakthrough experiments with wet feed gas flow rates. The symbol FGT-25-BT-25: Feed gas flow rate temperature (FGT) at 25 ^{0}C with bed temperature (BT) at 50 ^{0}C.

4.4.2b CO_2 desorption from the two fiber membrane bed immobilized with 80 wt. % dendrimer in ionic liquid.

Table 4.3 summarizes the results of these experiments, where the hollow fiber bed was first saturated with the simulated dry feed gas mixture at a feed gas flow rate of 12.7 cm^3/min. A temperature swing absorption- desorption study up to 97 °C was studied in the presence of sweep helium. Desorption experiments were done with stripping temperatures of 85 °C, 90 °C, 95 °C, 97 °C. Due to the high hot water flow rate through the solid PEEK hollow fibers (380 cm^3/min), the temperature of the bed rose quickly to the desired temperature. The thermocouples at the ends of the module ensured the bed was maintained at the desired temperature. After passing hot water for 10 min, the two inlet and the outlet valves connected to the porous hollow fibers were quickly opened and a helium sweep gas stream having a flow rate of 4.78, 7.18, 12.1 cm^3/min was passed though the bore of the porous PVDF hollow fibers. The outcoming CO_2 rich sweep helium stream flow rates varied between 6.66 - 15.8 cm^3/min. Rate of CO_2 stripped (cm^3/min) $[Q_o * C_{out} - Q_{in} * 0]$ out was calculated and the values are reported in Table 4.2.

Table 4.3 Variations of temperature and sweep helium and its effect on CO_2 desorption for a 12.7 cm^3/min dry and wet (RH = 91%) feed gas flow rate

Feed Flue Gas	Bed Temperature Absorption / Desorption (°C)	Sweep He Incoming Flow Rate (cm^3/min) Q_{in}	CO_2 Concentration (%) in Sweep Helium Stream C_{out}	Sweep He Outcoming Flow Rate (cm^3/min) Q_o	Stripper CO_2 Production Rate (cm^3/min)
Dry	25/85.1 - 84.2	12.1	19.2	15.8	3.034
Dry	25/90.2 - 89.8	12.1	22.3	15.8	3.523
Dry	25/95 - 94	12.1	27.1	15.8	4.282
Dry	25/97 - 96	12.1	28	15.8	4.424
Dry	25/97 - 96	7.18	40	11.15	4.460
Wet	50/97 - 96	7.18	44.8	11.15	4.995
Wet	50/97 - 96	4.78	31	6.66	2.065
Wet	60/97 - 96	7.18	28	10.27	2.876

Temperature plays an important role in stripping out the absorbed CO_2. Table 4.3 clearly shows that the CO_2 desorption flux is increased, with an increase in the bed temperature. In runs with the stripping (bed) temperature of 85 °C, the CO_2 outlet concentration was only about 19.2 %. The low stripping (bed) temperature was not sufficient to regenerate the bed completely. Temperature has a direct effect on CO_2 equilibrium partial pressure, chemical reaction equilibrium and CO_2 diffusion coefficient.

For the desorption bed temperatures of 90 °C, 95 °C, 97 °C, the corresponding CO_2 outlet concentrations in sweep helium measured 22.3%, 27.1% and 28% respectively. Therefore, the increase in the bed temperature leads to an increase in the driving force for desorbing CO_2 from the 80 wt% dendrimer in ionic liquid sorbent. As the sweep helium flow rate was decreased from 12 to 7.18 cm^3/min, the product purity at the CO_2 outlet increased from 28 % to 40%. This is the highest value achieved in the dry feed gas experiments.

Table 4.3 also shows the results with the variation in the absorption temperature and variation in sweep helium flow for wet feed gas mixture. A highest CO_2 outlet concentration of 44.8 % in He was recorded for the feed flow rate of 12.7 cm^3/min for the absorption bed at 50 °C and desorption bed ~ 97 °C with a sweep helium flow at 7.18 cm^3/min. This CO_2 % recovery achieved with the current absorbent is higher than that reported by Plaza et al. [67], where they recovered only 40 % CO_2 for a desorption flowrate of 2.6 cm^3/min using activated carbons. Though the sweep helium flow rate was decreased to 4.8 cm^3/min, the CO_2 outlet concentration reported was only about 32 % under same operating conditions. Reduction in the sweep helium gas flow rate can also reduce the driving force for stripping CO_2 from the loaded absorbent; this is the basis for the observed reduction in the outlet concentration of CO_2.

If the volume of the internal diameter region of the PVDF hollow fiber were smaller, the partial pressure of the desorbed CO_2 would have been higher. If the fibers were longer, they would have generated more CO_2 at the outlet of the fibers ultimately a pure wave of CO_2 have driven itself out. Employing pure PAMAM instead of 80 wt% PAMAM would have improved the situation even further.

The CO_2 sorption capacities of all the above experiments were calculated from the CO_2 breakthrough curves, by integrating the area under the curve and subtracting it from the total area. Figure 4.8 shows the data interpretation from a sample breakthrough curve.

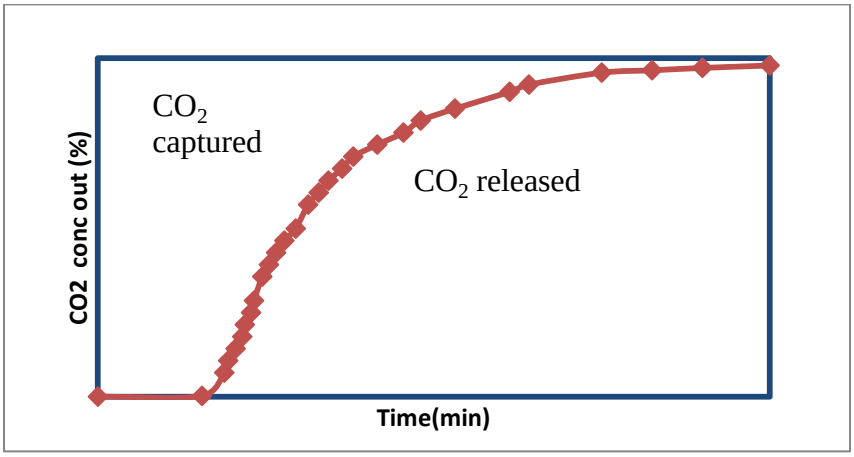

Figure 4.8 Interpretation of sorption capacities from breakthrough curve.

The volume of CO_2 captured in each experiment was calculated from which the number of mmol of CO_2 absorbed was calculated using ideal gas law. Most of the CO_2 is captured till the onset of the bed breakthrough, followed by partial capture of CO_2. Table 4.3 summarises the results of the mmol of CO_2 captured. It is clear from the table that, when the absorption temperature was at 25 °C, the time taken for the saturation of the bed was higher compared to the one with higher bed temperatures. For the feed gas flow rate 9.1 cm^3/min, the number of mmoles captured increased from 1.18 to 1.72 with the introduction of the moisture in the feed gas. The increase in the mmoles captured can mean that the already dormant tertiary amines are activated with the introduction of moisture.

For the feed gas flow rate 12.7 cm^3/min, the bed saturation time decreased with increase in temperature. At the bed temperature 25 °C, the number of millimol decreased from 1.77 to 1.02 with the introduction of moisture when using a wet humidified gas. The presence of moisture may have not helped in facilitating the reaction between CO_2 and tertiary amines at room temperature. The presence of moisture helped in increasing the mmoles from 1.23 to 1.73 for the bed temperature 50 °C. For a further increase in the bed temperature to 60 °C, the capture of number of millimol decreased to 0.92. This may be because the solubility of gases decreases with increase in temperature. Similar behavior was seen for a feed gas flow rate of 24.1 cm^3/min; similar behavior was seen with variation in absorbent bed temperatures and presence of moisture. In one experiment, the feed gas was heated to 40 °C; only 0.71 mmol of CO_2 were captured.

Based on the Happel's free surface model, only a portion of the fluid surrounding the fiber is considered for absorption purpose, this may be approximated as a circular cross section as shown in Figure 4.9. (Calculation shown in appendix)

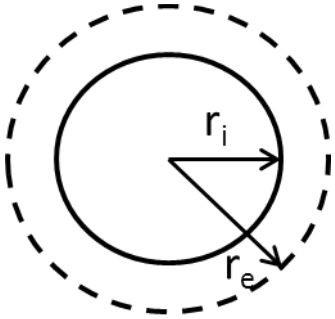

Figure 4.9 Happel's radius approximation around hollow fiber.

It is expected that the mass transfer takes place only in this portion of the fibers. Calculating the happels radius and thereby calculating the volume and amount of 80 wt%

dendrimer in ionic liquid around the hollow fiber, about 2.14 gm of the solvent is covered. Table 4.4 reports the values of mmole CO_2/g of absorbent. The sorption swing capacities vary 0.331-0.8257 mmol/g absorbent. These are the CO_2 sorption swing capacities for the saturation time upto 119 min. The swing absorption capacity reported by Lively et al. [43] using Zeolite 13-X was about 0.89 mmol/g

Table 4.4 CO_2 uptake by the two-fiber sorbent bed

Feed Gas Type	Absorption Temperature (°C)	Feed Flow Rate (cm^3/min)	Mmoles CO_2 Captured (mmol)	Time taken for Saturation (min)	Mmole of CO_2 per g Absorbent
Dry	25	9.1	1.18	119	0.551
Wet	50	9.1	1.72	103	0.803
Dry	25	12.7	1.77	105	0.827
Wet	25	12.7	1.02	78	0.476
Dry	50	12.7	1.23	58.15	0.574
Wet	50	12.7	1.73	55.58	0.808
Wet	60	12.7	0.92	35	0.429
Dry	25	24.1	1.65	70	0.771
Dry	50	24.1	1.01	24	0.471
Wet	50	24.1	1.45	40	0.677
Dry	25	24.1@40 °C	0.71	24.31	0.331

CHAPTER 5

CONCLUSIONS AND RECOMMENDATION FOR FUTURE WORK

Proof-of-concept studies on absorption-based CO_2 capture from flue gas were carried out using pure ionic liquid [bmim][DCA] and 20 wt% dendrimer solution in IL [bmim][DCA]. The parameters, e.g, simulated flue gas flow rate, absorbent liquid flow rate and stripping methods and temperature were varied to carry out a preliminary study of the process in terms of 90%> CO_2 recovery from the amount of CO_2 absorbed and considerable CO_2 removal from the feed gas. For tube-side flow of the absorbent liquid, redesigning of the hollow fiber I.D. and the material of the fiber is required to eliminate pore wetting and decrease the liquid-side pressure drop. It has been demonstrated that CO_2 from flue gas can be absorbed at a high rate in a dendrimer-IL solution and solution regeneration can be carried out at temperatures as low as 85 °C in the stripper. Variation of the CO_2 partial pressure affected CO_2 capture. As the CO_2 partial pressure increased, the capture rate increased as well since the driving force for the mass transfer increased. This value will eventually level off due to complete saturation of the absorbent liquid. High CO_2 percent recovery, 90-92% from the amount absorbed was achieved while using 20 wt% dendrimer solution in IL, [bmim] [DCA]. A study of the effect of reduced liquid flow rate on removal efficiency was not feasible since a certain liquid flow rate was needed in order to maintain needed stripping and absorption temperatures for the fixed heat transfer area and limited heat transfer coefficients.

Additional membrane area is needed for higher CO_2 removal from the feed gas for given feed gas and liquid flow rates. Lowest CO_2 concentration in the purified flue gas achieved was 4.1% which corresponds to around 70% removal. In order to achieve

higher CO_2 removal rates, feed gas flow rate, membrane area and liquid flow rate should be optimized in addition to increasing the membrane area. The CO_2 removal rate was varied by different stripping methods, e.g., helium sweep gas flow rate, vacuum level or a combination of both.

In the CO_2 capture using 80 wt% dendrimer solution in IL [bmim][DCA], CO_2 breakthrough curves in every case is not very sharp indicating the role of diffusional processes in the shell-side absorbent liquid. The thickness of the absorbent liquid on the shell side in between the two contiguous hollow fibers is considerable in the module studied; this thickness is contributing to the not-so-sharp-a-rise in the CO_2 concentration at the outlet. There were few fibers in the module; further the fiber ODs were quite large. If we had a higher packing density of the porous hollow fibers for gas absorption and the PVDF hollow fiber ODs were considerably smaller than 925 μm, the thickness of the absorbent liquid in between the contiguous porous/nonporous hollow fibers would be much reduced leading to a quicker saturation and a sharper CO_2 breakthrough.

Further in these short modules the effects of the two end-sections of the module are considerable. The gap between the individual contiguous fibers suddenly increase by an order of magnitude or more near the two module ends where the two sets of fibers are separated and are taken out through two separate inlets/outlets. Such effects can be reduced considerably when the length of the module is increased significantly. In the sets of experiments reported here, it should be clear that the module configuration used probably prevented a very large fraction of the liquid absorbent being utilized.

There are a few steps which can be implemented to substantially increase the CO_2 concentration in the stripped gas stream and therefore the partial pressure of CO_2. For a given amount of desorbed CO_2, the volume of the gas space in the bore of the porous

absorption hollow fibers should be considerably reduced. In the current hollow fiber membrane module, the porous hollow fibers for gas absorption have an ID of 691 μm; this diameter may be conveniently reduced to around 300-400 μm (these values are quite common). That will substantially increase the stripped CO_2 partial pressure. The reduction in the diameter will have other benefits. The OD of the hollow fiber will also be reduced leading to a higher surface area for gas absorption and reduced thickness of the absorbent liquid in between contiguous hollow fibers. It will lead to a better utilization of the shell-side absorbent. The breakthrough during absorption will become sharper.

One can utilize a very mild vacuum to pull out the desorbed CO_2 instead of passing a sweep helium stream. One can expect that the purity of this desorbed CO_2 stream under such a condition will be very high since the absorbent has a very high selectivity for CO_2 over N_2. One can improve the partial pressure of the stripped CO_2 even further if we employ pure dendrimer as the absorbent liquid.

APPENDIX A

EXPERIMENTAL DATA

Table A.1 Preliminary CO_2 absorption/stripping results at room temperature using water

Initial Testing was done with pure water and air as sweep gas and a single absorption MXFR#061 and a single stripping module stripping module MXFR #062

Feed gas mixture: 14.1% CO_2; 1.98% O_2/N_2 balance @ 24 °C

Liquid Flow Rate (gal/h)	Gas Flow Rate (cc/min)	Absorption module		Heat Exchanger		Sweep Gas Flow (scfh)	Vacuum (mmHg)/ He sweep (cc/min)	CO_2 Conc. Absorber Outlet (%)	CO_2 Conc. Stripper Outlet (%)
		P_i	P_{out}	P_{in} (psig)	P_{out} (psig)				
				Tube/Shell	Tube/Shell				
12.86	14.7	1.0	0.0	0.0/negative	0.0/negative	-	350/0.0	11.9	-
12.86	14.7	2.0	1.0	1.0/negative	0.5/negative	10.0	-	5.	0.01
12.74	7.50	5.0	3.5	3.5/1.5	3.0/0.5	26.0	-	3.	-
12.86	14.7	2.0	1.0	1.0/negative	0.5/negative	-	Full vacuum/ 15.0	5. 2	5.5

Table A.2 CO_2 absorption/stripping results at room temperature using pure water as absorption liquid at room temperature

Initial Testing was done with pure water and air as sweep gas and single absorption and stripping modules MXFR#061 and MXFR#62

Feed gas mixture: 14.1% CO_2; 1.98% O_2/N_2 balance @ 24°C.

Liquid Flow Rate (gal/h)	Gas Flow Rate (cc/min)	Absorption module		Heat Exchanger		Sweep Gas Flow (cc/min)	CO_2 Conc. Absorber Outlet (%)	CO_2 Conc. Stripper Outlet (%)
		P_{in} (psig)	P_{out} (psgi)	P_{in} (psig)	P_{out} (psig)			
				Tube/Shell	Tube/Shell			
12.74	7.3	4.0	3.0	3.0/1.0	2.0/0.0	35.0	3.3	-
12.99	14.7	3.0	2.0	2.0/0.0	2.0/0.0	25.0	6.4	-
12.74	7.5	5.0	3.0	3.5/1.5	3.0/0.5	26.5	3.6	-
12.74	7.5	3.0	2.0	2.0/0.0	1.5/0.1	30.0	4.1	-

Table A.2 CO_2 absorption/stripping results at room temperature using pure water as absorption liquid at room temperature (continued)

Feed Gas mixture + He sweep gas + Water @ 24°C								
Liquid Flow Rate (gal/h)	Gas Flow Rate (cc/min)	Absorption module		Heat Exchanger		Sweep Gas Flow (cc/min)	CO_2 Conc. Absorber Outlet (%)	CO_2 Conc. Stripper Outlet (%)
		P_{in} (psig)	P_{out} (psig)	P_{in} (psig)	P_{out} (psig)			
				Tube/Shell	Tube/Shell			
12.9	14.7	4.5	3.2	3.2/1.0	3.0/0.5	60.0	6.0	-
12.9	14.9	4.0	3.0	3.0/1.0	2.5/1.0	66.0	6.1	-

Feed Gas mixture + Sweep Gas + Vacuum Stripping @ 24°C Vacuum at 500mm Hg (12.74 gal/hr) and 720 mm Hg (12.86 gal/hr)								
Liquid Flow Rate (gal/h)	Gas Flow Rate (cc/min)	Absorption module		Heat Exchanger		Sweep Gas Flow (cc/min)	CO_2 Conc. Absorber Outlet (%)	CO_2 Conc. Stripper Outlet (%)
		P_{in} (psig)	P_{out} (psig)	P_{in} (psig)	P_{out} (psig)			
				Tube/Shell	Tube/Shell			
12.7	14.9	1.0	0.0	Negative	0.0	15.0	-	1.6
12.9	14.9	2.0	1.0	Negative	0.0	15.0	-	1.6

Feed Gas mixture + He sweep gas + Water @ 24°C								
Liquid Flow Rate (gal/h)	Gas Flow Rate (cc/min)	Absorption module		Heat Exchanger		Sweep Gas Flow (cc/min)	CO_2 Conc. Absorber Outlet (%)	CO_2 Conc. Stripper Outlet (%)
		P_{in} (psig)	P_{out} (psig)	P_{in} (psig)	P_{out} (psig)			
				Tube/Shell	Tube/Shell			
12.9	14.7	4.5	3.2	3.2/1.0	3.0/0.5	60.0	6.0	-
12.9	14.9	4.0	3.0	3.0/1.0	2.5/1.0	66.0	6.1	-

Table A.3 CO_2 absorption/stripping results at room temperature using 16 wt% dendrimer solution in water as absorption liquid at room temperature

Feed gas + 16.6% (wt) dendrimer + Vacuum stripping @ 23°C Vacuum 20 mm Hg								
Liquid Flow Rate (gal/h)	Gas Flow Rate (cc/min)	Absorption module		Heat Exchanger		Sweep Gas Flow (cc/min)	CO_2 Conc. Absorber Outlet (%)	CO_2 Conc. Stripper Outlet (%)
		P_{in} (psig)	P_{out} (psig)	P_{in} (psig)	P_{out} (psig)			
				Tube/Shell	Tube/Shell			
12.0	14.7	6.0	2.5	2.5/0.0	2.0/negative	-	3.0	9.0

Note: Excessive water condensation in vacuum trap was observed

Feed Gas + 16.6% (wt) dendrimer solution @ 24°C								
Liquid Flow Rate (gal/h)	Gas Flow Rate (cc/min)	Absorption module		Heat Exchanger		Sweep Gas Flow (cc/min)	CO_2 Conc. Absorber Outlet (%)	CO_2 Conc. Stripper Outlet (%)
		P_{in} (psig)	P_{out} (psig)	P_{in} (psig)	P_{out} (psig)			
				Tube/Shell	Tube/Shell			
0.98	14.9	6.0	5.5	5.5/5.0	5.0/4.0	14.4	2.0	-

Feed gas mixture+ Sweep Gas + 16.6% (wt) dendrimer @22.5° Exit Gas: 93.8 cc/min								
Liquid Flow Rate (gal/h)	Gas Flow Rate (cc/min)	Absorption module		Heat Exchanger		Sweep Gas Flow (cc/min)	CO_2 Conc. Absorber Outlet (%)	CO_2 Conc. Stripper Outlet (%)
		P_{in} (psig)	P_{out} (psig)	P_{in} (psig)	P_{out} (psig)			
				Tube/Shell	Tube/Shell			
12.0	102.0	6.0	3.0	3.0/0.0	2.0/0.0	125.0	11.8	3.6

Table A.4 CO_2 absorption/stripping results with pure [bmim][DCA] as absorption liquid and Helium sweep gas at room temperature

Inlet Feed gas composition: 14%CO_2/2% O_2/N_2 balance + ++ Sweep He gas									
Feed Gas Flow Rate		Liquid Flow Rate (gal/h)		Heat Exchanger Pressure (psig)		Heat Exchanger Temp. (°C)		Vacuum (mmHg)	Sweep Gas Flow Rate (cc/min)
In	Out	Pump I	Pump II	Tube In/Out)	Shell (In/Out)	Tube In/Out)	Shell (In/Out)		
3.54	3.13	0.36	-	1.0/0.5	0/0	At 20 °C		-	31.13
Absorption CO_2 Con. In (%)		Absorption CO_2 Con. Out		CO_2 Con. In Vacuum		CO_2 Com. He Sweep		CO_2 Com. Combo (%)	
14.1		9.32		-		0.50		-	

Calculation:

Absorber out (recorded in Quantek): 9.32 %

% CO_2 absorbed =>14.1-9.32 = 4.78%

Rate of CO_2 absorption => (4.78/100)*3.54 = 0.169 cc/min

Stripper:

Sweep He flow rate = 31.13 cc/min

% CO_2 reported from GC = 0.5024 %

Flowrate of CO_2 in Sweep Helium => 31.13*(0.5024/100) = 0.1564 cc/min.

CO_2 % recovery from the amount absorbed: (0.1564/0.169)*100 = 92.5%

Table A.5 CO_2 absorption/stripping results with pure [bmim][DCA] as absorption liquid and Helium sweep gas at room temperature

Inlet Feed gas composition: 14%CO_2/2% O_2/N_2 balance + [bmim][DCA]+ Sweep He gas										
Feed Gas Flow Rate		Liquid Flow Rate		Heat Exchanger Pressure (psig)		Heat Exchanger		Vacuum (mmHg)	Sweep Gas Flow Rate (cc/min)	Absorption In (psig)
In	Out	Pump I	Pump II	Tube In/Out)	Shell (In/Out)	Tube In/Out)	Shell (In/Out)			
9.6	8.9	0.24	-	0.5/0	0/0	At 20 °C		-	62.9	11
Absorption CO_2 Con. In		Absorption CO_2 Con. Out		CO_2 Con. In Vacuum		CO_2 Com. He Sweep		CO_2 Com. Combo (%)		Out (psi)
14.1		12.5		-		0.24		-		0.5

Calculation:

Absorber out (recorded in Quantek): 12.5 %;

% CO_2 absorbed =>14.1-12.5 =1.6 %

Rate of CO_2 absorption => (1.6/100)*9.6 = 0.153 cc/min

Stripper:

Sweep He flow rate = 62.9 cc/min

% CO_2 reported from Quantek = 0.24 %

Flow rate of CO_2 in Sweep Helium => 62.9*(0.24/100) = 0.150 cc/min.

CO_2 % recovery from the amount absorbed: (0.150/0.153)*100 = 98%

Table A.6 CO_2 absorption/stripping results with pure [bmim][DCA] as absorption liquid and Helium sweep gas at room temperature

Inlet Feed gas composition: 14%CO_2/2% O_2/N_2 balance + [bmim][DCA]+ Sweep He gas @ at 23.5 °C									
Feed Gas FlowRate (cc/min)		Liquid FlowRate (gal/h)		Heat Exchanger Pressure (psgi)		Heat Exchanger Temp. (°C)		Vacuum (mmHg)	Sweep Gas Flow Rate (cc/min)	Absorption module
In	Out	Pump I	Pump II	Tube In/Out)	Shell (In/Out | Tube In/Out)	Shell (In/Out)			In (psig)
3.57	-	0.3	-	1.0/0.0	0.0/0.0	At 23.5 °C		-	60.0	10.0
Absorption CO_2 Con. In		Absorption CO_2 Con. Out		CO_2 Con. In Vacuum		CO_2 Com. He Sweep		CO_2 Com. Combo (%)		Out (psi)
14.1		10.7		-		0.07		-		1.0

Table A.7 CO_2 absorption/stripping results with pure [bmim] [DCA] as absorption liquid and Helium sweep gas at elevated temperature

Inlet Feed gas composition: 14%CO_2/2% O_2/N_2 balance + [bmim][DCA]+ Sweep He gas										
Feed Gas Flow Rate (cc/min)		Liquid Flow Rate (gal/h)		Heat Exchanger Pressure (psi)		Heat Exchanger Temp. (°C)		Vacuum (mmHg)	Sweep Gas Flow Rate (cc/min)	Absorption module
In	Out	Pump I	Pump II	Tube (In/Out)	Shell (In/Out)	Tube (In/Out)	Shell (In/Out)			In (psig)
18.16	16.4	4.41	-	2.0/1.5	0/0	48.3/75.4	89.3/51.9	-	23.24	5.0/2.0
Absorption CO_2 Con. In (%)		Absorption CO_2 Con. Out (%)		CO_2 Con. In Vacuum (%)		CO_2 Com. He Sweep (%)		CO_2 Com. Combo (%)		$\frac{\#Module_{abs}}{\#Module_{str}}$
14.1		6.25		-		5.47		-		(63+65)/(72+70

Notes:

This experiment has two absorption and two stripper modules. Temperature of Ionic liquid at the inlet of two absorber modules: 52.4°C

Temperatures of Ionic liquid at the inlet/outlet of two stripping modules: 79.5°C/74.8°C

Calculations:

Rate of CO_2 absorption:

(14.1x18.16)/100 – (6.25x16.4)/100 => 2.56-1.025 = 1.535 cc/min

Flow rate of CO_2 from the Stripper modules: (23.24x5.475)/100 = 1.272 cc/min

CO_2 % recovery from the amount absorbed: (1.272/1.535)x100 = 82.89 %

Table A.7 Continued

Inlet Feed gas composition: 14%CO_2/2% O_2/N_2 balance + [bmim][DCA]+ Sweep He gas										
Feed Gas Flow Rate		Liquid Flow Rate		Heat Exchanger Pressure (psig)		Heat Exchanger Temp. (°C)		Vacuum (mmHg)	Sweep Helium Gas Flow Rate (cc/min)	Absorption Module(psig) (In/Out)
In	Out	Pump I	Pump II	Tube (In/Out)	Shell (In/Out)	Tube (In/Out)	Shell (In/Out)			
29.64	-	4.28	-	4/3	2/1.5	47.8/60.6		-	23.24	7/4
Absorption CO_2 Conc. In (%)		Absorption CO_2 Conc. Out (%)		CO_2 Conc. In Vacuum (%)		CO_2 Com. He Sweep (%)		CO_2 Com. Combo (%)		$\frac{\#Module_{abs}}{\#Module_{str}}$
14.1		7.03		-		6.20		-		(63+65)/ (72+70)

Calculation:

Absorber out (recorded in Quantek): 7.03 % ;

% CO_2 absorbed =>14.1-7.03 =7.07 %

Rate of CO_2 absorption => (7.07 /100)*29.64= 2.078cc/min

Stripper:

Sweep He flow rate = 23.24 cc/min

% CO_2 reported from GC = 6.20 %

Flow rate of CO_2 in Sweep Helium => 23.24*(6.20/100) = 1.44 cc/min

CO_2 % recovery from the amount absorbed: (1.44/2.078)*100 = 69.2%

Table A.7 Continued

Inlet Feed gas composition: 14%CO_2/2% O_2/N_2 balance + [bmim][DCA]+ Sweep He gas										
Feed Gas Flow Rate		Liquid Flow Rate		Heat Exchanger Pressure (psig)		Heat Exchanger Temp. (°C)		Vacuum (mmHg)	Sweep Helium Gas Flow Rate (cc/min)	Absorption Module(psig) (In/Out)
In	Out	Pump I	Pump II	Tube (In/Out)	Shell (In/Out)	Tube (In/Out)	Shell (In/Out)			
32.48	30.18	4.16	-	1.5/1.0	0.0/0.0	49.6/72.3		-	23.24	6.0/1.5
Absorption CO_2 Conc. In		Absorption CO_2 Conc. Out		CO_2 Conc. In Vacuum		CO_2 Com. He Sweep		CO_2 Com. Combo (%)		#Module$_{abs}$ / #Module$_{str}$
14.1		9.40		-		6.25		-		(63+65)/ (72+70)

Notes:

This experiment has two absorption and two stripper modules. Temperature of Ionic liquid at the inlet of two absorber modules: 52.6°C.

Temperatures of Ionic liquid at the inlet/outlet of two stripping modules: 78.1°C/74.7°C

Calculations:

Rate of CO_2 absorption:

(14.1x32.48)/100 – (30.18x9.4)/100 => 4.57-2.83= 1.74 cc/min

Flow rate of CO_2 from the Stripper modules: (23.24x6.25)/100 = 1.45 cc/min

CO_2 % recovery from the amount absorbed: (1.45/1.74)x100= 83.5%

Table A.7 Continued

Inlet Feed gas composition: 14%CO_2/2% O_2/N_2 balance + [bmim][DCA]+ Sweep He gas									
Feed Gas Flow Rate (cc/min)		Liquid Flow Rate (gal/h)		Heat Exchanger Pressure (psig)		Heat Exchanger Temp. (°C)		Vacuum (mmHg)	Sweep Helium Gas Flow Rate (cc/min)	Absorption Module (psig)
In	Out	Pump I	Pump II	Tube (In/Out)	Shell (In/Out)	Tube (In/Out)	Shell (In/Out)			(In/Out)
31.89	28.62	4.16	-	1.5/1.0	0.0/0.0	49.6/73.5		-	23.24	6.0/1.5
Absorption CO_2 Conc. In (%)		Absorption CO_2 Conc. Out (%)		CO_2 Conc. In Vacuum (%)		CO_2 Com. He Sweep (%)		CO_2 Com. Combo (%)		$\frac{\#Module_{abs}}{\#Module_{str}}$
14.1		9.68		-		6.42		-		(63+65)/ (72+70)

Notes:

This experiment has two absorption and two stripper modules. Temperature of Ionic liquid at the inlet of two absorber modules: 50.7°C.

Temperatures of Ionic liquid at the inlet/outlet of two stripping modules: 78.9°C/74.6°C.

Calculations:

Rate of CO_2 absorption:

(14.1x31.89)/100 – (28.62x9.68)/100 => 4.49-2.77=1.719 cc/min

Flow rate of CO_2 from the Stripper modules: (23.24x6.42)/100 = 1.49 cc/min

CO_2 % recovery from the amount absorbed: (1.49/1.719)x100= 86.6%

Table A.7 Continued

Inlet Feed gas composition: 14%CO_2/2% O_2/N_2 balance + [bmim][DCA]+ Sweep He gas									
Feed Gas Flow Rate (cc/min)		Liquid Flow Rate (gal/h)		Heat Exchanger Pressure (psig)		Heat Exchanger Temp. (°C)		Vacuum (mmHg)	Sweep Helium Gas Flow Rate (cc/min)	Absorption Module (psig)
In	Out	Pump I	Pump II	Tube (In/Out)	Shell (In/Out)	Tube (In/Out)	Shell (In/Out)			(In/Out)
10.91	9.88	4.26	-	2.0/1.0	0.0/0.0	49.6/72.3		-	23.24	7.0/2.0
Absorption CO_2 Conc. In		Absorption CO_2 Conc. Out		CO_2 Conc. In Vacuum		CO_2 Com. He Sweep		CO_2 Com. Combo (%)		$\frac{\#Module_{abs}}{\#Module_{str}}$
14.1		5.2		-		4.6		-		(63+65)/ (72+70)

Notes:

This experiment has two absorption and two stripper modules. Temperature of Ionic liquid at the inlet of two absorber modules: 50.1°C.

Temperatures of Ionic liquid at the inlet/outlet of two stripping modules: 80.1°C/71.4°C.

Calculations:

Rate of CO_2 absorption:

(14.1x10.91)/100 – (5.2x9.88)/100 => 1.53-0.513= 1.017 cc/min

Flow rate of CO_2 from the Stripper modules: (23.24x4.6)/100 = 1.069 cc/min

CO_2 % recovery from the amount absorbed: 1.069/1.017 ≥ 100

Table A.8 CO_2 absorption/stripping results with pure [bmim][DCA] as absorption liquid with vacuum and Helium sweep gas at room temperature

CO_2 Absorption-Stripping performance with pure IL [bmim][DCA] at 20 °C with Sweep He gas + vacuum									
Feed Gas Flow Rate (cc/min)		Liquid Flow Rate (gal/h)		Heat Exchanger Pressure (psig)		Heat Exchanger Temp. (°C)		Vacuum (mmHg)	Sweep Gas Flow Rate (cc/min)	Absorption Module Pressure(psig
In	Out	Pump I	Pump II	Tube In/Out)	Shell (In/Out)	Tube (In/Out)	Shell (In/Out)			(In/Out)
3.54	2.49	0.42	-	0/0	-	At 20°C		13.9	62.91	10/0
Absorption CO_2 Conc. In		Absorption CO_2 Conc. Out		CO_2 Conc. In Vacuum (%)		CO_2 Com. He Sweep		CO_2 Com. Combo (%)		#Module$_{abs}$ #Module$_{str}$
14.1		7.61		-		-		0.25 (using GC)		064/067

Notes:

The Sweep He gas was connected at the vacuum out in the combo mode.

Calculation:

Absorber out (recorded in Quantek): 7.61 % ;

% CO_2 absorbed =>14.1-7.61 =6.49 %

Rate of CO_2 absorption => (6.49 /100)*3.54= 0.229 cc/min

Stripper:

Sweep He flow rate = 62.9 cc/min

% CO_2 reported from GC = 0.256 %

Flow rate of CO_2 in Sweep Helium => 62.9*(0.256/100) = 0.161 cc/min

CO_2 % recovery from the amount absorbed: (0.161/0.229)*100 = 70.3%

Table A.9 CO_2 absorption/stripping results with pure [bmim][DCA] as absorption liquid with vacuum at room temperature.

CO_2 Absorption-Stripping performance with pure IL [bmim][DCA] at 20 °C with vacuum										
Feed Gas Flow Rate (cc/min)		Liquid Flow Rate (gal/h)		Heat Exchanger Pressure (psig)		Heat Exchanger Temp. (°C)		Vacuum (mmHg)	Sweep Gas Flow Rate (cc/min)	Absorption Module Pressure(psig
In	Out	Pump I	Pump II	Tube In/Out)	Shell (In/Out)	Tube (In/Out)	Shell (In/Out)			(In/Out)
3.54	2.79	0.36	-	0.5/0.0	0.0/0.0	At 20°C		15.3	-	12/0.5
Absorption CO_2 Conc. In		Absorption CO_2 Conc. Out		CO_2 Conc. In Vacuum (%)		CO_2 Com. He Sweep		CO_2 Com. Combo (%)		$\frac{\#Module_{abs}}{\#Module_{str}}$
14.1		10.15		9.5		-		-		064/067

CO_2 Absorption-Stripping performance with pure IL [bmim][DCA] at 20 °C with vacuum										
Feed Gas Flow Rate (cc/min)		Liquid Flow Rate (gal/h)		Heat Exchanger Pressure (psig)		Heat Exchanger Temp. (°C)		Vacuum (mmHg)	Sweep Gas Flow Rate (cc/min)	Absorption Module Pressure(psig)
In	Out	Pump I	Pump II	Tube (	Shell (In/Out)	Tube (In/Out)	Shell (In/Out)			(In/Out)
3.54	2.55	0.61/0.36	-	0.5/0.0	0.0/0.0	At 20°C		16.3	-	11/0.5
Absorption CO_2 Conc. In		Absorption CO_2 Conc. Out		CO_2 Conc. In Vacuum (%)		CO_2 Com. He Sweep		CO_2 Com. Combo (%)		$\frac{\#Module_{abs}}{\#Module_{str}}$
14.1		9.34		5.8		-		-		064/067

Table A.10 CO_2 absorption/stripping results with 20 wt% dendrimer solution in [bmim][DCA] solution as absorption liquid and Helium sweep gas at elevated temperature.

CO_2 Absorption-Stripping performance 20 wt% dendrimer solution in [bmim][DCA] at elevated temperature with									
Feed Gas Flow Rate (cc/min)		Liquid Flow Rate (gal/h)		Heat Exchanger Pressure (psig)		Heat Exchanger Temp. (°C)		Vacuum (mmHg)	Sweep Gas Flow Rate (cc/min)	Absorption Module Pressure(psig)
In	Out	Pump I	Pump II	Tube In/Out)	Shell (In/Out)	Tube (	Shell (In/Out)			(In/Out)
45.5	40.7	2.57	-	1.5/1.0	0.0/0.0	52.3/80.6		-	23.24	3.0/1.5
Absorption CO_2 Conc. In		Absorption CO_2 Conc. Out		CO_2 Conc. In Vacuum (%)		CO_2 Com. He Sweep		CO_2 Com. Combo (%)		$\frac{\#Module_{abs}}{\#Module_{str}}$
14.1		1.40		-		1.72		-		(69+66)/(70+72

Notes:

This experiment has two absorption and two stripper modules. Temperature of Ionic liquid at the inlet of two absorber modules: 59.1°C

Temperatures of Ionic liquid at the inlet/outlet of two stripping modules: 75.7°C/62.4°C

Calculations:

Rate of CO_2 absorption:

(14.1x45.5)/100 – (40.7x1.4)/100 => 6.41-0.56 = 5.84 cc/min

Flow rate of CO_2 from the stripper modules:

(23.24 x 5.475)/100 = 1.272 cc/min

CO_2 % recovery from the amount absorbed: (0.399/5.84)x100= 6.83%

Sweep gas flow rate was increased for better stripping of CO_2 and better recovery.

Table A.10 Continued

CO_2 Absorption-Stripping performance with 20 wt% dendrimer solution in [bmim][DCA] at elevated temperature with										
Feed Gas Flow Rate (cc/min)		Liquid Flow Rate (gal/h)		Heat Exchanger Pressure (psig)		Heat Exchanger Temp. (°C)		Vacuum (mmHg)	Sweep Gas Flow Rate (cc/min)	Absorption Module Pressure(psig)
In	Out	Pump I	Pump II	Tube In/Out)	Shell (In/Out)	Tube (In/Out)	Shell (In/Out)			(In/Out)
54.08	49.2	2.57	-	2.0/1.5	0.0/0.0	52.2/83.9	80.8/52.	-	78.87	4.0/2.0
Absorption CO_2 Conc. In		Absorption CO_2 Conc. Out		CO_2 Conc. In Vacuum (%)		CO_2 Com. He Sweep		CO_2 Com. Combo (%)		$\frac{\#Module_{abs}}{\#Module_{str}}$
14.1		4.1		-		3.93 (GC)		-		(69+66)/(70+72

Notes:

This experiment has two absorption and two stripper modules. Temperature of Ionic liquid at the inlet of two absorber modules: 58.8°C

Temperatures of Ionic liquid at the inlet/outlet of two stripping modules: 79.5°C/61.1°C

Calculations:

Rate of CO_2 absorption:

(14.1x54.05)/100 – (4.1x49.2)/100 => 7.62-2.01= 5.6 cc/min

Flow rate of CO_2 from the Stripper modules: (3.93x78.87)/100 = 3.09cc/min

CO_2 % recovery from the amount absorbed: (3.09/5.60)x100= 55.17%

Table A.10 Continued

CO_2 Absorption-Stripping performance with 20 wt% dendrimer solution in [bmim][DCA] at elevated temperature with Sweep He gas										
Feed Gas Flow Rate (cc/min)		Liquid Flow Rate (gal/h)		Heat Exchanger Pressure (psig)		Heat Exchanger Temp. (°C)		Vacuum (inch Hg)	Sweep Gas Flow Rate (cc/min)	Absorption Module Pressure(psig)
In	Out	Pump I	Pump II	Tube In/Out)	Shell (In/Out	Tube (In/Out)	Shell (In/Out)			(In/Out)
54.08	49.2	2.57	-	2.5/2.0	0.0/0.0	50.7/80.0		-	78.87	4.5/2.5
Absorption CO_2 Conc. In (%)		Absorption CO_2 Conc. Out (%)		CO_2 Conc. In Vacuum (%)		CO_2 Com. He Sweep		CO_2 Com. Combo (%)		$\frac{\#Module_{abs}}{\#Module_{str}}$
14.1		4.5		-		3.4 (Analyzer)		-		(69+66)/ (70+72)

Notes:

Temperature of Ionic liquid at the inlet of two absorber modules: 57.8°C

Temperatures of Ionic liquid at the inlet/outlet of two stripping modules: 78.1°C/63.6°C

Calculations:

Rate of CO_2 absorption:

(14.1x54.08)/100 – (4.5x49.2)/100 => 7.62-2.21=5.40 cc/min

Flow rate of CO_2 from the Stripper modules: (3.4x78.87)/100 = 2.68 cc/min

CO_2 % recovery from the amount absorbed: (2.68/5.40)x100= 49.6%

Table A.10 Continued

CO_2 Absorption-Stripping performance with 20 wt% dendrimer solution in [bmim][DCA] at elevated temperature with Sweep He gas										
Feed Gas Flow Rate (cc/min)		Liquid Flow Rate (gal/h)		Heat Exchanger Pressure (psig)		Heat Exchanger Temp. (°C)		Vacuum (inch Hg)	Sweep Gas Flow Rate (cc/min)	Absorption Module Pressure(psig)
In	Out	Pump I	Pump II	Tube (	Shell (In/Out	Tube (	Shell (In/Out)			(In/Out)
54.08	49.2	2.57	-	3.5/2.5	0.0/0.0	52.3/80.6		-	47.84	6.0/3.5
Absorption CO_2 Conc. In		Absorption CO_2 Conc. Out		CO_2 Conc. In Vacuum (%)		CO_2 Com. He Sweep		CO_2 Com. Combo (%)		$\frac{\#Module_{abs}}{\#Module_{str}}$
14.1		5.4		-		5.66 (Analyser)		-		(69+66)/(70+72)

Notes:

This experiment has two absorption and two stripper modules. Temperature of Ionic liquid at the inlet of two absorber modules: 59.1°C.

Temperatures of Ionic liquid at the inlet/outlet of two stripping modules: 77.2°C/64.2°C

Calculations:

Rate of CO_2 absorption:

(14.1x54.08)/100 – (5.4x49.2)/100 => 7.62-2.65 = 4.97 cc/min

Flow rate of CO_2 from the Stripper modules: (5.66x47.84)/100 = 2.70cc/min

CO_2 % recovery from the amount absorbed: (2.70/4.97)x100= 54.36%

Table A.11 CO_2 absorption/stripping results with 20 wt% dendrimer solution in [bmim][DCA] solution as absorption liquid and vacuum at elevated temperature using dry feed gas.

CO_2 Absorption-Stripping performance with 20 wt% dendrimer solution in [bmim][DCA] at elevated temperature with vacuum and dry feed gas										
Feed Gas Flow Rate (cc/min)		Liquid Flow Rate (gal/h)		Heat Exchanger Pressure (psig)		Heat Exchanger Temp. (°C)		Vacuum (inch Hg)	Sweep Gas Flow Rate (cc/min)	Absorption Module Pressure(psig)
In	Out	Pump I	Pump II	Tube (	Shell (In/Out	Tube (	Shell (In/Out)			(In/Out)
54.08	49.2	4.41	-	4.0/2.0	0.0 /0.0	47.4/86.7		29.0	-	6.0/4.0
Absorption CO_2 Conc. In		Absorption CO_2 Conc. Out		CO_2 Conc. In Vacuum (%)		CO_2 Com. He Sweep		CO_2 Com. Combo (%)		$\frac{\#Module_{abs}}{\#Module_{str}}$
14.1		5.29 (GC)/5,35 (Quantek)		82.0 (GC)/85.45 (Quantek)		-		-		(69+66)/(70+72)

Notes:

Calculations:

By Analyzer:

Rate of CO_2 absorption:

(14.1x54.08)/100 – (5.29x49.2)/100 => 7.62-2.60= 5.0 cc/min

Flow rate of CO_2 from the Stripper modules: (6.08x 85.45)/100 = 5.1cc/min

CO_2 % recovery from the amount absorbed: (5.1/5.0)x100= 102%

By GC:

Calculations:

Rate of CO_2 absorption:

(14.1x54.08)/100 – (5.35x49.2)/100 => 7.62-2.65= 4.99cc/min

Flow rate of CO_2 from the Stripper modules:

% CO_2 = 82%

(6.08x 82)/100 = 4.98cc/min

CO_2 % recovery from the amount absorbed: (4.98/4.99)x100= 99.7%

Table A.11 Continued

CO_2 Absorption-Stripping performance with 20 wt% dendrimer solution in [bmim][DCA] at elevated temperature with vacuum and dry feed gas										
Feed Gas Flow Rate (cc/min)		Liquid Flow Rate (gal/h)		Heat Exchanger Pressure (psig)		Heat Exchanger Temp. (°C)		Vacuum (inch Hg)	Sweep Gas Flow Rate (cc/min)	Absorption Module Pressure(psig)
In	Out	Pump I	Pump II	Tube (	Shell (In/Out	Tube (	Shell (In/Out			(In/Out)
98.4	94.63	4.41	-	4.5/2.5	0.0 /0.0	48.4/88.2		28.4	-	6.5/4.5
Absorption CO_2 Conc. In		Absorption CO_2 Conc. Out		CO_2 Conc. In Vacuum (%)		CO_2 Com. He Sweep		CO_2 Com. Combo (%)		#Module$_{abs}$ #Module$_{str}$
14.1		7.57 (GC)/7.91 (Quantek)		86.26 (GC)/94.63 (Quantek)		-		-		(69+66)/(70+72)

Notes:

Calculation:

By GC

Rate of CO_2 absorption:

(14.1x98.4)/100 – (94.63x7.91)/100 => 13.87-7.48 = 6.38 cc/min

Flow rate of CO_2 from the Stripper modules: (86.26x6.43)/100 = 5.54 cc/min

CO_2 % recovery from the amount absorbed: (5.54/6.38)x100= 86.8%

By Analyzer

Rate of CO_2 absorption:

(14.1x98.4)/100 – (94.63x7.57)/100 => 13.87-7.16 = 6.71 cc/min

Flow rate of CO_2 from the Stripper modules: (89.9x6.43)/100 = 5.78 cc/min

CO_2 % recovery from the amount absorbed: (5.78/6.71)x100= 86.1 cc/min.

Table A.12 CO_2 absorption/stripping results with 20 wt% dendrimer solution in [bmim][DCA] solution as absorption liquid and vacuum at elevated temperature using humidified feed gas.

CO_2 Absorption-Stripping performance with 20 wt% dendrimer solution in [bmim][DCA] at elevated temperature with vacuum and humidified feed gas									
Feed Gas Flow Rate (cc/min)		Liquid Flow Rate (gal/h)		Heat Exchanger Pressure (psig)		Heat Exchanger Temp. (°C)		Vacuum (inHg)	Sweep Gas Flow Rate (cc/min)	Absorption Module Pressure(psig)
In	Out	Pump I	Pump II	Tube (	Shell (In/Out	Tube (	Shell (In/Out)			(In/Out)
155.1	145.2	4.16	-	7.0/5.0	0.5 /0.0	46.8/81.1		28.6	-	9.0/7.0
Absorption CO_2 Conc. In		Absorption CO_2 Conc. Out		CO_2 Conc. In Vacuum (%)		CO_2 Com. He Sweep		CO_2 Com. Combo (%)		$\frac{\#Module_{abs}}{\#Module_{str}}$
14.1		7.67		91.6		-		-		(69+66)/ (70+72)

Table A.12 Continued

CO_2 Absorption-Stripping performance with 20 wt% dendrimer solution in [bmim][DCA] at elevated temperature with vacuum and humidified feed gas										
Feed Gas Flow Rate (cc/min)		Liquid Flow Rate (gal/h)		Heat Exchanger Pressure (psig)		Heat Exchanger Temp. (°C)		Vacuum (inHg)	Sweep Gas Flow Rate (cc/min)	Absorption Module Pressure(psig)
In	Out	Pump I	Pump II	Tube (In/Out)	Shell (In/Out	Tube (In/Out)	Shell (In/Out)			(In/Out)
155.1	145.2	4.16	-	7.0/5.0	0.5 /0.0	48.0/85.5		28.8	-	9.0/7.0
Absorption CO_2 Conc. In		Absorption CO_2 Conc. Out		CO_2 Conc. In Vacuum (%)		CO_2 Com. He Sweep		CO_2 Com. Combo (%)		$\frac{\#Module_{abs}}{\#Module_{str}}$
14.1		7.32 (GC)/8.3 (Quantek)		91.5 (GC)/92.5 (Quantek)		-		-		(63+71)/(70+72)

Calculation:

By GC

Rate of CO_2 absorption:

(14.1x155.1)/100 – (145.17x7.32)/100 => 21.86-10.62 = 11.24 cc/min

Flowrate of CO_2 from the Stripper modules: (91.5x11.03)/100 = 10.09 cc/min

CO_2 % recovery from the amount absorbed: (10.09/11.24)x100= 89.7%

By Analyzer

Rate of CO_2 absorption:

(14.1x155.1)/100 – (145.17x8.27)/100 => 21.86-12.00 = 9.86 cc/min

Flow rate of CO_2 from the Stripper modules: (92.5x11.03)/100 = 10.2 cc/min

CO_2 % recovery from the amount absorbed: (10.2/9.86)x100= 103%

APPENDIX B

B.1 Overall mass transfer coefficient calculation

For the case with 20% dendrimer+ IL DCA+ moisture:

Feed flow rate: 157.8 cm^3/min

Feed in (% CO_2): 14.1

Feed out (% CO_2): 7.2

Total Pressure (P_t) = 1 atm

Temperature: 298K

Membrane Area: 2 x 521.8 =1043.6 cm^2

Gas Constant: 82.05 $\frac{cm^3\ atm}{K\ gmol}$

Calculating the molar CO_2 Flux:

$y^{in}_{co_2}$ = 0.14 (mole fraction of CO_2 in feed flue gas)

$y_{co_2}^{out}$ =0.072 (mole fraction of CO_2 in treated flue gas)

$N_{co_2} = \frac{Q_g (C_{co_{2,in}} - C_{co_{2,out}})}{A}$ = Molar flux of CO_2

Conc. Of CO_2 in: $C_{co_{2,in}} = p_{co_2} / RT$

$= y^{in}_{co_2} \times P_t / RT$

$= 0.14 \times 1/ (82.05 \times 298)$

$= 5.72 \times 10^{-6}$ gmol/cm^3

Conc. Of CO_2 out: $C_{co_{2,out}} = p_{co_2} / RT$

$= y_{co_2}^{out} \times P_t / RT$

$= 0.072 \times 1/ (82.05 \times 298)$

$= 2.94 \times 10^{-6}$ gmol/cm^3

Molar Flux $N_{co_2} = \frac{157.8 \times (5.72 \times 10^{-6} - 2.94 \times 10^{-6})}{1043.6 * 60 \times 10^{-4}} = 7 \times 10^{-5}\ gmol / m^2 s$

Also, $N_{co_2} = K_{og} \frac{\Delta y_{lm} P_t}{RT}$

$$\Delta y_{lm} = \frac{(y_{co_2}{}^{in} - y^*_{in}) - (y_{co_2}{}^{out} - y^*_{out})}{\ln\left(\frac{(y_{co_2}{}^{in} - y^*_{in})}{(y_{co_2}{}^{out} - y^*_{out})}\right)}$$

Assuming $y^*_{in} \approx y^*_{out} \cong 0$; $\Delta y_{lm} = 0.102$

Therefore, calculating K_{og}

$$7 \times 10^{-5} = K_{og} \frac{0.102 \times 1}{(298 \times 82.05 \times 10^{-6})}$$

K_{og} =1.67x10^{-5}m/s.

B.2 Calculation of Mean Free Path (λ)

Mean free path of a gas molecule is given by = $RT/1.414*d^2*N_A*P*\pi$

Where, R = 8.205 x 10^{-5} m^3 atm/ K. mol

P = 1 atm

T = 273 + 25 = 298 K

d= CO_2 molecule of diameter = 3.3 Å

N_A = Avogadro number = 6.023 x 10^{23} / mol

Substituting these values in the above equation we get,

λ= 8.39 x 10^{-8} m.

B.3 Calculation of Interstitial Velocity

Interstitial velocity: Flow rate / open area for flow through the shell side

Open area for flow through the shell side => frame cross -sectional area (6.4 x 2.5 cm^2) – fiber projected area (number of fibers in 1 layer x D_0 x L, cm^2)

⇨ (6.4 x 2.5) – (38 x 0.029 x 6.35)

⇨ 16 – 6.99 cm^2

⇨ 9.00 cm^2.

B.4 Sample Calculation of k_g

For gas flow rate of 18.16 cm^3/min through the tubes

Length of fiber (L)(m)	0.0635		
Flowrate (Q)(m3/s)	1.81833E-07	--------->	Unit Conversion
Number of fibers	2128		

Flowrate in each tube(m3/s)	8.5448E-11	---------> Flowrate/ number of fibers
Inner Diameter (d_i)(m)	0.00024	
Outer Diameter (d_o)(m)	0.00029	
Area based on ID (m2)	4.5216E-08	---------> $A = \pi d_i^2$ = Q/A
Mean velocity (m/s)	0.001889773	
Temperature (F)	77	
Density (lb/ft3)	0.0775	
Kinematic Viscosity (ft2/s)	0.000152	
Dynamic Viscosity (lb/ft/s)	0.00001162	
d ($d_o - d_i$) (m)	0.00005	

Reynolds Number : $\frac{\text{Length*Mean velocity*density}}{\text{dynamic viscosity}}$

$$Re = \frac{\rho * \upsilon * d}{\mu}$$

Density(kg/m3)	1.233
Dynamic Viscosity(Pa.s)	0.0000172
Reynolds number	0.0113

Schmidt Number : $\frac{\text{dynamic viscosity}}{\text{Diffusivity*density}}$

$$Sc = \frac{\mu}{D * \rho}$$

0.0000158

Diffusivity (m^2/s)	
Density (kg/m^3)	1.233
Dynamic Viscosity(Pa.s)	0.0000172
Sc Num	0.882893427
Sherwood Number	**0.0003164**

$Sh = 1.096 \{Re\ Sc\ (d/h)\}^{0.80}$

d = outer diameter - inner diameter

Kg (m/s)	1.00E-04

B.5 Calculation of Interfacial Area (m^2/m^3)

Interfacial Area (m^2/m^3): (a) Effective area

Shell volume

Total surface area = $n\pi dl$

= 3.14 x 0.029 x 6.35 x1064

= 615 cm^2

For 2 modules = 1230 cm^2

Fiber Volume

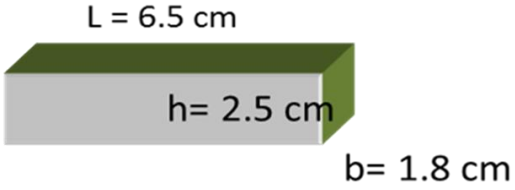

Volume = 6.5x2.5x1.8 = 29.25 cm^3 => 2x29.25 = 58.5 cm^3

Interfacial area (a) cm^{-1} = 1230/58.5 = 21.025 cm^{-1} = 2102.56 m^{-1}

B.5 CO_2 Diffusivity in IL- PAMAM mixture

Due to lack of literature, the CO_2 diffusivity in IL-PAMAM was assumed to be the same as with other amines

The diffusivity of N_2O in DEA- ethanol is 2.59 x 10^{-9} m^2/s.

Using N_2O analogy to calculate CO_2 diffusivity in IL- PAMAM mixture

N_2O analogy

$$(D_{CO2})_{amine} = (D_{N2O})_{amine} \frac{(D_{CO2})_{water}}{(D_{N2O})_{water}}$$

Diffusivities of CO_2 and N_2 in water are calculated using

$$D_{CO2} = 2.35 \text{ X } 10^{-6} \exp(-2119/T(K)) \ m^2/s$$

$$D_{N2O} = 5.07 \text{ X } 10^{-6} \exp(-2371/T(K)) \ m^2/s$$

Calculating the diffusion coefficients at 323K and substituting in the above equation

$$(D_{CO2})_{amine} = 2.2 \text{ x } 10^{-9} \ m^2/s.$$

B.6 Calculation of happel's radius and volume of 80 wt% dendrimer in ionic liquid around PVDF hollow fiber.

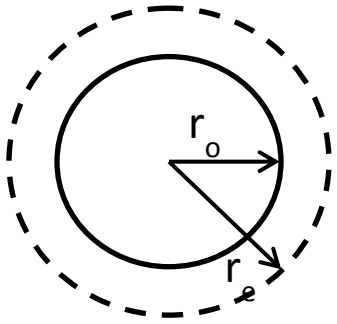

Where,

r_o = outer radius of the hollow fiber

r_e = happel's radius

Outer radius of PVDF hollow fiber = 0.0925/2 = 0.046 cm.

Active length of the fiber = L = 35.5 cm.

Shell radius of the module = r_s = 0.45 cm.

Number of PVDF fibers = 11.

To calculate the grams, we first calculate the volume between the two radii.

Happel's radius $r_e = (1/1-\varepsilon)^{0.5}. r_o$

where, $\varepsilon = 1- \frac{N\Pi r_o^2}{\Pi r_s^2}$

$\varepsilon = 1- \frac{11*0.046*0.046}{(0.45*0.45)}$

$\varepsilon = 0.885$

$r_e = 0.1357$ cm.

Volume between fibers = $\Pi*L*(r_e^2 - r_o^2) = 1.815$ cm^3.

Since ρ= 1.18 gm/ cm^3; weight of 80 wt% dendrimer in ionic liquid = 2.14 g of absorbent.

REFERENCES

1. J.D. Fiqueroa, et al., Advances in CO_2 Capture Technology—The U.S. Department of Energy's Carbon Sequestration Program, International Journal of Greenhouse Gas Control 2 (2008) 9-20.

2. Energy Information Administration (EIA), 2006a. Annual Energy Outlook 2006. http://www.eia.doe.gov/oiaf/aeo/. (last accessed on March, 2014)

3. IPCC, 2005: IPCC Special Report on Carbon Dioxide Capture and Storage, Prepared by Working group III of the Intergovernmental Panel on Climate Change. Cambridge University Press, Cambridge, United Kingdom and New York NY, USA, 422pp.

4. J. Gibbins and H. Chalmers, Carbon Capture and Storage, Energy Policy 36 (2008) 4317-4322.

5. J. Kuropka, Removal of Nitrogen Oxides from Flue Gases in a Packed Column, Environment Protection Engineering, 37 (2011) 13-22.

6. I. Furuta, Nitrogen Oxide Removal from Waste Gas by Scrubbing with Calcium and Magnesium Hypochlorites (36372), 1975.

7. F.J.G. Ortiz, et al., Pilot-plant Technical Assessment of Wet Flue Gas Desulfurization using Limestone, Ind. Eng. Chem. Res. 45 (2006) 1466-1477.

8. Z. Yi, et al., Experimental Study on Simultaneous Desulfurization and Denitrification based on Highly Active Absorbent, Journal of Environmental Sciences 18 (2006) 281-286.

9. A. L. Kohl, et al., Gas Purification, Fifth edition, Houston, State: Gulf Publishing Company, 1997.

10. G.T. Rochelle, Amine Scrubbing for CO_2 Capture, Science 325 (2009) 1652-1654.

11. J. Zhou, Hybrid Membrane Absorption Process for Acid Gas Removal in FLNG Applications, Gas Technology Institute.

12. D.M.D' Alessandro, Carbon Dioxide capture: Prospects for New Materials, 49 (2010) 6058-6082.

13. S. Karoor and K.K. Sirkar, Gas Absorption Studies in Microporous Hollow Fiber Membrane Modules, Ind. Eng. Chem. Res. 32 (1993) 674-684.

14. W. Ho and K.K. Sirkar, Membrane Handbook, Cambridge University Press, 1992, Chap. 5.

15. K. Esato et al., Experimental Evaluation of Gore-Tex Membrane Oxygenator, J. Thorac. Cardivas. Surg. 69 (1975) 690-675.

16. T. Tsuji et al., Development and Clinical Evaluation of Hollow Fiber Membrane Oxygenator, Trans. Am. Soc. Artif. Intern. Organs. 27 (1981) 280-284.

17. A. Gabelamn, et al., Hollow Fiber Membrane Contactors, J. of Membrane Science 159 (1999) 61-106.

18. J.L. Anderson, et al., Measurement of CO_2 Solubility in Ionic Liquids, Ind. Eng. Chem. Res. 43 (2004**)** 6855-6860.

19. A. Berthod et al., Ionic liquid in Separation Techniques, J. Chromatogr. A 1184 (2008) 6–18.

20. Process Insight: Comparing Physical Solvents for Acid Gas Removal, Bryan Research & Engineering, Inc.

21. A. Marciniak, The Solubility Paramètres of Ionic liquid, Int. J. Mol. Sci. 11 (2010**)** 1973-1990.

22. A.H. Jalili, Solubility and diffusion of CO_2 and H_2 S in the Ionic Liquid 1-ethyl-3-methylimidazolium Ethylsulfate, J. Chem. Thermodynamics 42 (2010) 1298–1303.

23. J.L. Anthony, N.V.K.A. Sudhir, E.J. Maginn and J.F. Brennecke, Feasibility of using Ionic Liquids for Carbon Dioxide Capture, Int. J. Environmental Technology and Management 4 (2004) 105-115.

24. J. Chau, G. Obuskovic, X. Jie, T. Mulukutla and K.K. Sirkar, Solubilities of CO_2 and Helium in an Ionic liquid containing Poly(amidoamine) Dendrimer Gen 0, Ind. Eng. Chem. Res. 52 (2013) 10484-10494.

25. P. Vaidya et al., CO_2-Alkanolamine Reaction Kinetics: A Review of Recent Studies, Chem. Eng. Technol. 30 (2007) 1467-1474.

26. H. Matsuyama et al., Facilitated transport of CO_2 through Polyethylenimine/poly (vinyl alcohol) Blend Membranes, J. Membr. Sci. 163 (1999) 221-227.

27. A.S. Kovvali, H. Chen, K.K. Sirkar, Dendrimer Membranes: A CO_2-selective Molecular Gate, JACS 122 (2000) 7594-7595.

28. A.S. Kovvali, K.K. Sirkar, Dendrimer Liquid Membranes: CO_2-separation from Gas Mixtures, Ind. Eng. Chem. Res. 40 (2001) 2502-2511.

29. A.S. Kovvali, and K.K. Sirkar, Carbon Dioxide Separation with Novel Solvents as Liquid Membranes, Ind. Eng. Chem. Res. 41 (2002) 2287-2295.

30. S. Duan, T. Kouketsu, S. Kazama, K. Yamada, Development of PAMAM Dendrimer Composite Membranes for CO_2 Separation, J. Membrane Sci. 283 (2006) 2-6.

31. I. Taniguchi, S. Duan, S. Kazama, Y. Fujioka, Facile Fabrication of a Novel High Performance CO_2 Separation Membrane: Immobilization of Poly (amidoamine) Dendrimers in Poly (ethylene glycol) Networks, J. Membrane Sci. 322 (2008) 277-280.

32. S. Duan, T. Kouketsu, T. Kai, S. Kazama, K. Yamada, PAMAM Dendrimer Composite Membrane for CO_2 Separation: Formation of a Chitosan Gutter Layer, J. Membrane Sci. 287 (2007) 51-59.

33. B. Li and K. K. Sirkar, Novel Membrane and Device for Direct Contact Membrane Distillation-based Desalination Process, Ind. Eng. Chem. Res. 43 (2004) 5300-5309.

34. L. Song, B. Li, K.K. Sirkar and J. Gilron, Direct Contact Membrane Distillation-based Desalination: Novel Membranes, Devices, Larger-scale Studies and a Model, Ind. Eng. Chem. Res. 46 (2007) 2307-2323.

35. L. Song, and K.K. Sirkar, Pilot plant Studies of Novel Membranes and Devices for Direct Contact Membrane Distillation-Based Desalination, J. Membrane Sci. 323 (2008) 257-270.

36. P. Kosaraju, A. Korikov, A. Kovvali and K.K. Sirkar, Hollow Fiber Membrane Contactor-Based CO_2 Absorption-Stripping Using Novel Solvents and Membranes, Ind. Eng. Chem. Res. 44 (2005) 1250-1258.

37. X. Ma, X. Wang and C. Song, Molecular Basket Sorbents for Separation of CO_2 and H_2S from Various Gas Streams, JACS 131 (2009) 5777-5783.

38. R. Banerjee et al., High-Throughput Synthesis of Zeolitic Imidazolte Frameworks and Application to CO_2 Capture, Science 319 (2008) 939-942.

39. J.C. Hicks et al., Designing Adsborbent for CO_2 Capture from Flue Gas-Hyperbranched Aminosilicas Capable of Capture CO_2 Reversibly, JACS 130 (2008) 2902-2903.

40. A. Geoppert et al., Carbon Dioxide Capture from the Air Using a Polyamine

Based Regenerable Solid Adsorbent, JACS 133 (2011) 20164 – 20167.

41. N.R. Stuckert and R.T. Yang, CO_2 Capture from the Atmosphere and Simultaneous Concentration Using Zeolites and Amine- Grafted SBA- 15, Environ. Sci. Tech. 45 (2011) 10257-10264.

42. D.M. Pacheco, J.R. Johnson and W. Koros, Aminosilane-Functionalized Cellulosic Polymer for Increased CO_2 Sorption, Ind. Eng. Chem. Res. 51 (2012) 503-514.

43. R.P. Lively et al., Hollow Fiber Adsorbents for CO_2 capture: Kinetic Sorption Performance, Chem. Eng. Journal 171 (2011) 801-810.

44. T.L. Donaldson and Y. N. Nguyen, Carbon Dioxide Reaction Kinetics and Transport in Aqueous Amine Membranes, Ind. Eng. Chem. Fundam. 19 (1980) 260-266.

45. M. Caplow, Kinetics of Carbamate Formation and Breakdrown, J. Am. Chem. Soc. 90 (1968) 6795 - 6803.

46. P. V. Danckwerts, The Reaction of Carbon Dioxide with Ethanol-Amines. Chem. Eng. Sci. 34 (1979) 443-446.

47. P. Vaidya, et al., CO_2- Alkanolamine Reaction Kinetics: A Review of Recent Studies, Chem. Eng. Technol. 30(2007) 1467-1474.

48. C.W. Jones, et al, Adsorbent materials for Carbon Dioxide Capture from Large Anthropogenic Point Sources, ChemSusChem 2 (2009) 796-854.

49. D. Barth, et al, Kinetic study of Carbon Dioxide Reaction with Tertiary Amines in Aqueous Solutions, J. Phys. Chem. 85 (1981) 3660-3667.

50. Y. G. Ko, et.al, Primary, Secondary and Tertiary Amines for CO_2 Capture: Designing for Mesoporous CO_2 Adsorbents, Journal of Collodial and Interface Science 361(2011) 594-602.

51. S.R. Rubero et al., Surface Characterization of 1-Butyl-3-methylimidazolium Br^-, I^-, PF_6^-, BF_4^-, $(CF_3SO_2)_2N^-$, SCN^-, $CH_3SO_3^-$, $CH_3SO_4^-$, and $(CN)_2N^-$ Ionic Liquid by Sum Frequency Generation, J. Phys. Chem. B, 110(10), 4756-4765.

52. R.K. Khanna, et al., Carbamic acid: molecular structure and IR spectra, Spectrochimica Acta Part A 55 (1999) 961-967.

53. J. Albo, P. Luis and A. Irabien, Carbon Dioxide Capture from Flue gases using a Cross-flow Membrane Contactor and the Ionic Liquid 1-Ethyl-3-methylimidazolium Ethylsulfate, Ind. Eng. Chem. Res. 49 (2010) 11045-11051.

54. J.L. Li, B.H. Chen, Review of CO_2 Absorption using Chemical Solvents in Hollow Fiber Membrane Contactors, Separation and Purification Technology 41 (2005) 109-122.

55. M.C. Yang and E.L. Cussler, Designing Hollow-Fiber contactors, AIChE Journal 32 (1986) 1910-1916.

56. S.R. Wickramasinghe, M.J. Semmens, E.L. Cussler, Mass transfer in various hollow fiber geometries, J. Membrane Sci. 69 (1992) 235-250.

57. D. Bhaumik, S. Majumdar, K.K. Sirkar, Absorption of CO_2 in a Traverse Flow Hollow Fiber Membrane Module having a New Wraps of the Fiber Mat, J. Membrane Sci. 138 (1998) 77-82.

58. C.A. Fuster, N. Midoux, A. Laurent and J.C. Charpentier, Chemical Kinetics of the Reaction of CO_2 with Amines in Pseudo m-nth Order Conditions in Polar and Viscous Organic Solutions, Chem. Eng. Sci. 36 (1981) 1513-1518.

59. M.A. Pacheco, Mass transfer, Kinetics and Rate-based Modeling of Reactive Absorption, PhD Dissertation, The University of Texas, Austin, Texas, 1998 <http://www.che.utexas.edu/rochelle_group/Pubs/Pacheco%20Dissertation.pdf >.

60. N. Nishikawa, M. Ishibashi, H. Ohta and N. Akutsu, CO_2 Removal by Hollow Fiber Gas Liquid Contactor, Energy Convers. Mgmt 36 (1995) 415-418.

61. H.A. Rangwala, Absorption of Carbon Dioxide into Aqueous Solutions using Hollow Fiber Membrane Contactors. J. Membrane Sci. 112 (1996**)** 229-234.

62. J.L. Anthony; N.V.K.A. Sudhir et al. Feasibility of Using Ionic Liquids for Carbon Dioxide Capture, Int. J. Environ. Techn. Mgmt. 4 (2004) 105-109.

63. M. Ramdin,; T.W. de Loos,; T.J.H. Vlugt, "State-of –the –Art of CO_2 capture with Ionic Liquids", *Ind. Eng. Chem. Res.* 51 (2012**)** 8149-8153.

64. C.P. Fredlake, J.M. Crosthwaite, D.G. Hert, et al., Thermophysical Properties of Imidazolium-Based Ionic Liquids, J. Chem. Eng. Data. 49 (2004) 954-959.

65. Y. Kuwahara, et al., Dramatic Enhancement of CO_2 uptake by Poly(ethyleneimine) Using Zirconosilicate Supports, J. Am. Chem. Soc. 134 (2012) 10757–10760.

66. A. Samanta, et al., Post Combustion CO_2 Capture using Solid Sorbents: A Review, Ind. Eng. Chem. Res. 51 (2012) 1438-1463.

67. M.G. Plaza, et al., Post combustion CO_2 Capture with a Commercial Activated

Carbon: Comparison of Different Regeneration Strategies, Chem. Eng. Journal 163 (2010) 41-47.